Dispersion in a Mountain Environment

By
John D. Reid

Department of Atmospheric Science
Colorado State University
Fort Collins, Colorado

This report was prepared with support provided by the National Science Foundation
Grant ERT 71-01885.
Principal investigator: Lewis O. Grant
July 1976

Colorado State University

Department of Atmospheric Science

Paper No. 253

DISPERSION IN A MOUNTAIN ENVIRONMENT

BY

John D. Reid

This report was prepared with support provided by
National Science Foundation Grant ERT 71-01885
Principal Investigator, Lewis O. Grant

Department of Atmospheric Science
Colorado State University
Fort Collins, Colorado

July 1976

Atmospheric Science Paper No. 253

ABSTRACT OF DISSERTATION

DISPERSION IN A MOUNTAIN ENVIRONMENT

This study attacks the problem of identifying the key atmospheric parameters governing dispersion in mountainous terrain, particularly as it relates to modification of cold orographic clouds by ice nucleant released near the surface. Three lines of investigaton are followed: (i) post hoc analysis of the Climax randomized weather modification data set, (ii) case study tracer experiments, (iii) numerical simulation.

The ten year Climax randomized orographic seeding experiment data set is examined to identify variables influencing the dispersion stage of the seeding process which also influenced precipitation. Wind speed at 700 mb, which governs the time available for dispersion to occur as the seeding agent is transported from the generator to the target, is indicated to be a significant parameter. Speeds in the range 12 to 14 mps are found optimum for seeding effect. However, for low (< 8 mps) wind speed the seeding effect is found dependent on wind direction, with winds from the southwest quadrant (generators distant from the target and more complex terrain) showing precipitation increases with seeding but winds from the northwest quadrant (generators closer to the target) showing precipitation decreases with seeding. No diurnal influence on seeding effect is found.

Field tracer experiments were conducted during the winters of 1973-74 and 1974-75 with AgI seeding agent released from valley based generators and sensed with a acoustical ice nucleus counter aboard an NCAR Queenair aircraft. The majority of experimental tracer days showed

greater low-level stability than is typical for orographic cloud conditions. Under these circumstances the seeding agent is strongly constrained in the valley and frequently found to be transported considerable distances by low-level drainage flow. Thus transport of the seeding agent far "upwind" of the generator site as well as downwind is possible. Presence of an orographic cloud inhibits drainage flow on the shallower slopes leading to zones of low level flow convergence and forced vertical motions near marked terrain slope changes. This apparently provides one mechanism for seeding agent vertical transport during orographic conditions.

The University of Virginia two-dimensional mesoscale model coupled with a new Monte Carlo simulation of atmospheric dispersion is employed to investigate transport and dispersion of seeding agent to cloud base for a situation representing an idealization of that at Climax in northwesterly airflow. For stable low-level conditions drainage flow persists on the mountain side for low geostrophic wind speeds. For somewhat higher geostrophic wind speeds (higher speeds for greater stability) a zone of low-level wind convergence, as found in the field study, is evident. For strong geostrophic winds the drainage flow is eliminated. The dispersion simulation shows a maximum in the cloud base area subject to seeding for intermediate geostrophic wind speeds where the rate of dispersion is compensated by the rate of terrain rise to keep cloud base ice nucleus concentrations in the range effective for seeding for a maximum distance between the generator and ridge crest target.

These studies show that the most critical parameter governing dispersion of seeding agent to orographic cloud base for a fixed source and target configuration is wind speed. Although diurnal diabatic

effects are generally dominant in mountainous terrain it appears that for orographic cloud situations simulations of neutral stratification conditions may be adequate to define close to optimum seeding configurations.

John D. Reid
Atmospheric Science Department
Colorado State University
Fort Collins, Colorado 80523
Summer, 1976

ACKNOWLEDGEMENTS

The outstanding contribution of Professor L.O. Grant, adviser, for this research, is gratefully acknowledged. His counsel throughout the course of this study was indispensable to its completion.

Thanks are also due to my graduate committee, Dr. F. Hall, Dr. D. Lenschow, Dr. J. Peterka and especially Dr. W. Cotton for numerous helpful discussions.

The research was funded under contract ERT 71-01885-A03 from the RANN division of the National Science Foundation. The author's time was partially supported by his continuing employer, the Atmospheric Environment Service, Environment Canada.

Aircraft facilities for this project were provided by the National Center for Atmospheric Research. Particular thanks go to NCAR pilots Mr. T. McQuade, Mr. R. Burris and to Mr. A. Rodi for ground coordination. Computer facilities were also provided in part by NCAR, which is funded by the National Science Foundation.

Completion of this study would not have been possible without the able computer programming assistance of Mr. D. Blanchar and Mr. G. Walters, the field services of Western Scientific Services and the help in data services of Mr. D. Friday and Ms. L. McCall.

Finally, I am especially pleased to acknowledge the contributions of Ms. G. Holt who did a splendid job in preparing the manuscript and Ms. L. McCall who did an equally outstanding job in drafting the figures.

TABLE OF CONTENTS

		Page
TITLE PAGE		i
SIGNATURE PAGE		ii
ABSTRACT		iii
ACKNOWLEDGEMENTS		vi
LIST OF TABLES		x
LIST OF FIGURES		xii
LIST OF SYMBOLS		xv
CHAPTER		
ONE	INTRODUCTION	1
	1.1 Specific Objectives of the Research	2
	1.2 Organization of the Material	2
TWO	REVIEW OF AIRFLOW AND DISPERSION IN MOUNTAINOUS TERRAIN	4
	2.1 Airflow in Mountainous Terrain	4
	2.2 Dispersion in Mountainous Terrain	16
THREE	COLD OROGRAPHIC CLOUD MODIFICATION	27
	3.1 Outline of Cold Orographic Cloud Modification Theory	27
	3.2 Review of Statistical Results from the Climax Experiment	30
	3.3 Further Results from the Climax Experiments	33
	3.4 Diurnal Effects of Seeding	37
FOUR	THE FIELD EXPERIMENTAL PROGRAM	42
	4.1 Area of Study	42
	4.2 Surface Based Instrumentation	42
	4.3 Airborne Instruments	47
	4.4 Aircraft Data Processing	49
	4.5 Experimental Design and Procedures	52
	4.6 Data Obtained	55
FIVE	OBSERVATIONS	57
	5.1 Near Surface Flow	57
	5.2 Background Levels of Ice Nuclei	61

TABLE OF CONTENTS (Continued)

CHAPTER		Page
	5.3 Dispersion Case Studies	62
	5.3.1 December 15, 1973	62
	5.3.2 January 13, 1975	73
	5.3.3 January 14, 1975	79
	5.4 Conclusions	82
SIX	SIMULATION OF MOUNTAIN ENVIRONMENT AIRFLOW	85
	6.1 Previous Modelling Studies	85
	6.2 Modelling Constraints and Requirements	87
	6.3 The University of Virginia Two-Dimensional Meso-scale Model	89
	6.3.1 Restriction on the Applicability of the Model	90
	6.4 Case Studies with the University of Virginia Model	93
	6.4.1 The Daytime Case	93
	6.4.2 The Nighttime Case	98
SEVEN	MONTE CARLO METHODS FOR ATMOSPHERIC DISPERSION STUDIES	101
	7.1 The Monte Carlo Method	101
	7.1.1 Specification of Component Winds	103
	7.2 Numerical Method for Statistical Simulation of Near Neutral Stability Condition Dispersion	104
	7.3 Numerical Method for Statistical Simulation of Dispersion in Energy Containing Eddy Fields	106
	7.4 Variance Reduction Techniques	108
	7.4.1 Random Number Sharing	108
	7.4.2 Time-Step Expansion for Quasi-Uniform Regions	109
	7.4.3 Cloning and Russian Roulette	110
	7.5 Disadvantages of the Model	110
EIGHT	A MOUNTAIN ENVIRONMENT DISPERSION SIMULATION	112
	8.1 The Turbulence Model	112
	8.2 Application	115
	8.3 Case Studies	116
	8.3.1 The Daytime Situation	117
	8.3.2 The Nighttime Situation	121
NINE	SUMMARY AND CONCLUSIONS	125
	9.1 Summary and Specific Conclusions	125
	9.2 A Conceptual Model of the Orographic Cloud Seeding Process	128
	9.3 Suggestions for Further Research	130

TABLE OF CONTENTS (Continued)

		Page
REFERENCES		132
APPENDIX		
A	THE UNIVERSITY OF VIRGINIA TWO-DIMENSIONAL MESOSCALE MODEL	138
	A.1 Boundary Layer Formulation	139
	A.2 Initial and Boundary Conditions	141
	A.3 Numerical Aspects	142
B	NUMERICAL METHOD FOR STATISTICAL SIMULATION OF DISPERSION IN A CONVECTIVE PLUME FIELD	143

LIST OF TABLES

Table		Page
3.1	Effect of 500mb (near cloud top) temperature on seeding effect in the Climax experiment	31
3.2	Effect of 700mb wind direction on seeding effect in the Climax experiment	31
3.3	Effect of 700mb wind speed on seeding effect in the Climax experiment	31
3.4	Precipitation modification at Climax indicated by a multiple stratification of wind speed, wind direction and 500mb temperature	34
3.5	Precipitation efficiency at Climax for multiple stratification of meteorological parameters	34
3.6	Diurnal variation of precipitation during the Climax experiment for seeded and non-seeded low wind speed cases	39
3.7	Same as table 3.6 except for moderate wind speed cases	40
4.1	Anemometer sites during the field study	46
4.2	Conventional equipment aboard the NCAR Queenair for the 1973-74 season, after NCAR (1973)	48
4.3	Intensive observation days during the field experiment	56
5.1	Climatology of diurnal wind direction variation for winter months in Camp Hale	58
5.2	Diurnal variation of wind direction at the Camp Hale station for 500mb up-valley flow cases stratified according to whether precipitation fell on the day or not	60
5.3	Wind variation at a number of stations within the experiment area for 15 December 1973	72
8.1	Variation of von Kármán scale length in the winter LO-LOCAT wind conforming subset taken west of Colorado Springs, Colorado	114
8.2	Variation of turbulent velocity variances in the LO-LOCAT wind conforming subset taken west of Colorado Springs, Colorado	114

LIST OF TABLES (Continued)

Table		Page
8.3	Seeding efficiency index and overseeding index for neutral stratification conditions with various wind speeds	118
8.4	Same as table 8.3, except for 10 mps wind speed and stable low level air under an orographic cloud . .	120
8.5	Same as table 8.3, except for low level stable conditions with 10 and 15 mps prevailing wind speed .	123

LIST OF FIGURES

Figure		Page
2.1	Potential flow for horizontal deviations in the vicinity of two mountains	6
2.2	Potential flow over an isolated mountain ridge	7
2.3	Precipitation profile across the Rocky Mountains in Colorado, after Grant and Kahan (1974)	9
2.4	The Lee Wave and associated phenomena, after Flohn (1970)	9
2.5	Vertical profile of a down-slope wind, after Defant (1949)	12
2.6	Schematic illustration of the normal diurnal variations of air currents in a mountain valley, after Defant (1949)	15
2.7	Vertical variation of eddy diffusivity in mountainous terrain near Climax, Colorado, after Wooldridge and Lewis (1975)	20
2.8	Vertical variation of eddy diffusivity in Cache Valley, Utah, after Wooldridge (1974)	21
2.9	Spectrum of kinetic energy in the atmosphere, after Vinnichenko et al. (1973)	23
3.1	Schematic representation of the orographic cloud seeding process	29
3.2	Comparative seed/no seed precipitation ratios as related to estimated cloud-top temperatures for seven cloud seeding experiments, after Grant and Elliott (1974)	32
4.1	Major topographic features of the area of the study at climax	43
4.2	The immediate area of concern in the field experiments	44
4.3	Calibration of the ice nucleus generator used in the field experiments	56
5.1	Synoptic situation at 12Z 15 December 1973	63

Figure		Page
5.2	Aircraft temperature sounding obtained at about 12 Noon MST north of Camp Hale on 15 December 1973 . .	65
5.3	Concentration of ice nuclei for the lowest 250m above terrain for the 15 December 1973 experimental day	66
5.4	Same as Figure 5.3, except for 250-500m above the surface	67
5.5	Comparison of non-dimensionized potential temperature profiles for the Barostromatic wind tunnel case of Orgill (1971) and the case of 15 December 1973 . .	69
5.6	Surface IN concentration pattern found in Barostromatic conditions in the wind tunnel by Orgill (1971) . .	70
5.7	Synoptic situation at 12Z 13 January 1975	74
5.8	Composite upper air sounding from flight operations on 13 January 1975	75
5.9	Surface ice nucleus concentration pattern for 13 January 1975	77
5.10	Cross-section along the prevailing wind direction showing IN concentrations and wind flow for 13 January 1975	78
5.11	Synoptic situation at 12Z 14 January 1975	80
6.1	Streamlines of neutral stratification airflow over a mountain ridge for a case with geostrophic wind 10 mps	95
6.2	Isotachs of vertical velocity for the case of figure 6.1	96
6.3	Streamlines of orographic flow for an early morning situation with an orographic cloud present, geostrophic wind 10 mps	97
6.4	Streamlines of orographic flow for a stable nighttime situation simulating clear sky conditions except with an orographic cloud over the mountain	99
7.1	Comparison of analytic and Monte Carlo concentration estimates for a simple line source case	107

LIST OF FIGURES (Continued)

Figure		Page
B.1	Crosswind integrated concentration as a function of height and distance downstream from an elevated point source, after Willis and Deardorff (1975)	146
B.2	Plume vertical velocity profile satisfying boundary constraints	147
B.3	Monte Carlo simulation of concentration as a function of height and distance downstream from an elevated line source	149

LIST OF SYMBOLS

C	Ensemble mean concentration
C_o	Drag coefficient
C_i	Concentration in cell i given by the Monte Carlo dispersion method
DV_i	Volume of a cell in the Monte Carlo dispersion method
Dx, Dy, Dz	Dimension of a cell in the Monte Carlo dispersion method
f	Coriolis parameter
$F_E(n)$	Eulerian turbulence spectrum function for wavenumber n
g	Acceleration of gravity
$\overline{h}$	Mean depth of a slope wind
J_o, J_1	Zero and first order Bessel Functions
K_{ij}	The i,j'th element of the eddy diffusion tensor
$K_{x,y,z}$	Eddy diffusivity coefficients along and across the wind, and vertically, respectively
K_z^m	Vertical eddy exchange coefficient for momentum
K_z^q	Vertical eddy exchange coefficient for moisture
K_z^θ	Vertical eddy exchange coefficient of heat
k_o	von Kármán's constant
L_{u_i}	Scale length for the von-Kármán spectrum in the i direction
L_*	Reduced Monin-Obukhov stability length
M	Separation constant, in Appendix B
N	Total number of trajectories in the Monte Carlo dispersion method
n_{eff}	Number of independent contributions to a concentration estimate from a single particle
n_i	Total number of time increments accumulated in cell i in the Monte Carlo dispersion method

Q	Pollutant source strength
q	Specific humidity
R	Plume radius, in Appendix B
r	Radial distance, in Appendix B
$R_E(\kappa)$	Eulerian time correlation between turbulent velocities at times separated by κ
$R_L(\tau)$	Lagrangian time correlation between turbulent velocities at times separated by τ
S	Pollutant sink strength
s	The material surface top of the numerical model
$S_i(k)$	Component of the von-Karman spectrum function at wave-number k in the i direction
$\overline{s}$	Initial height of the material surface top of the numerical model
t	Time
T_c	Local temperature of cold slope wind
T_E	Environment temperature
u, v, w	x, y, z direction winds
u	Radial velocity, in Appendix B
u_g	Geostrophic wind in the x direction
u_i	Wind component in the i direction
$\overline{u_i'^2}_{eff}$	Effective velocity variance employed with large time steps in the Monte Carlo dispersion method
U_{slope}	Slope wind-speed
u_*	Surface friction velocity
v_g	Geostrophic wind in the y direction
x_i	Distance in the i direction

w^*	Vertical velocity in the airflow model transformed coordinate system
x, y, z	Coordinate directions
z_G	Height of the topography in the numerical model
z_o	Roughness parameter
z^*	Transformed vertical coordinate
α	Slope angle, in Chapter Two
α	Lagrangian autocorrelation between turbulent velocities at times separated by Δt
α	Horizontal scale factor, in Appendix B
β	Ratio of Lagrangian to Eulerian time scales
β	Coefficient in the expression for a turbulent velocity equal to $(1-\alpha^2)^{1/2}$
γ	Lapse rate of temperature
Δt	Time increment used in the Monte Carlo dispersion method
ϵ	Time
θ	Potential temperature
θ_*	Surface friction temperature
ξ	Non-dimensional stability length, $= z^*/\lvert L_* \rvert$
π	Exner's function
ρ_1	Lagrangian time correlation for lag Δt
$\sigma^2_{x_i}$	Variance of a concentration distribution in the x_i direction
ϕ_i	Non-dimensional profile functions

CHAPTER ONE

INTRODUCTION

Mountainous regions offer a particular challenge for assessing the turbulent diffusion of gaseous and aerosol pollutants. The dispersion regime of mountain valleys is quite different from that of more open areas. Pollution tends to remain in more concentrated form. It is thus more hazardous. The increasing development of mountain areas for industry and recreation along with more stringent restrictions on polluting has motivated greater efforts to understand this phenomena.

The problem of dispersion in mountainous terrain is also of interest in that it affects orographic cloud seeding. Such seeding conducted in Colorado has involved releasing silver iodide smoke from a ground based seeding generator. The silver iodide particles are dispersed into the orographic cloud by the mountain airflow. It has been estimated that such seeding might increase runoff an additional two million acre feet a season from Colorado alone.

With these practical concerns in mind, the overall objective of this investigation has been to improve our understanding of the physical processes contributing to, and so ability to predict, dispersion in mountainous terrain. In particular the research has been motivated by the need to understand orographic cloud seeding from ground based generators. The results presented here are, of course, also immediately applicable to the pollution dispersion problem in general.

Two approaches have been adopted in this study. An extensive field tracer study program has been undertaken in the vicinity of the Continental Divide at Climax, Colorado. The program was conducted during

selected days of the winters of 1973-74 and 1974-75. Such case studies, along with climatological/statistical studies, provide direct evidence with which to determine the important processes in operation. In the second approach an attempt is made to numerically model the dispersion of seeding agent in orographic airflow. A comprehensive study of a third approach, wind tunnel simulation, has been made by Orgill (1971) for the area of concern and the results achieved here are compared to those investigations.

1.1 Specific Objectives of the Research

Two specific objectives are identified for the field study:

1. Determine the significant mechanisms by which the mountains and synoptic weather conditions interact to produce characteristic mountain-valley dispersion patterns.
2. Relate the transient wind fluctuations responsible for dispersion to larger scale and thus more easily determined parameters.

An additional two objectives for the numerical modeling study are:

3. Investigate numerical models which may permit inclusion of all the significant physical mechanisms found in the field investigation.
4. Develop a method capable of predicting seeding concentrations from a ground based seeding generator.

1.2 Organization of the Material

The structure of this dissertation is presented now as a brief guide. In Chapter Two a review of our understanding of airflow and dispersion in mountainous terrain, as obtained from the literature, is presented. The material is intended to emphasize knowledge gained from

observation. Chapter Three discusses cold orographic cloud modification, reviewing our previous knowledge and extending it by additional analysis of the data obtained from the Climax experiments. The thrust of the chapter is to determine the importance of the transport-dispersion regime on seeding effect.

Observational work done in this study is then presented. In Chapter Four the details of the observational procedures are given and the instrumentation described. The experimental results are discussed in Chapter Five, particularly the important implications for cold orographic cloud seeding are emphasized. A comparison with wind tunnel simulations is included.

Based on the experimental results and other considerations, the important features that need to be included in a numerical model of airflow in an orographic environment are outlined in Chapter Six. A simplified two-dimensional version of this model is discussed in detail and calculations for sample cases included. The importance of including the physical processes identified as important earlier is thus emphasized. Chapter Seven develops a Monte Carlo dispersion model for atmospheric dispersion studies. The disadvantages of this method, compared to others which have been used, are indicated.

The mountain airflow and Monte Carlo dispersion models are combined to study seeding concentrations at orographic cloud base for several atmospheric conditions in Chapter Eight. Finally, in Chapter Nine a summary of this work and its primary conclusions are given. A brief discussion of the further work that needs to be done is included.

CHAPTER TWO

REVIEW OF AIRFLOW AND DISPERSION IN MOUNTAINOUS TERRAIN

2.1 Airflow in Mountainous Terrain

Mountains affect all scales of atmospheric motion. On the hemispheric scale they play a role in anchoring the long waves. On the synoptic scale the lee of mountain ranges are favored locations for cyclogenesis. Of primary concern here are smaller scales of motion. On the mesoscale, mountain forced wind systems are quite predominant. Even on the microscale strong effects of the rough surface and presence of turbulent wakes to the lee of terrain irregularities are manifest.

Mountains interact with other atmospheric environmental conditions to affect flow in two ways. Firstly, they act as a physical barrier to the airflow. The predominant airstream is forced to find a way over or around a topographic barrier, or it may be entirely blocked establishing a pressure gradient such that the airflow is locally completely stopped or even turned around. This interaction may be thought of as the pure adiabatic (sometimes called mechanical) type. The second type involves diabatic forcings. Mountains act as elevated sources (and sinks) of heat and to a lesser extent moisture. They also act as elevated friction sources. Usually these two types of forcing are confounded and it is difficult to establish their relative role in any particular situation.

Adiabatic forcing is perhaps the easier to treat theoretically and there is considerable history of observation of these phenomena. The energetics of the flow and topographic situation determine the partition between horizontal and vertical flow deviation.

Horizontal deviation of the wind results in the phenomena of "gap winds". The flow is locally strengthened and canalized. Figure 2.1 shows this feature for a potential flow situation (frictionless, incompressible, adiabatic, no coriolis acceleration) in the vicinity of two model mountains. For this case, with no vertical deviation allowed at all, the strengthening of the wind, as portrayed by the streamlines, is quite marked. A good example of this type of situation occurs with the "Mistral", a northerly flow of winter and early spring, which is intensified in the gap between the Alps and Cevennes. Similar strong winds are observed at Gibralter and at the large mountain gaps and passes of central Asia. In North America the "Chinook" wind appearing along the lee of the Rocky Mountains is often strengthened in geographically favored locations by gaps in the mountain range.

Where horizontal deviation of the flow is not energetically favored, such as for a long mountain ridge orientated normal to the prevailing large-scale flow, vertical deviation may occur. Figure 2.2 shows a potential flow for such a situation. A wind maximum occurs at the ridge crest. It should be remembered that no constraint of zero wind at the mountain surface has been imposed. Imposing this constraint would shift the wind maximum above the surface.

Observations of such vertical deviation are commonplace. Birds and glider pilots often take advantage of orographic uplift. Strong winds above the tops of mountain ridges are often observed by aircraft attempting to fly over them. The architecture of plants on mountain ridges is frequently dominated by the flow. Indirect evidence is afforded by the mean precipitation pattern in the vicinity of a mountain barrier. As an example, figure 2.3 shows the considerable enhancement

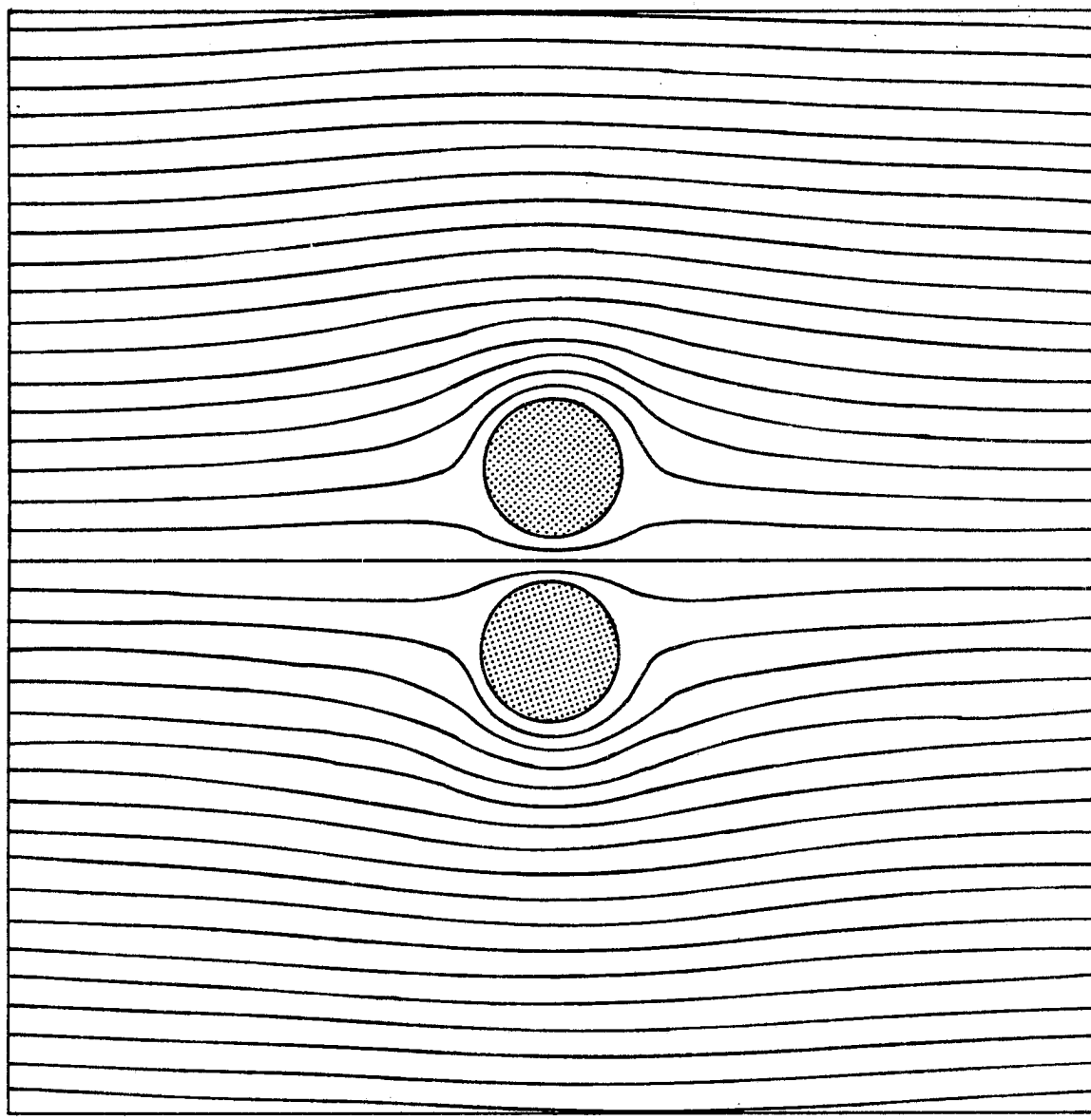

Figure 2.1. Potential flow for horizontal deviations in the vicinity of two mountains.

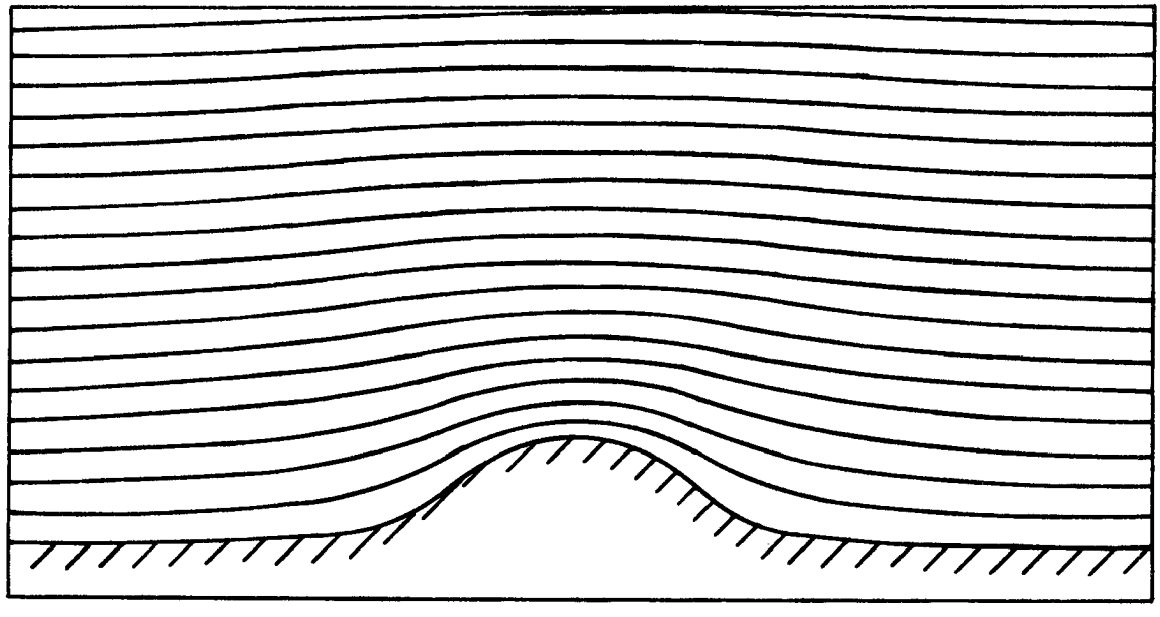

Figure 2.2. Potential flow over an isolated mountain ridge.

upwind and "rain shadow" effect downwind caused by the Rocky Mountains in Colorado.

Where the stratification of the air approaching the barrier is different from neutral a considerable difference in the flow over the ridge may be expected. For example:

1. If the low level air is stably stratified the kinetic energy of the flow may be dissipated before the air can rise over the barrier. This situation is called blocking.
2. If a stable layer is found somewhat above ridge crest the airflow above the crest can be considerably strengthened as air is forced between the crest and stable layer. It is this type of situation which gives rise to the lee slope wind storms (Chinooks) in the Rocky Mountain region.

A simplified model to account for the effects of stratification on flow over a long ridge has been proposed by Myers (1962).

An additional feature associated with vertical displacement of the air flowing over a mountain barrier, which has received considerable study, is the lee wave and associated phenomena. Figure 2.4 shows typical features diagramatically. A good review is given by Queney et. al. (1960).

Diabatic forcings are the second type that have been identified as having an important influence on airflow in mountainous terrain. These enter in two ways: by cloud condensation effects, primarily latent heat release, and by turbulent interaction with the surface. Cloud condensation effects are examined in section 6.3.4 in detail. Because flow near the surface is of prime interest in this study, the diabatic heat transfers near the surface will be of prime interest here. Such diabatic

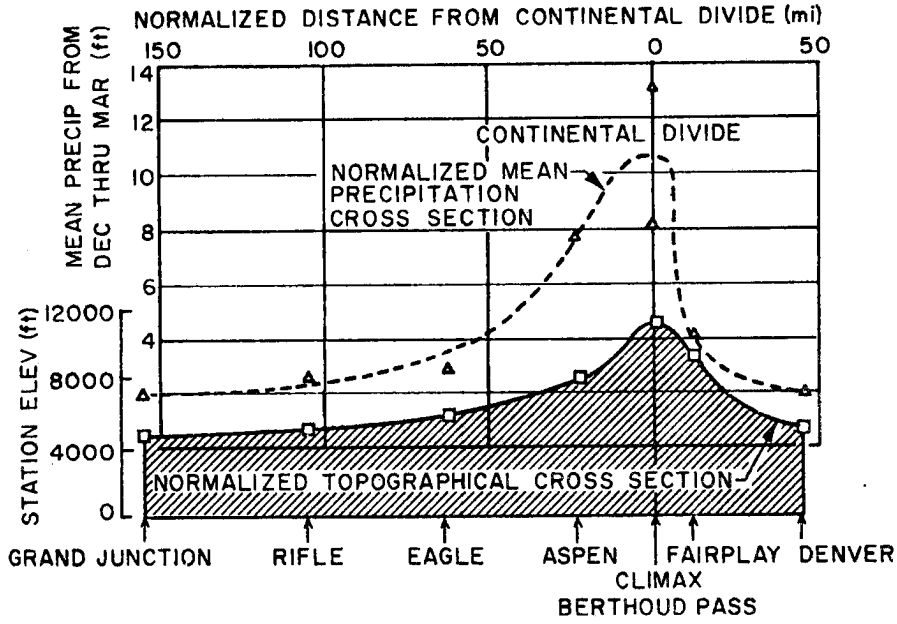

Figure 2.3. Normalized east-west cross-section of topography and mean precipitation for the central Colorado Rockies. Mean precipitation computed for period December through March (1960-1964). (After Grant and Kahan, 1974.)

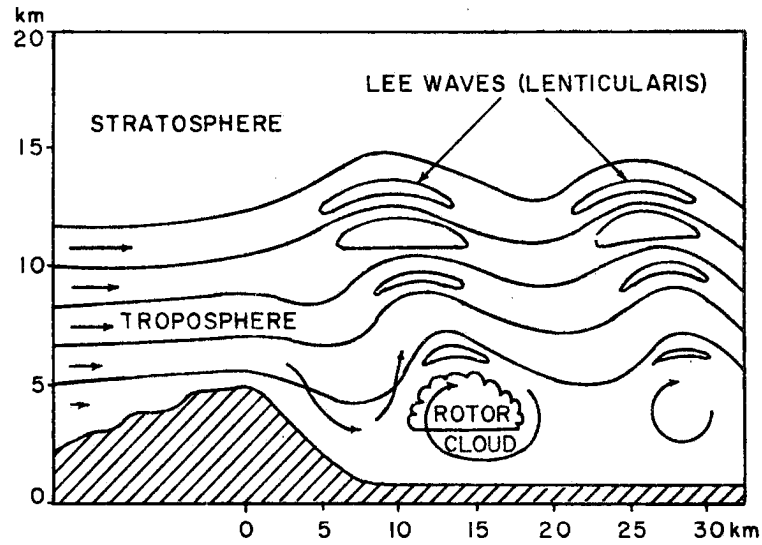

Figure 2.4. Leewaves and lenticularis clouds behind an obstacle. (After Flohn, 1970.)

effects are readily identified in the diurnal oscillations of winds in mountain valleys. Some of the early observations and theories advanced to explain them were conflicting. It appears possible to reconcile observation and theory by reference to two ways in which diabatic forcing can enter into the fundamental equations of motion. Two types of diabatically driven winds are defined, slope winds and valley winds.

Slope winds are microscale breezes which blow normal to the topographic contours, up-slope during the day and down-slope at night. Radiative cooling of a slope at night will cool the air just above it. This air becomes more dense than air which is at the same altitude but further above the slope surface. As a result the cold air slides downward along the slope to the valley floor. The reverse process occurs during the day.

In terms of the equations of motion, the origin of the motion is from the buoyancy term in the vertical equation of motion. The steady state speed of a cold current gliding down a slope of elevation angle α may be expressed, after Defant (1933),

$$U_{slope} = \left[\frac{g \bar{h} (T_c - T_E) \sin \alpha}{C_D T_c} \right]^{\frac{1}{2}}$$

where C_D is the drag coefficient, $\bar{h}$ is the mean height of the cold current and T_c and T_E the temperature of the current and environment respectively. This theory predicts that the stronger the radiation, the deeper the slope flow and the steeper the slope the stronger the flow. Some compensation can be expected between these; a steep slope would probably predicate against a deep slope flow.

Observational results appear to be in qualitative accord with this theory. The up-slope wind begins shortly after sunrise and ceases around sunset when the down-slope wind sets in. Cross (1950) found that during winter months in the Columbia River valley of British Columbia the slope wind system was quite weak. A similar observation by Jelinek (1937) in Europe was attributed to generally small vertical temperature gradients during this season, there being little heating of the slopes by the sun during the day. Further, a large part of the radiation incident is reflected by the winter snow surface. Slope wind systems are found to be more predominant during the remainder of the year.

The down-slope wind is observed to be shallow. Initially cold air drainage is in a layer only a few centimeters deep, but can increase to 20 to 50 meters quite commonly and to 200 to 400 meters over the Greenland and Antarctic ice caps. Figure 2.5 shows a typical vertical profile of down-slope wind velocity after Defant (1949). A wind maximum is found at 27m in this composite profile. Evidence from other studies, Bergen (1967), is that this maximum will frequently occur even lower, with the suggestion that the down-slope flow is normally a more shallow phenomenon than up-slope flow.

Little quantitative field study appears to have been made on the effect of the magnitude of the slope on slope winds. Bergen (loc cit) in a thorough literature review finds that generally small scale-height drainage flow is associated with steep slopes, while large scale-height flow is associated with low speeds and areas of pooling such as valley bottoms. It is found also that quite minor "microrelief" features, such as gullies and vegetative boundaries of a meter or so scale, can have considerable influence on slope flow, particularly cold air drainage.

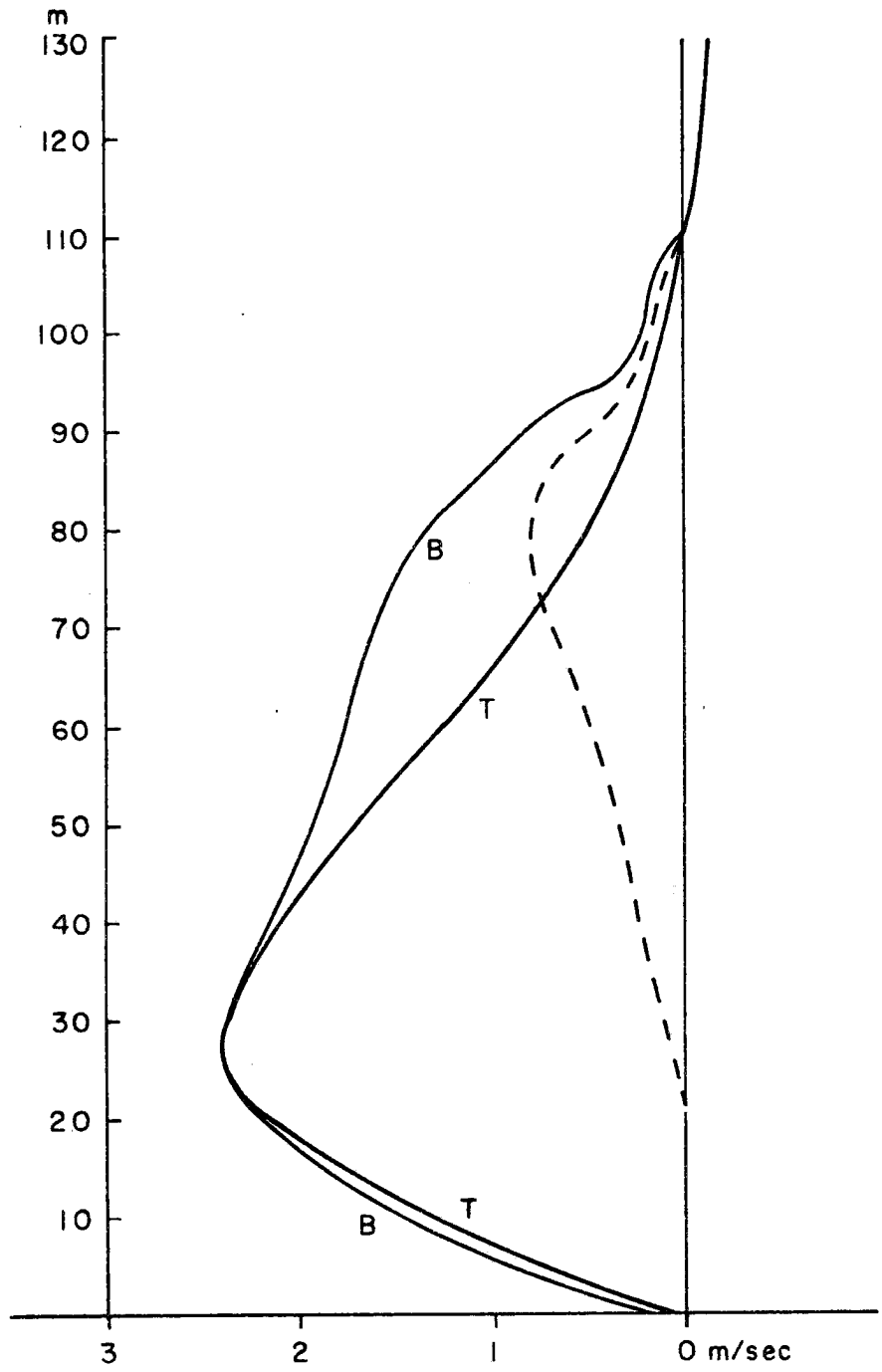

Figure 2.5. Wind profiles, normal to the slope, for downslope winds. B: - according to observation, T: - according to theory, Broken Line: - |T-B|. (After Defant, 1949.)

In reviewing the previous work it becomes clear that there is, still a considerable lack of detailed understanding of slope flow. Rather substantial fluctuations (5 to 30 minute periodicities) in these flows are commonly observed denoting a problem with the applicability of steady state theory predictions. Fluctuations can probably be traced to topographic variations on small scales. A further factor that needs to be considered in a complete treatment is the variation in time of the drag forces at the slope surface. More recent theoretical work attempts to tackle these complexities [see Benjamin (1968)].

A second type of diabatically induced wind is mesoscale valley wind. During the day the up-valley winds blow up along the main axis of the valley. The situation is reversed at night. Cross (1950) has described the mechanism as follows. "These winds result from differences in temperature between the small body of air in a valley and the much larger body of air over the adjacent plain into which the valley opens or in a wider portion of the valley downstream. On a sunny day the same amount of insolation is received on similar horizontal areas at any level over the valley and over the plain. Consider now the relative volumes of air in the columns below these given horizontal areas. It will be seen that, owing to the space occupied by the land mass which makes up the valley sides and floor, the volume of air in the column over the valley will be considerably smaller than the corresponding volume over the plain. Insolation first heats the ground which in turn warms the air above by turbulent conduction and convection. As the same amount of heat is added to the small volume of air over the valley and the large volume over the plain, the temperature of the valley air becomes progressively greater than that of the air over the plain. As

this happens the pressure of the air in the valley decreases relative to that of the air at the same level over the plain, resulting in the development of a local pressure gradient. In response to the resulting pressure gradient force there is a flow of air from the plain toward and up the valley." Similar arguments can be followed to explain the down-valley wind.

In terms of the equations of motion the valley wind results from changes in the horizontal pressure gradient terms. Horizontal pressure gradients are formed by differential heating and hydrostatic adjustments of air columns inside and outside the mountain valley.

Observations show that valley winds are much better developed in winter than slope winds. The diurnal up-valley wind starts, almost simultaneously at all levels, at about the time of most rapid warming. It ceases a couple of hours after sunset to be replaced by down-valley wind. The valley wind typically fills the valley with a maximum speed, greater than that of the slope wind, at one quarter to one third of ridge height.

Of course, the slope and valley wind systems, by their nature, occur together and interact. Figure 2.6, after Defant (1949), indicates the complexity this implies. Moreover, it should go without saying that these are model wind systems and idealizations of the field situation. Varying topography, gradient wind influences, thermal advection, transient mesoscale systems embedded in the larger scale flow and many other factors will interact with these model flow systems to make any particular situation deviate from the ideal. The complexities of these interactions will only be understood by more complete (and complex) model calculations guided by more exhaustive field observations.

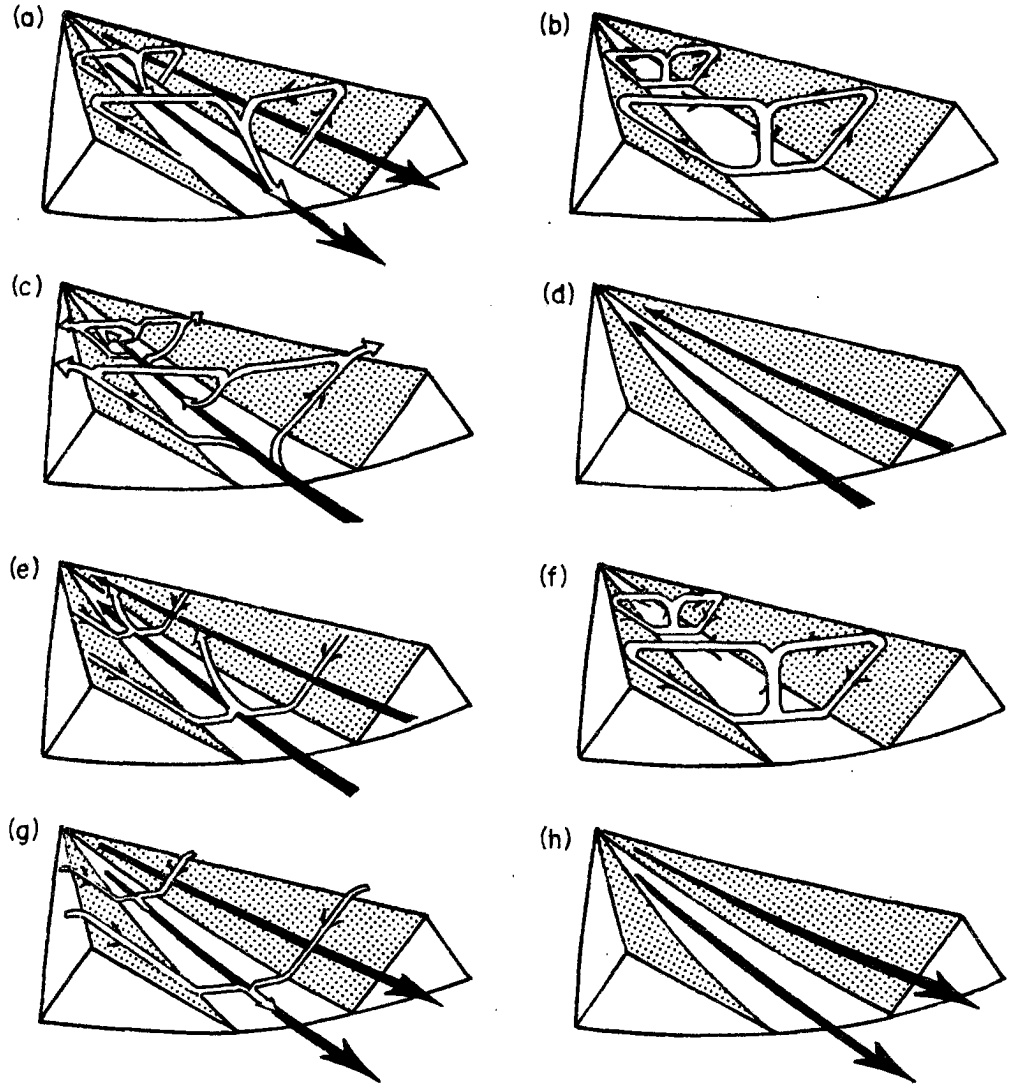

Figure 2.6. Schematic illustration of the normal diurnal variations of the air currents in a valley. (After F. Defant, 1949.)

(a) Sunrise; onset of upslope winds (white arrows), continuation of mountain wind (black arrows). Valley cold, plains warm.

(b) Forenoon (about 0900); strong slope winds, transition from mountain wind to valley wind. Valley temperature same as plains.

(c) Noon and early afternoon; diminishing slope winds, fully developed valley wind. Valley warmer than plains.

(d) Late afternoon; slope winds have ceased, valley wind continues. Valley continues warmer than plains.

(e) Evening; onset of downslope winds, diminishing valley wind. Valley only slightly warmer than plains.

(f) Early night; well-developed downslope winds, transition from valley wind to mountain wind. Valley and plains at same temperature.

(g) Middle of night; downslope winds continue, mountain wind fully developed. Valley colder than plains.

(h) Late night to morning; downslope winds have ceased, mountain wind fills valley. Valley colder than plains.

2.2 Dispersion in Mountainous Terrain

Atmospheric dispersion is the name given to the process by which dilution of concentration of contaminant occurs. It may profitably be thought of as a process increasing the mean separation of contaminant particles while conserving the total mass of contaminant in the air.

From an engineering standpoint standard formulations for estimating contaminant concentrations, primarily the "Gaussian plume model", have been derived empirically from observation. They are applicable only in simple situtations (flat terrain, spacial and temporal uniformity of winds). While estimates so derived may be helpful for short range transport-dispersion within open mountainous areas, in general this formulation will not be useful here.

A simple model which has found application in mountain areas is the box model. The details of the transport-dispersion are ignored and a gross concentration is calculated based on total contaminant released divided by the volume of air containing it. In the case of a mountain valley this volume is given by the topography of the valley defining the sides and bottom of the box and the height of an impenetrable inversion defining the top. Temporal variation is given by the accumulation of emissions, variation of the inversion height and a crude ventilation effect. The deficiencies of this model are obvious and include limited applicability and particularly lack of any spacial resolution.

More comprehensively formulated models for predicting pollutant concentration have been attempted. These will be discussed in a later section. In practical circumstances tracer studies are resorted to because of the lack of development of the sufficiently sophisticated models.

The amount of quantitative information obtained on the mechanisms of dispersion in mountainous terrain from tracer studies is rather disappointing. These studies have largely been financed by companies interested in the practical problem of whether a proposed development would meet pollution standards rather than to learn more about dispersion physics. Some interesting qualitative and semi-quantitative results of general applicability do seem to recur.

1. The strong diabatic influence on the transport is frequently mentioned, Start et al. (1974), Smith (1968), Kao et al. (1974).
2. Low level inversions strongly restricting dispersion appear enhanced in frequency in mountain valleys. This is confirmed, within the limits imposed by the radiosonde network, by the inversion climatology of Hosler (1961).
3. Pollutants are found to be strongly constrained in mountain valleys, Smith (1968). This might be deduced from the previous two items.
4. Horizontal dispersion is stronger in mountain valleys than over flat terrain up until the constraining influence of the valley walls is felt. Hovind et al. (1974) claim that in rugged mountain canyons the "average dispersion power" is enhanced tenfold. The effect is attributed to terrain induced mechanical turbulence not necessarily reflected in the vertical temperature profiles. Start et al. (1974) reported for an inversion condition in Huntington Canyon, Utah, that axial concentrations are 15 times less than would be predicted by the Pasquill-Gifford version of the Gaussian plume model.

In the remainder of this section the background to two methods for calculating dispersion are outlined. The observational base used in employing these methods for mountainous terrain is discussed.

The equation of continuity for mass of a passive contaminant for incompressible flow may be written using Cartesian tensor notation

$$\frac{\partial C}{\partial t} = -\bar{u}_i \frac{\partial C}{\partial x_i} - \frac{\partial}{\partial x_i} (\overline{u_i' C'}) + Q - S$$

where C is the ensemble mean concentration, $\bar{u}_i$ the mean wind, u_i' and C' are deviations from these means, Q represents sources and S sinks of contaminant. Molecular diffusion has been neglected as its effect is generally quite insignificant. The divergence of the fluctuation product term is intractable. The thrust to overcome this difficulty has led to parameterization of this term by analogy between the turbulent transport it represents and Fickian molecular diffusion. The continuity equation is then written

$$\frac{\partial C}{\partial t} = -\bar{u}_i \frac{\partial C}{\partial x_i} + \frac{\partial}{\partial x_i} (K_{ij} \frac{\partial C}{\partial x_j}) + Q - S$$

Calder (1965) has pointed out that in general all nine elements of the K tensor need to be specified as functions of space and time for the formulation to be strictly valid. In practice a coordinate system is defined conforming to the local mean wind field and only the three main diagonal elements used. Even so, many theoretical and practical deficiencies remain in this formulation, [see Scorer (1972), Lettau (1967), and Reid (1974)]. The qualitative success in simple cases and simplicity of formulation motivate continued application of this parameterization.

Experimental evidence on the spacial variation of K in mountainous terrain is extremely limited and conflicting. Figure 2.7 from dual release balloon data taken during slightly stable winter conditions in the Eagle River Valley of Colorado lends support to all three components of K increasing as height scaled by mean ridge height for regions below ridge top. Figure 2.8 shows data obtained by a similar technique in Cache Valley in Utah during the month of September. These data, although showing considerable scatter, also suggest K_y and K_z increasing exponentially with height. The coefficient K_x shows a decrease with height, the reverse of that found in the Colorado study. Some additional boundary conditions that might be inferred are that the K's should go to zero at the surface as the turbulent fluctuations vanish, and that above the mountains the K's will revert to small values because away from the surface the mechanical, and in unstable situations buoyant, sources of turbulence are less prevalent.

A second method of calculating dispersion requires a closer examination of the dispersion mechanism.

Any sufficiently small and neutrally charged particle in the atmosphere will exactly follow the wind down to the smallest scale. It is commonly observed that the wind fluctuates on a variety of scales. Thus two particles released from different points in space-time phase space will follow different trajectories. For a situation in which winds are fluctuating about some mean value, two particles initially related closely in phase space will tend to diverge owing primarily to the action of fluctuations with wavelength near twice that of the two particles separation.

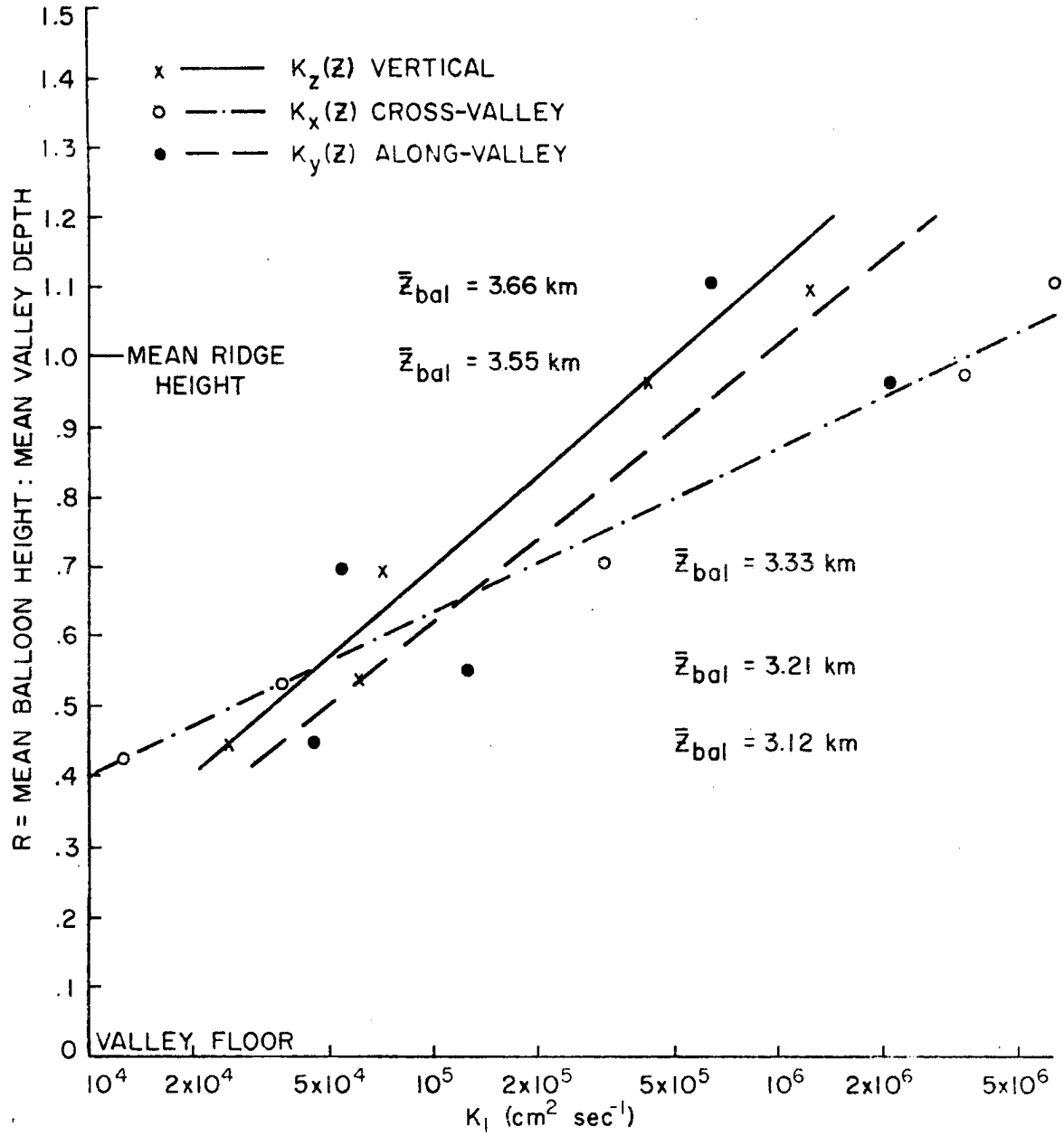

Figure 2.7. Vertical variation of Eddy diffusivity as a function of height scaled by mean ridge height. (After Wooldridge and Lewis, 1975.)

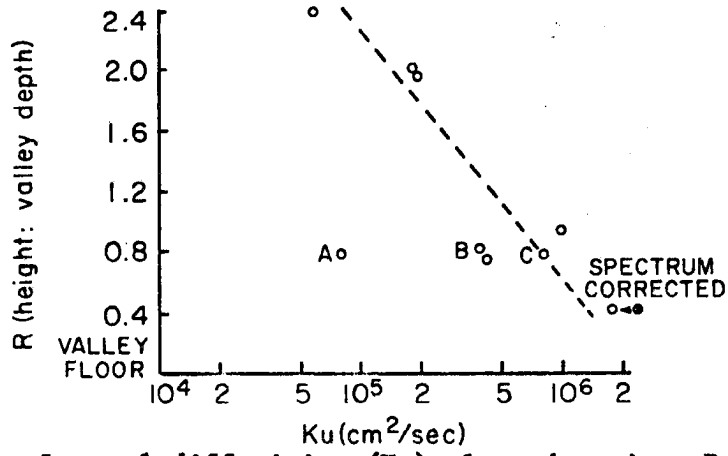

Figure 2.8a. Lateral diffusivity (K_u) plotted against R for constant volume balloon pairs released from Cache Valley. A, B and C represent pairs released on September 15, 1972.

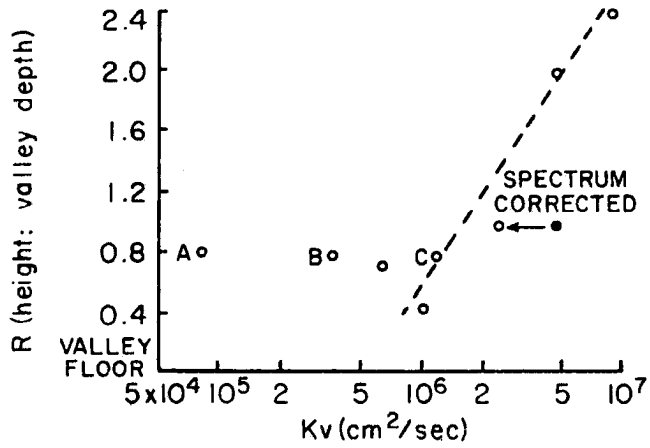

Figure 2.8b. Longitudinal diffusivity (K_v) plotted against R for constant volume balloon pairs released from Cache Valley. A, B and C represent pairs released on September 15, 1972.

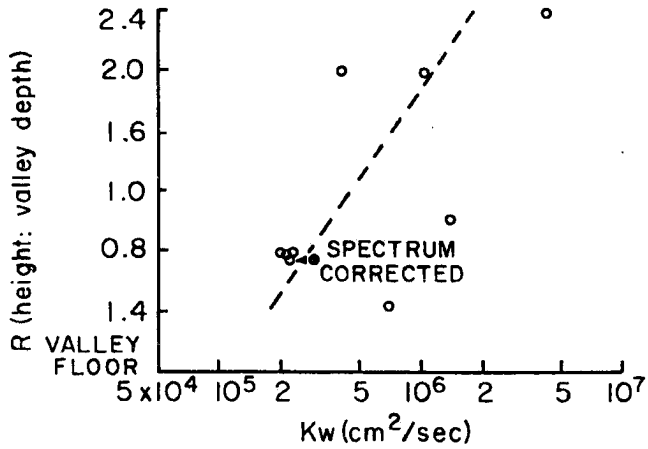

Figure 2.8c. Vertical diffusivity (K_w) plotted against R for constant volume balloon pairs released from Cache Valley. (After Wooldridge, 1974.)

For an ensemble of like particles released, this divergence will manifest itself at a certain time after release as a dispersion of the particles about some center of mass. The mean displacement defines the mean wind. The scatter of particles about their center of mass is controlled by the turbulence of the wind. It is clear that to understand and predict the dispersion of the particles it is necessary to understand at least some aspects of turbulence. This statistical approach to dispersion was pioneered by G. I. Taylor in his famous paper of 1921.

Sutton (1949) defines turbulence as a state of fluid flow "in which instantaneous velocities exhibit irregular and apparently random fluctuations so that in practice only statistical properties can be recognized and subject to analysis". Lumley and Panofsky (1964) list some essential features of turbulence: a three-dimensional continuum fluid phenomenon; rotational, dissipative, non-linear, stochastic, and diffusive with transport occuring at time and length scales typically the same as those of the properties being transported.

Classically, turbulence theory has been formulated for stationary turbulence. Here the lowest frequency in the turbulence spectrum is much shorter than the time over which the statistical properties are accumulated. Unfortunately, for atmospheric turbulence this is not the case. Figure 2.9 shows that the spectrum of kinetic energy in the atmosphere is continuous up to the planetary scales of motion. Thus no obvious natural separation of mean and turbulent wind components is found in our atmosphere. The idea of turbulent fluctuations about an ensemble mean is not strictly applicable in this situation, but studies

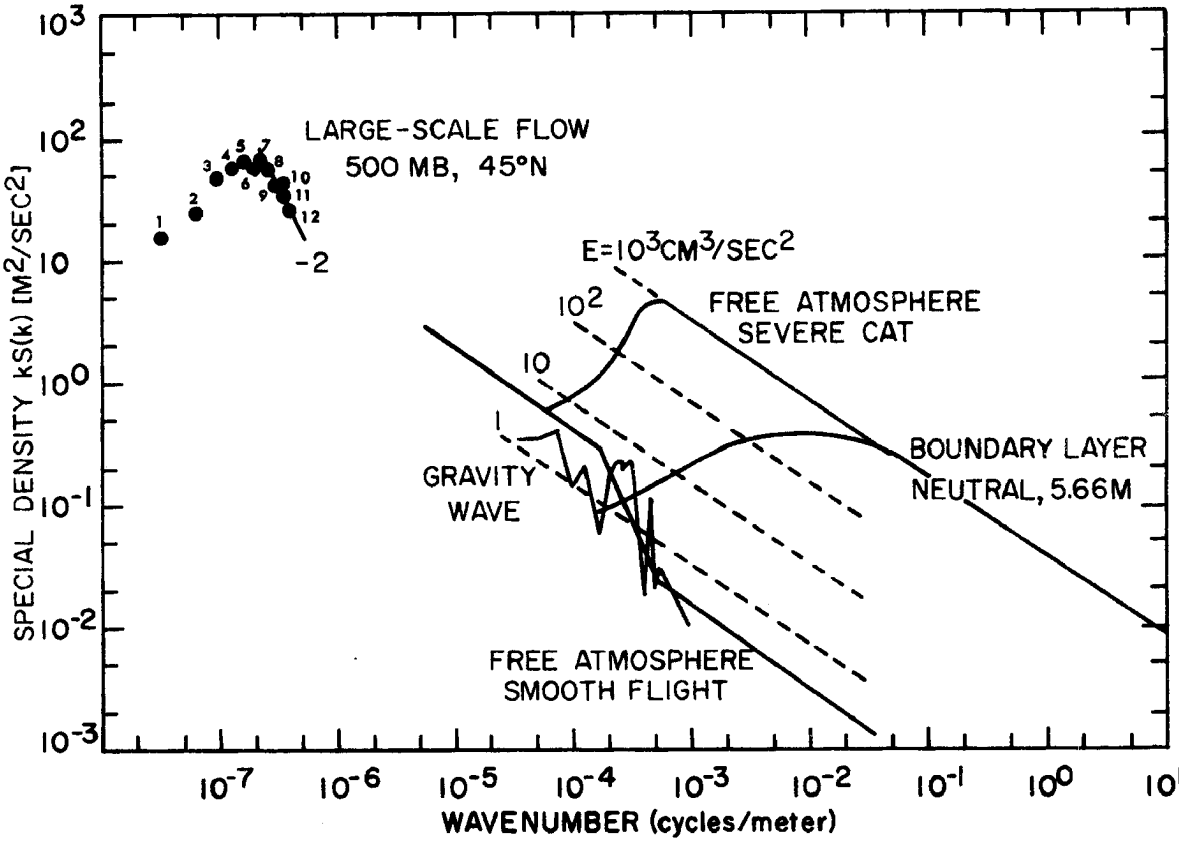

Figure 2.9. The spectrum of kinetic energy in the atmosphere. (After Dutton in Vinnichenko et al., 1973.)

are normally conducted in situations where a local minimum exists to separate "mean" and "turbulent" winds.

Taylor (1921) showed that for one-dimensional diffusion within a homogeneous turbulence field

$$\sigma^2_{x_i}(t) = 2\,\overline{u_i'^2} \int_0^t \int_0^\varepsilon R_L(\tau)\, d\tau\, d\varepsilon$$

where $\sigma^2_{x_i}$ is the mean squared displacement of particles diffused about the center of mass after time t and $R_L(\tau)$ is the Langrangian time correlation between turbulent velocities of a typical particle at times separated by τ. Kampé de Fériet (1939) has shown an equivalent formulation is

$$\sigma^2_{x_i}(t) = 2\,\overline{u_i'^2} \int_0^t (t - \tau)\, R_L(\tau)\, d\tau$$

Hay and Pasquill (1959) suggest that the Langrangian and Eulerian (fixed in space) time correlations can be related by

$$R_L(\tau) = R_E(\kappa) \quad \text{where} \quad \tau = \beta\kappa$$

Applying the Wiener-Khintchine theorem

$$\sigma^2_{x_i}(t) = \overline{u_i'^2}\; t^2 \int_0^\infty F_E(n) \left[\frac{\sin \pi n t/\beta}{\pi n t/\beta}\right]^2 dn$$

where $F_E(n)$ is the Eulerian spectrum function and n is wavenumber. This expression is valid when all turbulence scales contributing to $\overline{u_i'^2}$ are covered by the duration of release. A number of analytic functions have been used to describe $F_E(n)$. Typical is the von-Kármán spectrum given by

$$S_i(k) = \overline{u_i'^2}\; 4\, L_{u_i} / [1 + 70.78\, L^2_{u_i}\, k^2]^{5/6}$$

for longitudinal, and

$$S_i(k) = \overline{u_i'^2}\, L_{u_i} [2 + 377.5\, L_{u_i}^2\, k^2]/[1 + 70.78\, L_{u_i}^2\, k^2]^{11/6}$$

for lateral and vertical fluctuation spectra. This simplifies the problem in that it describes the effect of turbulence on dispersion in terms of only three parameters of the tubulence, $\overline{u_i'^2}$, L_{u_i}, and β for each of the three coordinate directions.

Pasquill (1962) reviews the experimental data on the β parameter. He concludes that a good average value is four. He also shows that the effect of a moderate error on the dispersion variance is rather small. Panofsky and Mizuno (1974) tentatively conclude that β decreases with increasing roughness and decreasing stability. From data taken over smooth Nebraska terrain they find $\beta = 4.5$ in near neutral conditions and $\beta = 2$ in unstable air. No investigations of β variations appear to exist for mountainous terrain.

Basic data to determine the variation of the turbulence parameters in mountainous terrain is extremely scarce. One excellent study has been made, the LO-LOCAT atmospheric turbulence study. This was undertaken to determine the turbulent environment below 1000ft above ground for a wide variety of conditions. The data were collected for aircraft design purposes. Extensive summaries, Gunter et al. (1969) and Jones et al. (1970) have been published. Unfortunately the turbulence parameters were expressed in a coordinate frame fixed with respect to the aircraft heading instead of following the mean wind direction as is common in atmospheric turbulence studies. The effect of this on the statistics is uncertain. Burns and Rider (1965) show changes in the cross-correlation between vertical and lateral turbulent velocities depending upon the

angle of heading relative to the wind direction. Lenschow (1970) found in an unstable boundary layer that the convective plumes contributed differently to turbulence statistics flying along and across the wind. Data from a wind conforming subset of the LO-LOCAT data are discussed and employed in Chapter Eight to parameterize turbulence scale lengths and velocity variances.

One additional property of the turbulent velocity distribution, which will be useful later, is its Gaussian nature. For the LO-LOCAT data set approximately 87 percent of the vertical, 88 percent of the longitudinal and 89 percent of the lateral turbulent velocity distributions sampled were accepted as Gaussian, using a Chi-square test, at the 0.02 level of significance. This means that in most cases the variance of the distribution completely specifies the distribution.

CHAPTER THREE

COLD OROGRAPHIC CLOUD MODIFICATION

Bergeron (1949) was the first to point out the potential of orographic clouds as candidates for precipitation augmentation by cloud seeding. Ludlam (1955) carried out calculations to demonstrate the efficacy of seeding such clouds with ice nuclei. Encouraged by the promise shown by these calculations Grant and co-workers at Colorado State University have performed a long series of randomized experiments, the Climax experiments, to field test this seeding.

In this chapter, after a brief review of the theory of cold orographic cloud seeding, statistical examination of data from the Climax experiments is performed to investigate whether low level transport and dispersion significantly influenced the results at Climax.

3.1 Outline of Cold Orographic Cloud Modification Theory

Almost casual observation of natural orographic clouds is sufficient to convince one that, as precipitation producers, these are often rather inefficient systems. Water droplets form as air rises over a mountain barrier and becomes saturated. Because these drops are small they frequently fail to fall to the ground, but pass over the barrier and evaporate in the subsiding, warming air to the lee of the barrier. The objective in modifying these clouds is to promote the growth of larger precipitation particles within the cloud which can fall to the surface during the short time available as they pass over the mountain barrier. This can be achieved by taking advantage of the Bergeron-Findieson mechanism whereby when ice crystals and supercooled water droplets coexist in a cloud the crystals tend to grow by diffusion while

the droplets evaporate. The modification is initiated by introducing artificial ice nuclei into the cloud.

Figure 3.1 illustrates schematically a typical chain of events culminating in enhanced precipitation. A typical artificial ice nucleus is generated and released at a site considerably upwind of the mountain barrier at time zero. It moves with the wind and turbulence until, at time t_1, it finds its way into the orographic cloud. Here, all the time moving with the wind, it nucleates an ice crystal which grows by diffusion and in some cases accretion and, accumulating mass, begins to fall. Growth and settling continue until it leaves cloud base at time t_2. Below cloud base it may sublime, settling to the surface at time t_3 if it has survived. Of course, it may be that the mountain surface is in direct contact with the cloud in which case times t_2 and t_3 are the same.

The time for each of these stages will be strongly dependent on the individual situation. Time t_1 will depend on plume rise at the generator, the total wind regime, and the height of cloud base. The additional time to t_2 will depend on the trajectory the particle follows as it moves through the cloud, is activated, grows and falls. Nucleation and growth are temperature and supersaturation dependent. Ludlam (loc cit) estimated optimal seeding concentrations would be 10 to 100 IN per liter and that overseeding could decrease precipitation. For the final stage of the process the important factors determining its duration will be height of cloud base above the ground, the crystal terminal velocity and sub-cloud wind field.

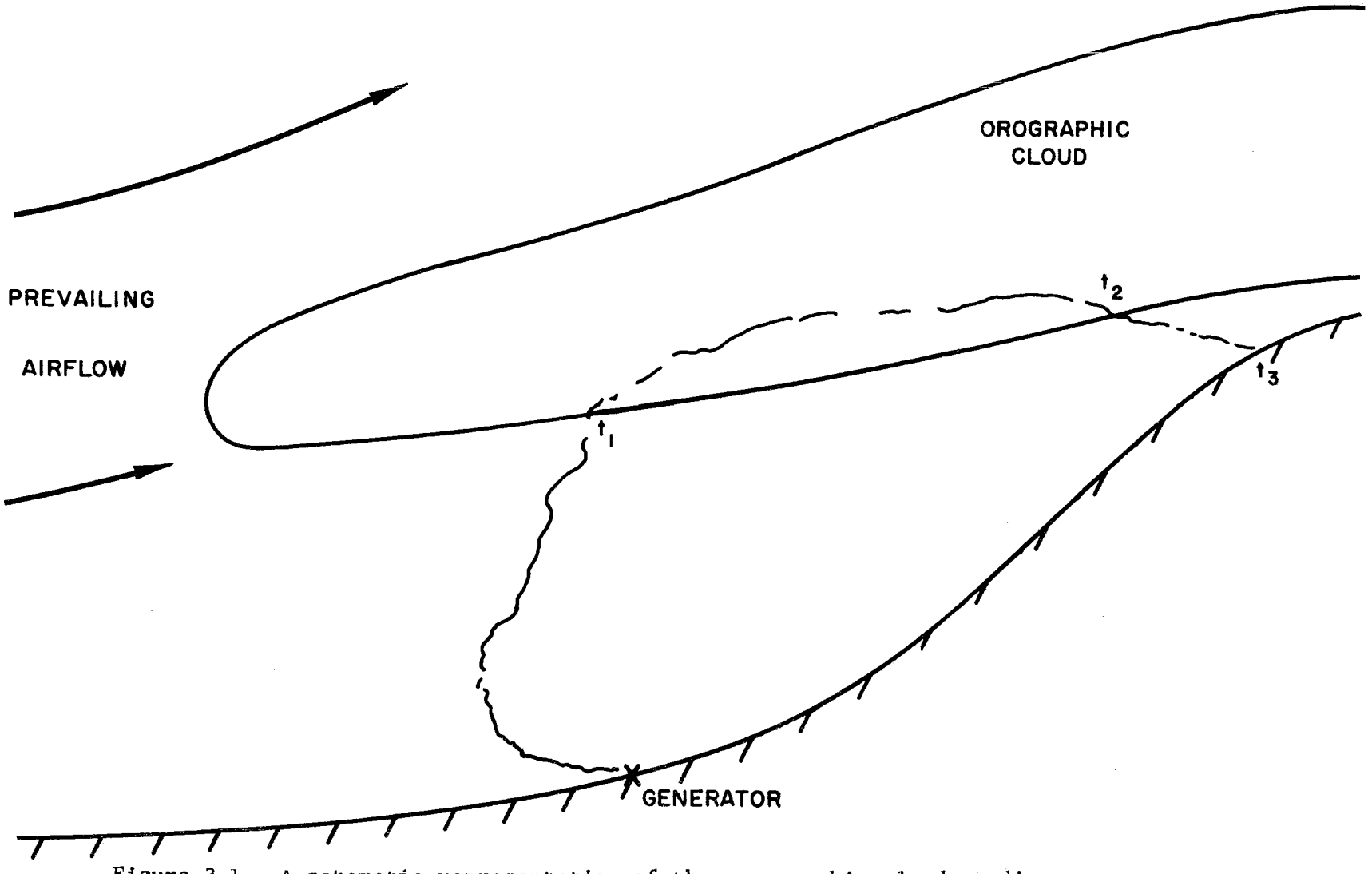

Figure 3.1. A schematic representation of the orographic cloud seeding process.

It is clear that in total this modification is a complex process and it would be difficult to predict a priori the result of any particular seeding.

3.2 Review of Statistical Results from the Climax Experiments

One method to obtain information on the major physical controls in this modification is to perform randomized experiments to search for factors correlated with any seeding effect noted. Of many such experiments the most definitive is the Climax experiment which has been summarized by Grant et al. (1971) and Grant and Kahan (1974). Tables 3.1, 3.2 and 3.3 show that 500 mb (near cloud top) temperature, 700 mb wind direction and 700 mb wind speed were critical parameters determining the effect of seeding for the Climax situation. One obvious conclusion is that, at least in some situations, seeding agent released near the ground is transported into and interacts with the orographic cloud.

Table 3.1 shows significant precipitation increases with seeding for 500 mb temperature warmer than -20°C and decreases indicated for temperatures colder than -27°C. Grant and Elliott (1974) examined the influence of cloud top temperature on seeding efficacy for a number of orographic seeding experiments. They show, figure 3.2, that for seven such experiments precipitation increases with seeding are found when the cloud top temperature is in the range -10°C to -24°C. The lack of effect at warm temperatures is attributed to the inefficiency of the artificial ice nucleant employed at these high temperatures. At cold temperatures the natural cloud processes are already efficient so that seeding has no effect. For cloud top temperature in the window region of -10°C to -24°C the natural ice nuclei available for diffusional growth are frequently insufficient to fully utilize the available

	A -20 to -11°C	B -26 to -21°C	C -39 to -27°C
Climax I	1.85 (.206)	0.97 (.436)	0.78 (.041)
Climax II B	1.74 (.034)	1.28 (.230)	1.18 (.732)
Total Sample	1.75 (.045)	1.10 (.350)	0.89 (.150)

Table 3.1. Ratios of Seeded to Nonseeded Mean Precipitation Amounts (Wilcoxon Statistic One-sided ρ-Values): A and B for Increases, C for a Decrease for 500-mb., Temperature Partitions (Climax I-251 Experimental Units, Climax IIB-296 Experimental Units, Climax I and Climax IIB Combined-547 Experimental Units).

	A 190 to 250°	B 260 to 300°	C 310 to 360°	D 10 to 180°
Climax I	1.94 (.031)	0.85 (.863)	1.41 (.095)	0.72 (.218)
Climax II B	2.27 (0.13)	1.06 (.508)	1.84 (0.28)	0.83 (.520)
Total Sample	2.08 (.004)	.92 (.800)	1.54 (.024)	0.77 (.360)

Table 3.2. Ratios of Seeded to Nonseeded Mean Precipitation Amounts (Wilcoxon Statistic One-Sided ρ-Values): A, B, C for Increases, D for Decreases for 700-mb Wind Direction Partitions Climax I-251 Experimental Units, Climax IIB-296 Experimental Units, Climax I and Climax IIB Combined-547 Experimental Units).

	A 0 to 8 m/sec	B 9 to 11 m/sec	C 12 to 14 m/sec	D 15 to 28 m/sec
Climax I	1.08 (.460)	1.24 (.236)	1.44 (.043)	0.73 (.093)
Climax II B	0.99 (.568)	1.17 (.367)	3.02 (<.001)	0.87 (.278)
Total Sample	1.03 (.600)	1.23 (.300)	1.90 (<.001)	0.70 (.13)

Table 3.3. Ratios of Seeded to Nonseeded Mean Precipitation Amounts (Wilcoxon Statistic One-Sided ρ-Values): A, B, C for Increases, D for Decreases for 700-mb Wind Velocity Partition (Climax I-251 Experimental Units, Climax IIB-296 Experimental Units, Climax I and Climax IIB Combined-547 Experimental Units).

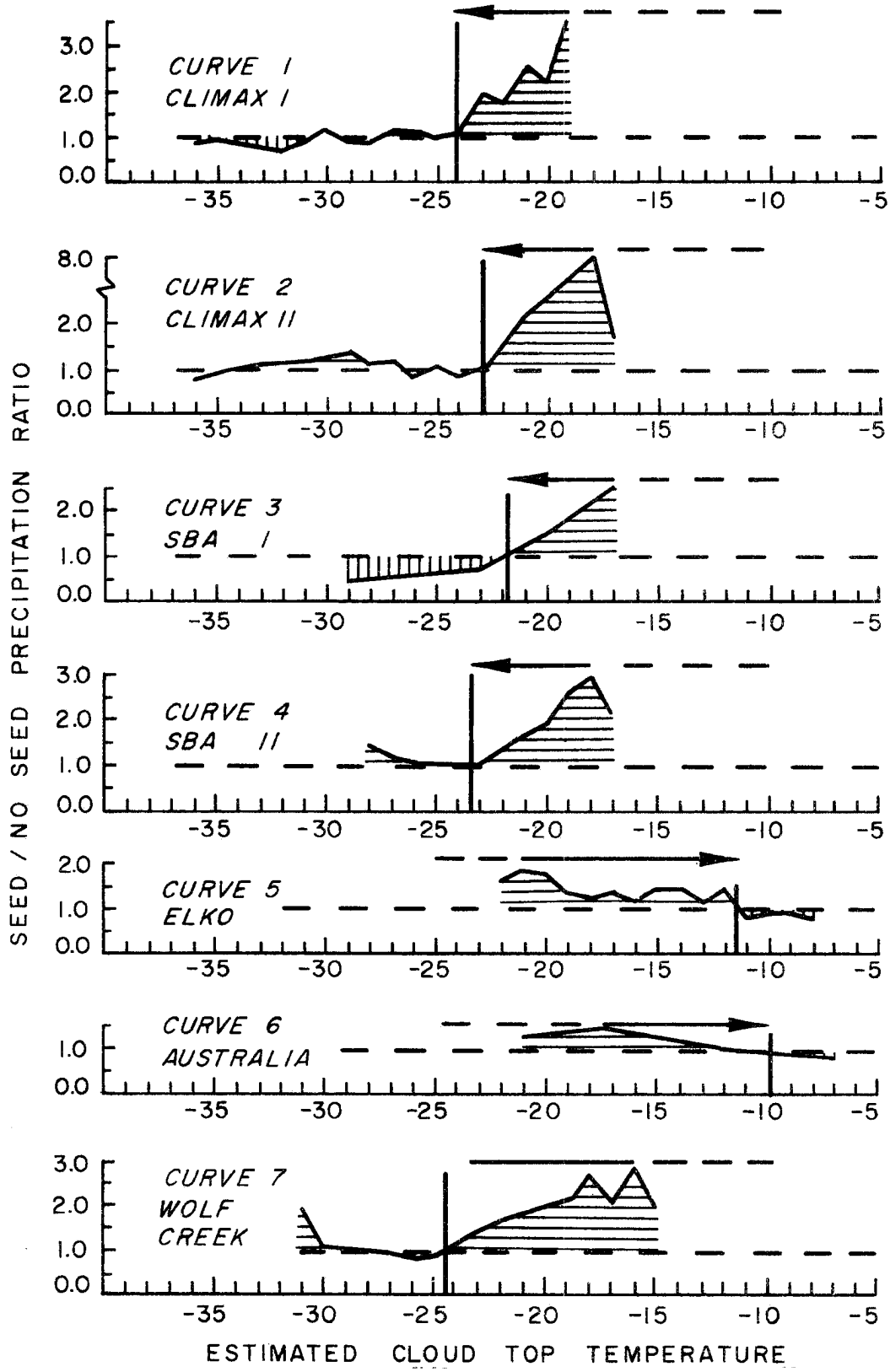

Figure 3.2. Comparative seed/no seed precipitation ratios as related to estimated cloud-top temperatures for seven seeding experiments. (After Grant and Elliott, 1974.)

moisture. Seeding increases the precipitation by increasing the nuclei available for diffusional growth.

The wind direction stratification of table 3.2 shows another good indication that seeding was effective. Relative to the target, the direction that generators were placed corresponded to wind directions showing precipitation modification.

Wind speed is the last critical parameter investigated. Significant precipitation increases for seeded cases occur for 700 mb wind speeds of 12 to 14 mps. For higher wind speeds the indication is that seeding decreases snowfall. It is noteworthy that the increases observed for moderate wind speeds are the most significant result of any of the stratifications shown.

3.3 Further Results from the Climax Experiments

To further unravel the effects of these meteorological parameters a triple stratification of the Climax data is shown in table 3.4. As might be expected, for warm 500 mb temperatures and wind speeds 12 to 14 mps highly significant target area precipitation increases are found with seeding. For higher wind speeds there are indications of decreases.

For northwesterly airflow cases and light winds significant precipitation decreases are found for both temperature classes. By contrast for southwest flow cases of low speed and warm temperature significant precipitation increases are found. This behavior for low wind speeds has not previously been found. The result suggests that there is a feature, as yet unresolved, of the seeding which is primarily effective only at low wind speeds and which is direction dependent.

To further investigate this effect the data for the triple stratifications of table 3.4 are examined in terms of precipitation efficiency,

WIND SPEED CATEGORY	NORTHWESTERLY FLOW WARM	NORTHWESTERLY FLOW COLD	SOUTHWESTERLY FLOW WARM	SOUTHWESTERLY FLOW COLD
v7 < 8 mps	0.52 (.015)	0.44 (.012)*	1.57 (0.38)	0.91 (.397)
8≤ v7 <11	1.23 (.215)	1.28 (.316)*	1.44 (.119)*	0.69 (.119)*
11≤ v7< 14	1.25 (.020)	1.07 (.488)*	1.94 (.012)*	1.09 (.129)*
14≤ v7	0.60 (.062)*	0.99 (.363)*	2.46 (.236)*	- *

Table 3.4: Ratio of Seeded to Non-Seeded Cases Precipitation Amounts at Climax and Wilcoxon Statistic one-sided probability value for a Triple Stratification of the Climax Experiment Data Set. Northwesterly Flow refers to 500 mb wind direction 290° to 360° inclusive. Southwesterly Flow refers to 500 mb wind direction 190° to 289° inclusive. Warm refers to 500 mb temperature greater than -25°C, cold to colder than or equal to -25°C. Data is stratified according to the 700 mb windspeed categories shown in column one. Asterisks indicate classes having less than 10 non-zero seed and no-seed cases.

700 MB WIND SPEED RANGE	NORTHWEST 500 MB FLOW				SOUTHWEST 500 MB FLOW			
	500 MB TEMPS WARM		500 MB TEMPS COLD		500 MB TEMPS WARM		500 MB TEMPS COLD	
	NO SEED	SEED	NO SEED	SEED	NO SEED	SEED	NO SEED	SEED
0 - 8	.028 (26)	.016 (14)	.024 (15)	.013 (5)	.024 (44)	.041 (50)	.035 (23)	.031 (17)
9 - 11	.023 (21)	.029 (19)	.011 (5)	.013 (9)	.013 (10)	.022 (18)	.015 (7)	.012 (9)
12 - 14	.016 (11)	.019 (12)	.012 (6)	.013 (5)	.012 (12)	.020 (18)	.013 (1)	.016 (3)
>14	.019 (6)	.010 (8)	.012 (2)	.012 (4)	.013 (9)	.028 (3)	- (0)	- (0)

Table 3.5: Triple stratification for Climax Precipitation Efficiencies (24 hour precipitation in inches divided by 700 mb windspeed in mps) and number of precipitation occurrences for each stratification. For remaining definitions see table 3.4.

precipitation divided by 700 mb wind speed, so factoring out the effect of wind speed on the condensate supply rate. The resulting average precipitation efficiencies are shown in table 3.5. It should be noted that the effect of warmer temperature air having greater moisture has not been compensated for. The table shows a dominant trend for higher efficiencies for low wind speeds than for higher wind speeds. Although this may be partly explained in that for light winds synoptic scale lifting effects will account for a larger proportion of the precipitation than in the stronger wind cases, nevertheless the evidence is clear that seeding decreases these high efficiencies, except for warm southwest wind cases.

The above observations are consistent with low wind cases being naturally efficient because ice crystals nucleated by abundant natural ice nuclei at high levels have a considerable time to fall to the surface before passing over the barrier crest. In warm cases such ice crystals produced at high levels collect moisture from the lower levels as they fall to the surface. In these low wind cases seeding produces an overabundance of ice crystals which, competing for the available moisture, grow only to much smaller size. Because in northwesterly flow the distance from the seeding site to the barrier crest is quite short the smaller crystals produced from seeding do not have sufficient terminal velocity to fall to the surface before passing over the ridge. By contrast, in southwesterly low speed warm cases the precipitation naturally falls short of the target. Seeding, by making smaller crystals allows these to be transported further, falling to the target. Overall these results are consistent with the role of seeding in low

wind speed cases being to overseed the cloud producing smaller crystals and a spacial redistribution of precipitation.

For moderate wind speeds (8 to 14 mps) the trend is for considerable increases with seeding for warm cases but only marginal changes for cold cases. Moreover the efficiencies are low compared to the low wind cases for these wind speed stratifications.

Consistent with the above observations one may hypothesize that these moderate wind situations produce precipitation at the target only from the lowest layers of the cloud. Most of the moisture fails to attain sufficient fall to impact the surface before being carried over the barrier. In seeding the lowest layers, for which the precipitation process is quite inefficient at warm temperatures, the efficiency is increased by presence of additional ice nuclei. At colder temperatures, for which the natural process is more efficient at the lower levels, the seeding effect depends on the trade-off between increasing the number of ice nuclei and decreasing the crystal size because of competition. The effect of seeding is then only a small effect.

Interpreting the above in terms of the primary concern in this work, the transport and dispersion of the seeding agent from a ground based generator site to the orographic cloud, it is clear that the situation is highly dependent on wind speed. For low winds the location of the target site relative to the seeding location is critical. The Climax experiment may have overseeded the cloud in low wind situations. For stronger winds the seeding site appears to be not as critical, although there is a suggestion that longer trajectories are more favorable to a seeding effect.

3.4 Diurnal Effects of Seeding

Throughout the ten years of the Climax experiment a recording precipitation gauge was in operation at Climax 2NW (HA0), so that hourly precipitation amounts are available at this site, which is near the target. In this section these data are used to investigate the variation of seeding effect with time of day for various stratifications of the meteorological parameters. It is worth emphasizing that the statistical evaluations used in this analysis are stricly post hoc, and thus the statistical significance is only a qualitative indicator of the effect. Also, for many of the stratifications the sample sizes are small. Trends are noted in what follows only when a succession of hours showing the same tendency are evident, and even this indicator should be treated with some caution as there is at least a moderate serial correlation in the precipitation record. Successive precipitation hours show a linear correlation in precipitation amount of 0.45 based on a limited sample of the data.

Taking the data set as a whole, without stratification except by hour of the day, twenty hours show precipitation increases correlated with seeding. During six of these hours the increases are twenty percent or greater while only one hour of the remaining four hours shows a decrease of more than ten percent.

Stratifications based on a single meteorological parameter show the most significant effects for the 700 mb wind speed category 12 to 14 mps. Twenty-two of the twenty-four hours show precipitation increases, eighteen of these hours having better than five percent confidence levels. The hours between 1000 and 1500 MST show least effect and least confidence levels. Lower wind speed categories show no significant

effect while stronger wind speeds indicate precipitation decreases for nineteen of the twenty-four hours, however, the significance level is not great. For a single stratification based on wind direction, southwesterly airflow shows precipitation increases correlated with seeding exceeding the five percent significance level for ten of the twelve hours from 2100 to 0900 MST and for all the remaining hours but without statistical significance. By contrast, for northwesterly airflow seventeen hours of the twenty-four show decreases. The only other single stratification showing a persistent effect is warm 500 mb temperatures with precipitation increases indicated for twenty-one of the twenty-four hours.

Table 3.6 presents the results of a triple stratification by meteorological parameters for the hourly data for the low wind speed cases (less than 9 mps). The sample sizes are too small to draw any conclusions regarding the northwest airflow cases, although the predominant trend is for precipitation decreases with seeding. Similarly for cold southwesterly airflow the sample size is too small to draw any conclusions. With warm southwest airflow, except for four hours of the day, the trend is for precipitation increases with seeding. In particular the hours between 2000 and 0400 MST show increases in excess of thirty percent. The hours showing precipitation decreases are around sunset and sunrise.

The triple stratification for moderate winds (9 to 14 mps inclusive) is shown in table 3.7. Again, for the cold 500 mb temperature cases the sample sizes are too small to be meaningful. Sample sizes are also fairly small for the warm southwesterly flow cases, but strong precipitation increases are indicated for most hours. Particularly

HOUR INTERVAL	NORTHWEST								SOUTHWEST							
	WARM				COLD				WARM				COLD			
09 - 10	.826	1	2	.44		0	2		2.146	1	8	.07	.714	2	6	.40
10 - 11		2	0			2	0		2.318	4	7	.19	3.074	4	5	.18
11 - NOON	.343	3	1	.34		0	0		2.625	5	8	.18	.748	4	4	.33
NOON - 13	.282	3	1	.24		2	0		1.968	5	6	.37	.510	5	3	.38
13 - 14	1.200	6	3	.32		1	0		1.169	6	7	.41	.571	5	3	.35
14 - 15	.563	6	2	.16		2	0		2.031	6	10	.13	1.905	5	4	.32
15 - 16	.626	6	2	.17		1	0		1.440	9	11	.29	.909	5	4	.40
16 - 17	.429	6	2	.15	2.167	1	1	.28	.908	12	14	.38	.821	7	8	.28
17 - 18	.357	7	2	.11	.179	3	1	.34	1.233	12	14	.39	.917	6	5	.32
18 - 19	.204	9	1	.02	.359	3	2	.41	.747	8	15	.11	.698	6	4	.47
19 - 20	.745	8	3	.17	.467	3	1	.39	2.151	7	9	.31	1.571	5	3	.48
20 - 21	.823	11	3	.05	.289	5	1	.20	6.000	8	12	.14	1.141	7	5	.43
21 - 22	.739	9	1	.03		2	0		5.948	5	14	.01	1.141	3	5	.31
22 - 23	.824	9	3	.14		2	0		2.544	6	14	.03	1.257	4	3	.43
23 - 00	.621	10	3	.10		5	0		1.315	4	10	.06	.838	5	4	.46
00 - 01	.337	13	3	.02	.191	4	1	.15	2.393	5	8	.21	1.333	7	5	.44
01 - 02	.423	11	4	.10	.191	5	1	.09	1.408	9	12	.29	.963	8	7	.42
02 - 03	.308	10	3	.07		4	0		1.411	11	17	.13	1.969	7	8	.09
03 - 04	.234	12	5	.05		6	0		2.090	10	17	.08	1.790	8	7	.19
04 - 05	.129	9	2	.04		4	0		1.182	9	12	.29	2.031	5	5	.28
05 - 06	.067	7	1	.04		2	0		1.218	5	7	.30	5.250	2	5	.04
06 - 07	.329	4	2	.32		3	0		.957	4	4	.48		0	2	
07 - 08		5	0			1	0		.538	4	5	.44		0	3	
08 - 09	.110	6	1	.07		2	0		1.074	7	10	.28		0	4	

Table 3.6. Statistics on seeding effect for low windspeed cases (700mb windspeed less than 9 mps) as a function of time of day (MS (MST). For definition of categories see table 3.4. Statistics tabulated are ratio of seeded cases to non-seeded cases precipitating, number of non-seeded cases precipitating, number of seeded cases precipitating and probability of such a ratio being achieved by chance.

HOUR INTERVAL	NORTHWEST								SOUTHWEST							
	WARM				COLD				WARM				COLD			
09 - 10	1.25	6	13	.30		0	4			0	4			0	2	
10 - 11	1.37	9	7	.50	.35	3	3	.27		0	1		.64	1	1	.37
11 - NOON	1.15	9	9	.35	1.83	2	3	.38		0	4			0	0	
NOON - 13	.97	11	12	.24	.94	3	4	.47	10.60	1	5	.06		0	0	
13 - 14	1.00	12	12	.32	1.96	2	6	.12		0	6		4.67	1	2	.39
14 - 15	.76	13	11	.50	3.40	2	7	.05	9.69	1	5	.06	1.62	2	2	.33
15 - 16	.74	11	12	.33		0	4		2.41	2	8	.04	2.96	1	2	.43
16 - 17	1.09	12	11	.37	4.00	2	5	.14	3.29	2	9	.03	1.17	2	4	.42
17 - 18	1.22	14	8	.20	2.57	2	4	.21	12.80	1	7	.03	1.33	1	4	.18
18 - 19	.63	13	6	.09	1.71	2	3	.35	1.96	4	9	.15	1.07	1	4	.20
19 - 20	.73	10	11	.35	10.29	1	4	.08	1.60	3	11	.03	1.00	1	3	.25
20 - 21	.87	11	13	.30	4.71	2	4	.20	3.64	5	14	.03	.80	2	4	.36
21 - 22	1.61	8	16	.01	2.60	2	4	.20	2.92	6	14	.05	.80	1	5	.09
22 - 23	1.04	13	12	.43	1.01	4	4	.43	1.16	5	12	.10	.46	2	2	.31
23 - 24	1.01	11	10	.48	.62	2	3	.41	4.18	4	15	.01	.16	2	1	.19
00 - 01	2.41	11	13	.11	.74	4	3	.29	2.09	5	15	.04	.61	3	4	.37
01 - 02	1.36	13	15	.20	1.21	4	5	.41	2.75	5	21	.00	1.02	4	5	.40
02 - 03	1.08	14	17	.14	.60	6	5	.24	3.07	7	19	.01	.99	4	5	.23
03 - 04	1.05	17	15	.42	.87	5	5	.29	1.86	6	20	.01	.70	3	3	.30
04 - 05	1.04	14	14	.41	1.64	5	5	.48	4.86	4	17	.00	.30	4	2	.09
05 - 06	1.23	16	9	.20	.87	4	2	.15	4.11	4	19	.00		2	0	
06 - 07	.72	8	9	.35	.35	3	1	.12	9.98	2	15	.00	.16	2	1	.19
07 - 08	1.11	8	9	.32	.87	2	1	.26	27.13	1	12	.00		0	0	
08 - 09	.64	7	8	.43	1.60	1	1	.46		0	13		.16	2	1	.13

Table 3.7. Same as table 3.6 except for moderate windspeed cases (700 mb windspeed between 9 mps and 14 mps inclusive).

notable is the high number of seeded hours precipitating compared to non-seeded hours precipitating although the number of experimental hours in each category was about the same. No such behavior is evident for warm northwesterly flow situations and although the sample sizes are quite large here the significance levels are unspectacular.

For strong winds the sample sizes are too small to warrant presentation of the triple stratifications.

In summary, hourly precipitation data for a site near the Climax target region show, in general, the same seeding effects as seen for daily data. The only notable diurnal variation between precipitation for seeded and non-seeded cases is that for wind speeds 12 to 14 mps significant precipitation increases with seeding are seen throughout most of the day, except that the hours from 1000 to 1500 MST show no significant effect. The major factor contributing to this result is that the warm northwesterly flow cases showing little seeding effect are predominant contributors to the 12 to 14 mps stratification during these hours around noon.

CHAPTER FOUR

THE FIELD EXPERIMENTAL PROGRAM

4.1 Area of Study

Figure 4.1 shows the major topographic features of the area of the study. Upstream from its junction with the Colorado River, the Eagle River runs with Highway 24 in a E-W orientated valley which turns NW-SE further upstream. Running through the towns of Minturn and Redcliff the river is in a deep valley which widens into Camp Hale (2800m) south of Redcliff. The mountains around this area are some of the highest in Colorado rising to over 4200m. The mountain ranges run generally N-S. Figure 4.2 shows the immediate area of concern in greater detail. Upstream of Camp Hale the Eagle River divides around the major barrier complex of Taylor Hill and Chicago Ridge. These rise over 1000m above Camp Hale. One branch of the Eagle, the South, ascends to the Continental Divide near Tennessee Pass (3177m); the other, the East Branch, meets the Divide near Freemont Pass (3444m). Close to Freemont Pass is the CSU Chalk Mountain Observatory (3662m). At the northern base of Chalk Mountain is the High Altitude Observatory (HAO). Treeline is at about 3500m with conifers being the primary tree type.

4.2 Surface Based Instrumentation

Studies conducted during the Climax randomized seeding experiments have led to the gradual installation of a modest surface based observation network. This includes hygrothermographs, precipitation gauges and anemometers. This is a climatological network in that it is designed for continuous operation. For this study the anemometer network was supplemented to give more intensive coverage. Anemometer locations are

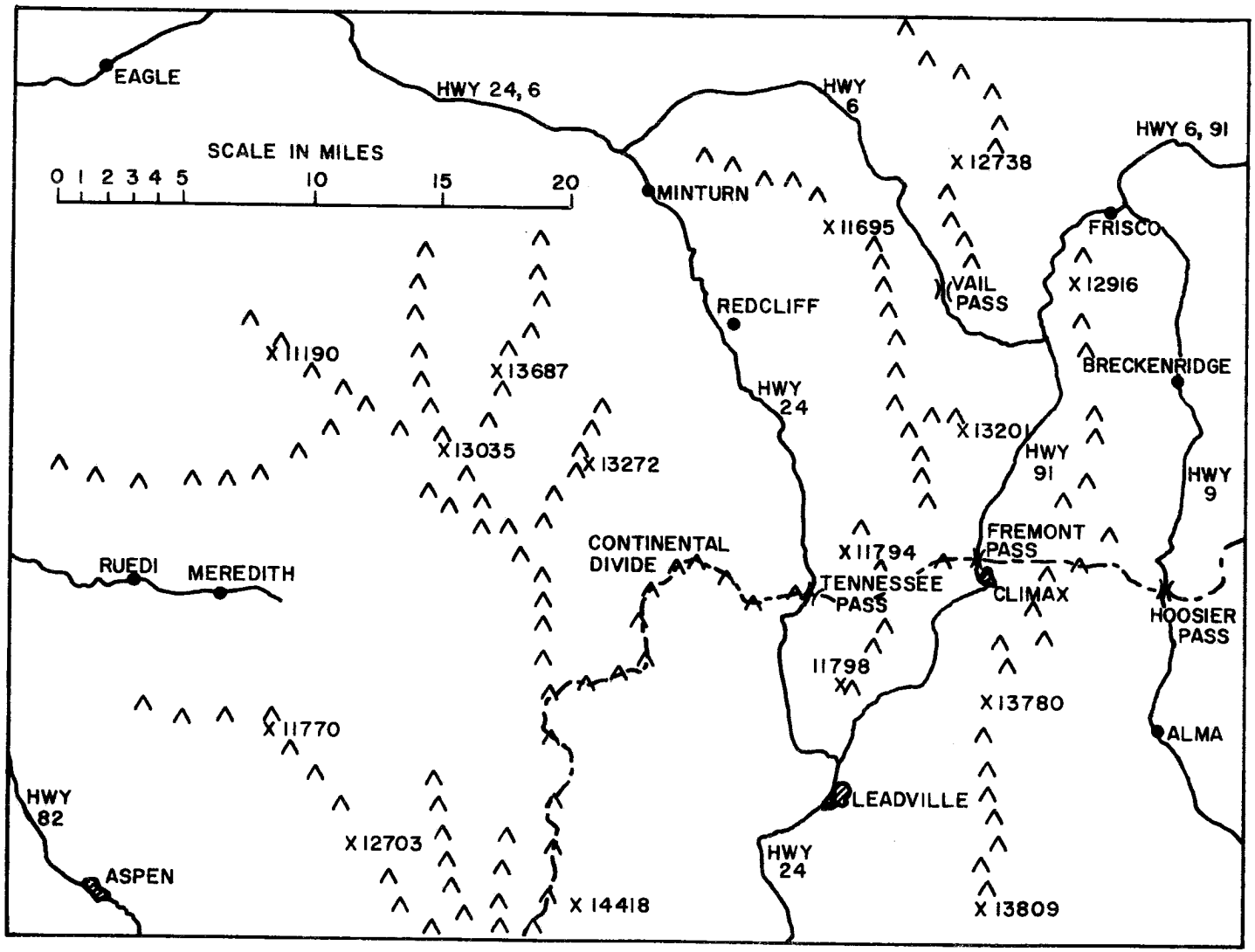

Figure 4.1. Climax experimental area showing major topographic features of the area of study.

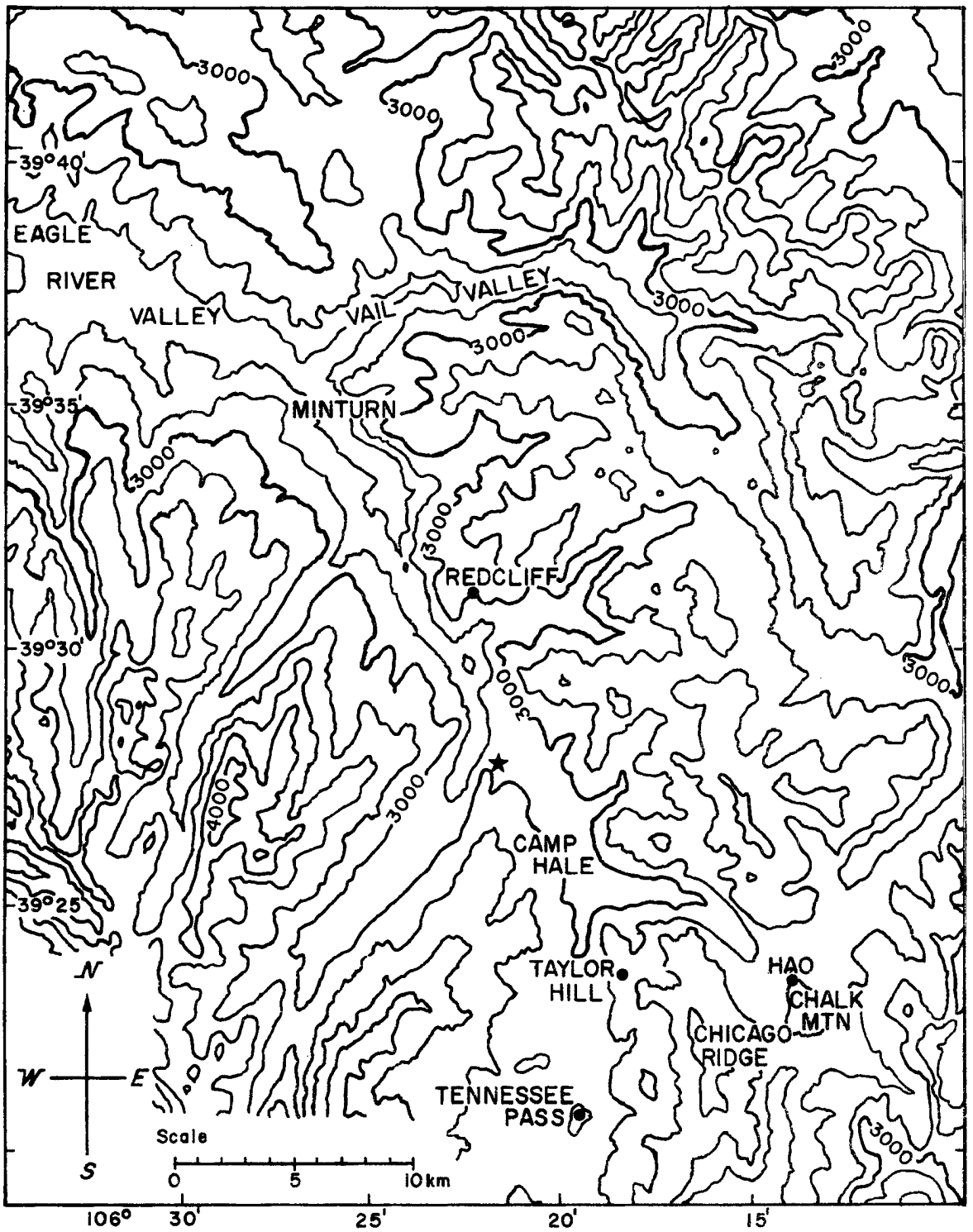

Figure 4.2. Major Topographic Features of the Immediate Area of Concern. ★ is location of S Bend Experimental Site.

listed in table 4.1. It was intended that data be collected throughout the winter months but logistical problems connected with the severity of the environment reduced the data set to a rather small part of the potential set. It is clear that for efficient operation such instrumentation in this type of environment requires extraordinary attention.

Anemometer data was recorded by pen and ink recorders on strip charts powered with clockwork drives. Inking problems and malfunction of the drive mechanisms were the main causes of data loss. A variety of anemometer types were employed (being the only ones available) and mounted on 10m towers. A few sites had up to 20m towers to minimize extraordinary sheltering effects. Strip charts were changed every two weeks. Data were normally abstracted every hour, when a data quality check showed it to be reliable, for mean wind speed and direction. For periods of special interest data for shorter time periods, as short as 10 minutes, were abstracted. Hygrothermograph data were similarly treated.

Two periods of intensive study were undertaken. The first such period was during December 1973. Conventional radiosonde ascents were taken from Chalk Mountain and S Bend Corner (see fig. 4.2). Pibals were released from Camp Hale and followed with dual theodolites. Data from these two sources were abstracted later at CSU. A "silver iodide" ice nucleus generator was operated at the S Bend radiosonde site. CSU ice nuclei counters were operated at the HAO and Chalk Mountain sites. Attempts were made to monitor ice nuclei with a mobile Mee counter. Also an acoustic sounder was evaluated for field serviceability and utility in such conditions.

LOCATION	LATITUDE (N)	LONGITUDE	ALTITUDE (meters)
TAYLOR RIDGE	39°24'16"	106°18'00"	3400
CAMP HALE	39°27'10"	106°19'42"	2800
GRAVEL PIT	39°27'48"	106°20'56"	2800
CATARACT CREEK	39°25'13"	106°16'24"	2900
SOUTH CAMP HALE	39°25'30"	106°19'45"	2800
S BEND	39°28'13"	106°21'31"	2700
JOHNS	39°22'54"	106°19'24"	3100
TOP CHALK	39°22'31"	106°12'23"	3700
TENNESSEE PASS	39°22'04"	106°18'45"	3200
TOP CHICAGO	39°22'54"	106°15'42"	3700
HAO	39°23'00"	106°12'29"	3400

Table 4.1. Anemometer sites and altitudes.

Additional intensive studies undertaken during the winter 1974-75 required fewer ground personnel. A "silver iodide" ice nucleus generator was operated and the two surface ice nucleus counters at HAO and Chalk Mountain activated. Radiosonde ascents from Chalk Mountain were made.

4.3 Airborne Instrumentation

The vast majority of the information collected during the fieldwork was obtained by aircraft observations. NCAR Queenair N306D was used during the intensive study periods. Details of this aircraft and its equipment may be found in NCAR (1973). In brief, the Queenair is a twin-prop craft with 1000nm cruising range, with a flight ceiling of 30,000ft. and a slow flight speed of 110 knots. Table 4.2 lists the conventional instrumentation aboard the Queenair for the 1973-74 season and performance characteristics. Data obtained from this instrumentation are recorded digitally during flight on ARIS (Aircraft Recording Instrumentation System). In addition an NCAR acoustical ice nucleus counter was employed. This instumentation is all rather routinely flown on the Queenair. Maintenance and calibration is by the NCAR Research Aviation Facility. After computer processing and incorporating calibrations, data from each sensor at one second intervals are available. Thus, for instruments with fast response, the slow flight speed available permits spacial resolution of about 60m.

The NCAR acoustical IN counter has been described by Langer et al. (1967). Tests of the system show an average time delay of thirty seconds, although delays of only 23 seconds occur when sudden large concentrations are encountered. Concentrations in IN/liter are recorded on a "Rustrak" analog chart system permitting convenient recording of 1

PARAMETER	INSTRUMENT TYPE	MANUFACTURER AND MODEL NO.	RANGE	ACCURACY	RESPONSE*
Stagnation Air Temperature	Platinum Resistance Total Temperature Probe	Rosemount Model 102E2AL	-70 to +30°C	±0.2°C	1 sec
	Platinum Resistance Reverse-Flow Total Temperature Probe	NCAR	-60 to +40°C	±0.5°C	8 to 10 sec
Moisture Content	Thermoelectric Dew-Point Hygrometer	EG&G 137-C3-S3	-50 to +50°C	±0.5°C above 0°C† ±1.0°C below 0°C	3°C/sec†
Pressure Altitude	Variable Capacitance Pressure Transducer	Rosemount Model 1301-A	300 to 1,035 mb	±1 mb†	0.025 sec†
Airspeed	Variable Capacitance Pressure Transducer	Rosemount Model 1301-B	0 to 140 m/sec	±0.14 m/sec†	0.025 sec†
Magnetic Heading	Flux-Gate Gyro Compass	Sperry Model N-1 (N304D)	0 to 360°	±1.0°	Undetermined
		Bendix C-11 (N306D)		±0.5°	Undetermined
Drift Angle and Ground Speed	Doppler Navigator	Singer-GPL Model APN-153V	0 to 500 m/sec -40 to +40°	Undetermined	Undetermined
Cloud Liquid Water	Hot-Wire Flowmeter	Johnson-Williams Model LWH	0 to 6 g/m^3	Undetermined	1.5 sec
Hydrometeor Liquid Water Content	Optical Flowmeter	NCAR	0.2 to 4.5 g/m^3	±10%	0.02 sec
Precipitation Particle Sampler	Lead Foil Impactor	NCAR	150 μm to 1 mm		
Radiometric Surface Temperature	Bolometric Radiometer (8- to 14-μm band)	Barnes Model PRT-5	-50 to +50°C	±0.5°C†	0.5 sec†
Visible Radiation	Spectral Pyranometer (280- to 2,800-μm band)	Eppley Model 2	0 to 2.5 ly/min	Unavailable	1 sec†
Thermal Mapping (N304D)	Inirared Line Scanner§	Texas Instruments Model RS-310	See article, "Airborne Infrared Imaging System"		
Weather Radar	X-Band Search Radar	RCA Model AVQ-55	0 to 45 n mi		
Photography	16-mm Time-Lapse Camera and Intervalometer	Giannini Model 111-B	0 to 16 frames/sec		

* A standard 63.2% time constant is implied unless otherwise specified.
† Manufacturer's specifications. These values may vary considerably depending on aircraft installation configuration and flight envelope.
§ This instrument is available to qualified users upon request through the National Hail Research Experiment (NHRE) at NCAR.

Table 4.2. Conventional instrumentation aboard the NCAR Queenair for the 1973-74 season. (After NCAR, 1973.)

to 10,000 counts per liter. All observations are for nuclei active at -20°C. The instumentation was calibrated at the Second International Workshop on Condensation and Ice Nuclei, Grant (1971). Measurements were shown reproducible within a factor of 10 almost 100 percent of the time. A systematic tendency to underestimate concentrations was shown and is compensated in the concentrations quoted. Langer (personnal communication) believes that the system as installed on the Queenair during December 1973 and with the calibration corrections determines IN concentrations to better than a factor 10.

For the second season a number of changes were made to the aircraft systems. The Doppler system used for wind sensing was replaced by an inertial navigation system which gave considerably enhanced data resolution and accuracy compared to that of the Doppler system. Late in the second season the wind sensing ability was again enhanced with a boom-vane system. Also for the second season arrangements were made to record the output from the IN counter on the ARIS. The analog chart was retained as a back-up. Finally, for the latter part of the 1974-75 season a radar altimeter was installed with recording on the ARIS. This gave aircraft height above ground when within 2000ft of the surface.

4.4 Aircraft Data Processing

The procedures used in processing the aircraft data were somewhat different in 1974-75 from those employed in 1973-74 because of the instrumentation differences.

During the first season ARIS data were processed by NCAR RAF to yield one second values of time, position relative to an arbitrary, but known, origin, pressure, true airspeed, ground speed, drift angle,

heading, Rosemount and Reverse flow measured temperature, wind speed and direction, PRT 5 indicated surface temperature, and liquid water content.

Examination of the indicated aircraft position, as calculated using the Doppler system at times when the aircraft was over a specific geographical location revealed a considerable accumulation of error over the course of a flight. While errors in the Doppler and airspeed sensing systems were anticipated sources of random error, an additional and significant source of systematic error was located in the compass heading. The compass appeared to stick in some circumstances. This made the validity of wind data as determined from the aircraft during the first season quite doubtful.

This error also produced errors in aircraft positioning. A crude, but satisfactory position correction was applied to reduce the error at any time to the accumulated error over about ten minutes as a maximum (and more usually about five minutes). This was achieved by examining the indicated aircraft position when the plane was over the S Bend corner site. This point was selected as it was always closely overflown. A linear time correction was applied to all positions between passages over the generator site ensuring the indicated position was always the same when the plane was known at this postition.

The position thus computed was used to determine the height of the terrain beneath the aircraft. Topographic data on an approximately 65m grid from the U.S. Topographic Data Center was employed. Despite the low level flying that was done, very few cases of topographic height apparently greater than indicated aircraft height were found. This lent confidence to the position correction.

Ice nuclei concentrations were abstracted at uniform (approximately 12 second) intervals along the flight path. Time marks on the Rustrack chart at about 15 minute intervals confirmed the uniform chart movement throughout the flights. Correction for the time delay was made and IN concentration interpolated to one second values to correspond to ARIS data. It should be noted that no allowance was made for faster response to the rapid encounter of high concentrations.

The instrumental changes during the second year eased the data processing task. Data were regularly processed by NCAR RAF to provide the following selected parameters at the specified data rates (samples per second)

Time	1	Latitude	2
Longitude	2	Ground Speed	2
Heading	16	Static Pressure	16
Rosemount Temperature	16	Reverse Flow Temperature	2
True Airspeed	16	Dew Point Temperature	2
Liquid Water Content	2	Ice Nucleus Conc.	2
Pressure Altitude	2	Aircraft Vert. Vel.	16
Aircraft Inertial Alt.	2	Aircraft Vert. Accel.	2
Wind Speed	2	Wind Direction	2
PRT 5 Surface Temp.	2	Event Markers	2
U Compt. of Wind	16	Pitot Pressure	16

The inertial position/wind sensing system proved to be considerably more reliable than the Doppler system. However, problems were encountered when the aircraft was in a turn. The system always gave increased indicated wind speed during this maneuver. Wind data obtained during turns of greater than 5° per second were rejected and replaced by a running average value from the previous few seconds. Topographic data was added to the data set based on the aircraft position. Apparent aircraft

height below terrain height was found to be rare. Ice nucleus counts were shifted forward in time to allow for the time delay in the instrument.

Full data quality control by visual inspection was employed on all case study data. Numerous errors were eliminated in this laborious but highly practical manner.

During the latter part of the second season turbulence sensing flights were made. Preliminary processing of these data revealed difficulties with the analysis. Owing to time limitations these data were not pursued further.

4.5 Experimental Design and Procedures

Based on the statistical results of the Climax experiments the following criterion was selected to specify an experimental day:

> A prevailing 500mb wind direction from 300° to 360° at greater than 5 mps.

In order to make operational flight safe an additional constraint was:

> Cloud sufficiently high (or absent) so as to permit safe VFR flying in the area of interest.

The ideal situation would have been a high-based orographic cloud in a moderate northwesterly airflow. The situations tended to be more subsident than would be desired from the orographic cloud seeding viewpoint.

A twenty-four hour decision cycle was instituted during the time the aircraft was available to the project. The probability of the next day meeting criteria was evaluated during the afternoon and evening and at about 2100 MST a go/no-go decision was made for the next day. Project personnel were informed. At this stage a no-go decision was final.

Early next morning (6-7am) a go decision was re-evaluated and if conditions remained favorable an experimental day commenced.

As soon as possible after the final go decision was made an AgI-acetone ice nucleus generator consuming 43 g of agent per hour was activated. A calibration of this generator performed by the CSU cloud simulation laboratory is shown in figure 4.3. For the first season the generator site was S Bend corner. One case study during the second season was made with the generator at a location northwest of Redcliff. It was originally anticipated that the prevailing flow would carry the seeding agent up-valley so that a steady state would be established by the time the aircraft arrived in the area between 10 and 11am.

During the first season the aircraft was flown along pre-selected tracks between ground reference points at specified altitudes above terrain. The time over each reference was noted to aid in location of the aircraft in space. Multiple passes through the area were made to delineate the plume and plume concentrations. Tracks during the first season were confined to the valley so that easily recognizable reference points could be used. It was felt that the IN would be confined to the valley. This type of track had the additional advantage that the meanders of the instantaneous plume would be smoothed out by the poor resolution of the IN counter.

Flight procedures during the second season were somewhat different. With greater positioning reliability from the inertial navigation system only part of the flight time was spent flying preselected tracks. More widespread flying in the horizontal and vertical was undertaken.

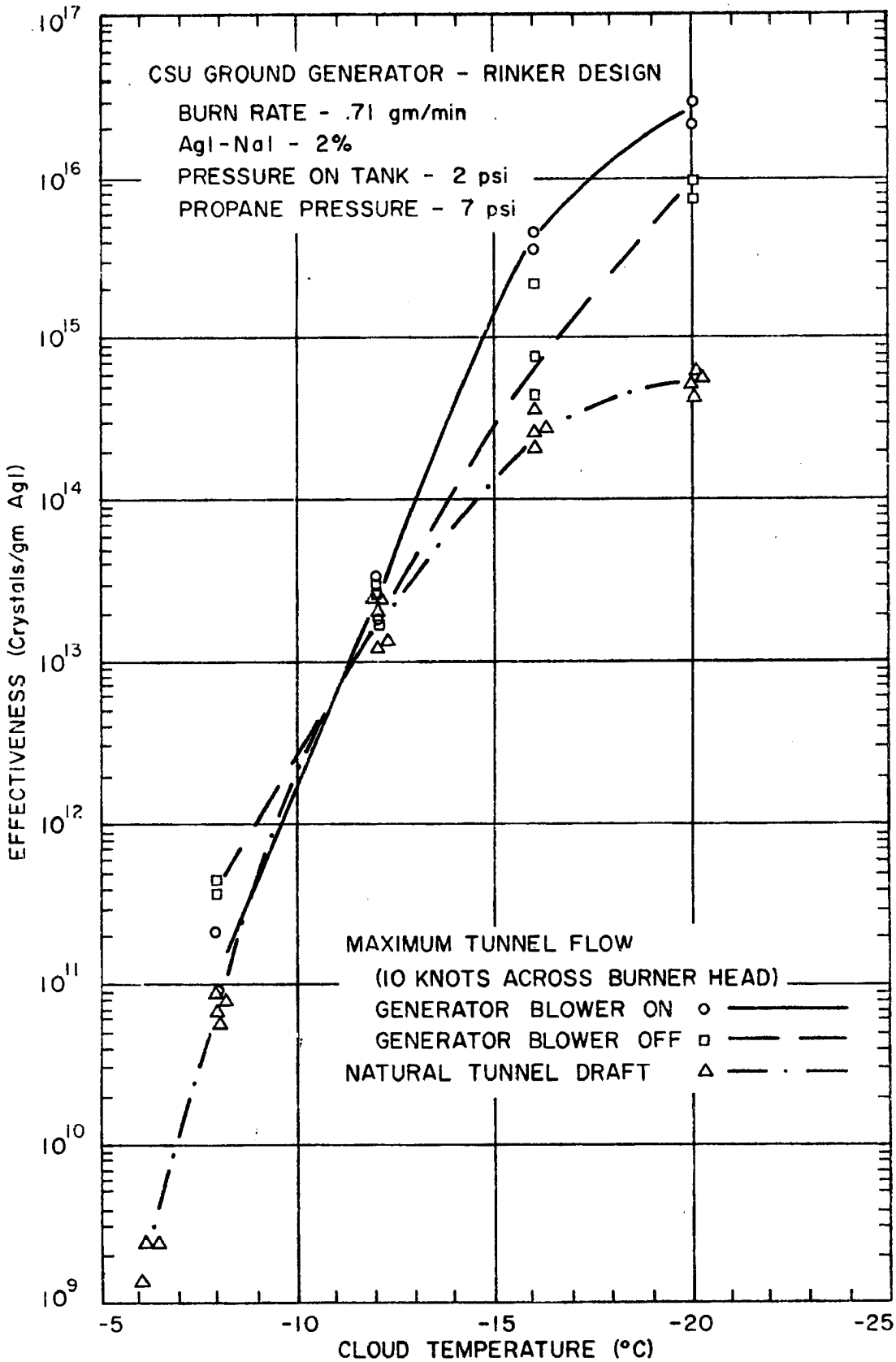

Figure 4.3. CSU Cloud Simulation Laboratory calibration of the ice nucleus generator used in the field experiments.

About four hours a day flying was a safe and practical limit due to the extrememly fatiguing nature of flying close to the surface at high altitude in mountainous terrain.

4.6 Data Obtained

Table 4.3 lists the intensive observation days during both seasons when the aircraft was flown. In comparison to the typical storm situation at Climax this set represents rather stable conditions. Orgill (1971) found that for storm situations dT/dz between 500mb and 700mb was -6.75°C/Km on the average. As far as wind speed and direction are concerned the data set meets the design criteria quite well. In general situations did not exhibit a high level orographic cloud, instead they tended to be cloud-free subsident situations.

Date	500mb Temp.	700mb Temp.	dT/dz	500mb WD/WS	Comments
15 Dec 1973	-22°C	-11°C	-4.35	315°/25mps	Seed Day
17 Dec 1973	-16°C	- 1°C	-5.75	300°/20mps	
20 Dec 1973	-18°C	- 5°C	-5.04	315°/15 mps	
21 Dec 1973	-15°C	- 1°C	-5.36	300°/12 mps	
11 Dec 1974	Background - Shakedown - IN Counter Malfunction				
16 Dec 1974	-23°C	-12°C	-4.36	350°/30 mps	Seed Day
17 Dec 1974	-20°C	- 6°C	-5.46	250°/25 mps	Post Seed Day
19 Dec 1974	-32°C	-11°C	-8.47	320°/15 mps	High Level Turb. Flt.
12 Jan 1975	Background				
13 Jan 1975$_{(1)}$	-18°C	- 3°C	-5.78	310°/35 mps	Snow Storm
13 Jan 1975$_{(2)}$	-21°C	- 6°C	-5.86	310°/35 mps	Seed Day
14 Jan 1975	-18°C	- 3°C	-5.79	300°/30 mps	Post Seed Day
12 Feb 1975	-18°C	1°C	-7.28	300°/10 mps	Turbulence Flt.
12 Mar 1975	Flight aborted due to insturment malfunction				
13 Mar 1975	-25°C	- 8°C	-6.72	300°/5 mps	Turbulence Flt.

Table 4.3. Intensive observation days during the field experiment.

CHAPTER FIVE

OBSERVATIONS

5.1 Near Surface Flow

The archetypes of valley and slope flows have already been presented. This section presents analysis of data from the surface anemometer network in Camp Hale in an attempt to determine how well this region fits the model. Table 5.1 shows the percentage frequency of wind occurrences from each quadrant, and calm, for four of our valley anemometer stations. Data are for the two winters of this experiment (November to February inclusive). The quadrant of maximum frequency for each hour is circled. The influences of up- and down-valley circulations are clear. Only Johns shows a rather weak regime for the down-valley flow. This is consistent with the station location. Being less than 2 Km from the Continental Divide this station is in the source region for the down-valley flow. By contrast Johns shows a strongly developed up-valley circulation.

For these months the down-valley circulation predominates between the hours of 1800 MST and 1100 MST the following morning. Official sunset time varies between 1630 MST and 1700 MST during these months. Typically onset of down-valley flow is delayed an hour or two after sunset. Sunrise varies between 0630 MST and 0720 MST but it takes four to six hour heating to establish the up-valley flow.

It is apparent from table 5.1 that the wind regime of this valley is influenced by factors in addition to the archetype diurnal diabatic circulations. To examine this further, data from the Camp Hale station was examined in depth.

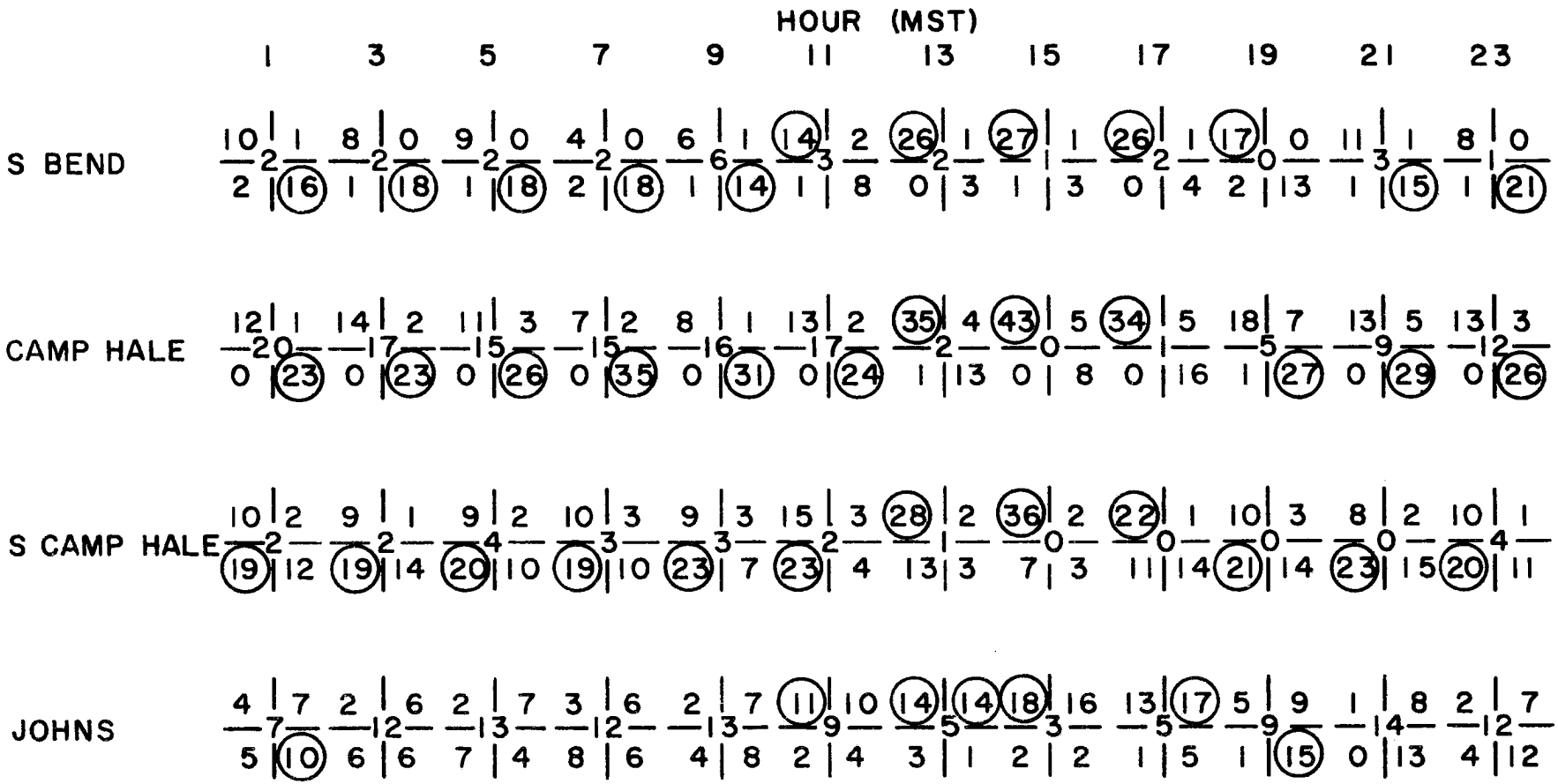

Table 5.1. Climatology of diurnal wind direction variation for winter months in Camp Hale.

Table 5.2 shows the diurnal variation of the wind direction for the Camp Hale station. The data are stratified so that only cases with 500mb flow up-valley are considered, and whether precipitation occurred in the 24 hour period or not. Data from the winters of 1969 to 1975 were considered.

For the majority of hours the surface flow for both stratifications is down-valley. Precipitation cases show three to six times more deviant up-valley flow cases during these hours than non-precipitation cases, with more deviant up-valley flow occurring when the 500mb wind is strong. This can probably be attributed to the cloud shield retarding the development of strong surface cooling and drainage winds, allowing the synoptic pressure gradient to be a greater factor in determining the flow. Grant et al. (1974) found that the diurnal temperature range at Climax under cloudy winter skies is typically 5 to 8°C whereas the average for all conditions is 11 to 17°C. Strong radiational cooling under clear night skies leads to the most persistent down-valley flow. Table 5.2 shows that even the greater short-wave radiation input to the surface in clear conditions over that in precipitation cases is not sufficient to overcome the excess nighttime cooling. During non-precipitation cases the down-valley flow persists longer into the day and is established sooner after the sun sets than for precipitation cases.

Two winters of data from the Camp Hale station show that during the prime-time for down-valley flow (0500 - 0800 MST) its speed averaged 0.5 to 1 mps for both precipitation and non-precipitation conditions. Up-valley flow between 1300 and 1600 MST averaged 4 mps for non-precipitation cases and 5 mps for precipitation cases.

Hour of the Day	Precipitation Cases					Non-Precipitation Cases				
	1-90°	91-180°	181-270°	271-360°	Calm	1-90°	91-180°	181-270°	271-360°	Calm
1	7	60	1	21	12	7	69	1	7	16
2	9	55	1	22	13	9	66	1	6	18
3	8	56	1	22	14	6	71	1	3	18
4	9	54	1	19	18	7	75	0	4	14
5	6	61	2	19	11	4	72	1	7	15
6	7	59	1	22	10	3	75	2	4	16
7	12	59	1	18	10	3	74	1	4	17
8	12	58	1	20	10	2	77	1	3	17
9	11	54	2	21	12	2	76	3	5	14
10	10	47	2	31	10	4	73	1	8	14
11	17	37	1	37	10	9	61	1	16	13
12	16	27	<1	50	6	10	43	1	37	8
13	10	20	0	68	2	8	25	1	63	4
14	13	12	2	69	5	7	15	1	75	2
15	12	13	1	74	1	7	13	1	78	1
16	15	11	1	72	2	9	18	1	70	2
17	15	14	1	64	5	14	32	0	50	4
18	16	29	1	45	9	14	53	1	23	9
19	15	39	2	35	8	11	67	1	9	12
20	17	43	2	29	9	7	70	1	9	13
21	13	48	2	26	11	4	81	1	4	10
22	11	49	1	28	11	2	84	1	4	8
23	7	55	1	25	11	4	80	2	4	10
24	10	50	2	25	12	2	79	1	4	13

Table 5.2. Diurnal variation of wind direction at the Camp Hale station for 500 mb up-valley flow cases stratified according to whether precipitation fell on the day.

In summary, data from the surface anemometer network show that the airflow in the mountain valley between Climax and Redcliff is fairly typical of the archetype mountain-valley circulations. Typically the airflow is strongly controlled by diabatic effects with a marked diurnal variation. In active precipitation situations surface heating by day and cooling by night are retarded resulting in stronger influence of the synoptic pressure gradient winds, particularly for stronger prevailing wind cases.

5.2 Background Levels of Ice Nuclei

Silver Iodide tracer used in this study is detected because of its property as an ice nucleant. Ice nuclei occur naturally in low concentrations. A number of flights were undertaken to confirm that background levels were in fact low in the region of this study. It has been suggested that many years of seeding experiments in this region may have contaminated the area with resultant elevated background levels. The statistical results of some seeding in the USA (Grant, 1963) and Australia (Smith, 1967) suggest this kind of effect.

Data for flights where no seeding was undertaken were examined. Typical is the case of 12 January 1975 where northwesterly flow conditions prevailed. No seeding had occurred in the region for about a month. Aircraft tracks were flown in the Camp Hale - Climax - Leadville region, similar to flight operations on seed days. About 100 seconds of the approximately three hour flight time showed counts elevated above the range 0.5 to 5 per liter active at -20°C. Two short periods of high counts caused by obvious instrument malfunction were also evident. The elevated counts assumed real occurred on two occasions, both in the

vicinity of the town of Leadville. Counts up to 500 IN per liter were recorded.

Similarly, for other days background counts were 0 to 5 per liter. Occasional extremes of up to 50 per liter were found which could not be attributed to anthropogenic sources with any certainty. Neither were these obvious instrument malfunctions. These occurrences could be either real or of more subtle instrument malfunctions.

5.3 Dispersion Case Studies

Of ten days in which aircraft data concerning dispersion in the Eagle River Valley were collected, three have been selected for study. These cases are of special interest to be noted in the text. The remaining flight days suffered from less complete data sets, primarily the result of trouble with the ARIS recording system or icing of the pitot tubes. Although there is useful data available for these days, time constraints prohibited anything but a cursory analysis.

5.3.1 December 15, 1973

Table 4.3 shows that this was the most stable situation encountered. It thus also represents a case of high air pollution potential. The 12Z 500 mb chart for this date (fig. 5.1) shows a major ridge near the west coast and deepening trough in mid-continent. Thus, Colorado was under the influence of strong northwesterly flow. The DEN and GJT rawinsondes for this time indicated 500 mb winds were from 310° at 20 to 25 mps. Temperatures at 500 mb were near -25°C at these stations. A noon radiosonde ascent from Camp Hale gave a 500 mb temperature of -20°C. The surface chart (fig. 5.1) shows that in association with the west coast ridge, a strong high pressure system was in the Great Basin with associated subsidence spreading into the Climax region.

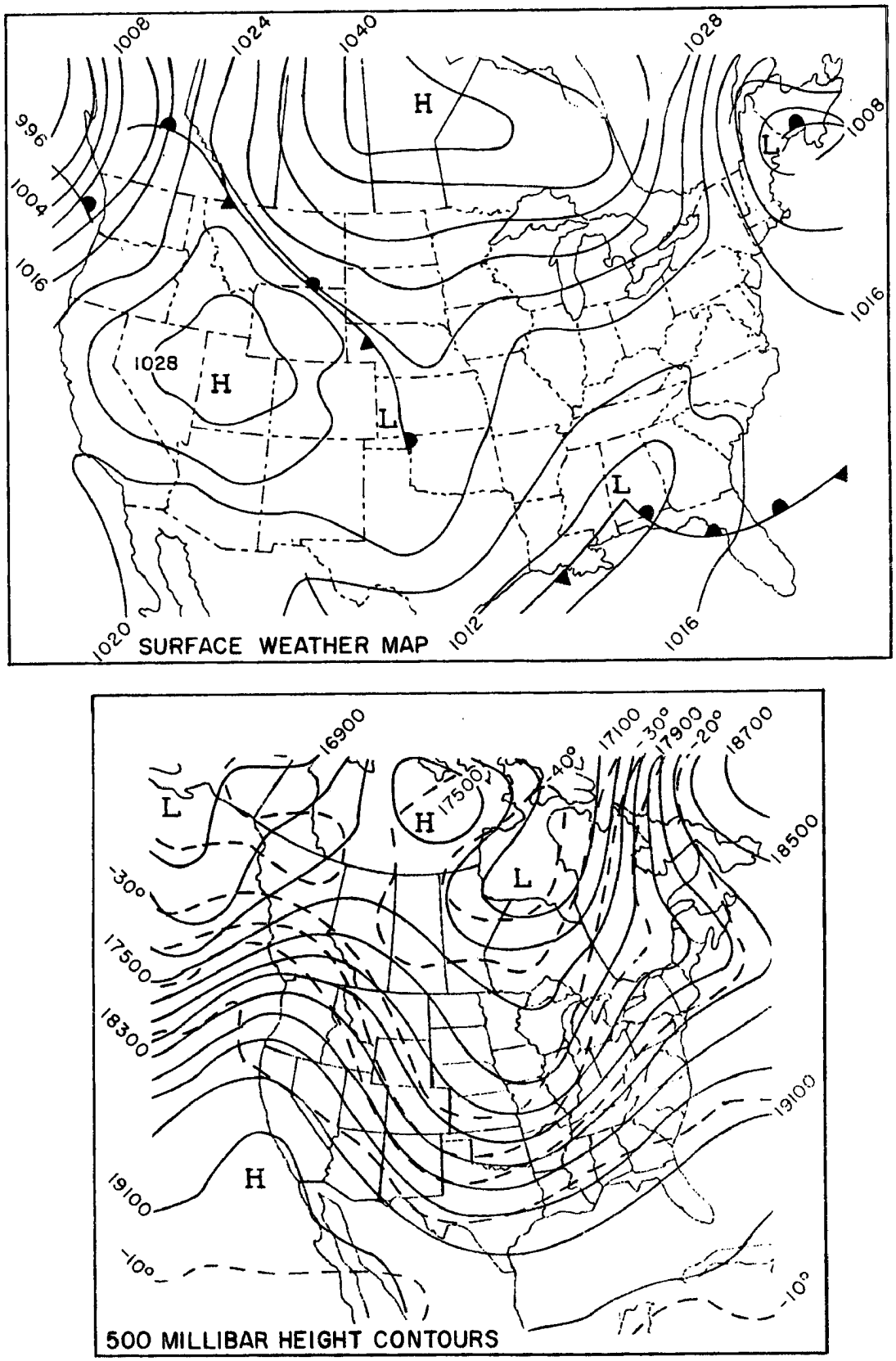

Figure 5.1. Surface and 500 millibar charts for 15, December 1973.

Figure 5.2 shows the aircraft temperature sounding, as determined at about 12 noon north of the experimental area in an ascent to 5300m and in the subsequent descent. As may be seen, there is considerable microstructure, particularly above 600 mb. Below that level the sounding shows a neutral or slightly stable structure. An approximately 2°C inversion is evident at about 600 mb topped by a 70 mb thick layer which is near isothermal. Again, above this level the thermal structure is close to neutral. The dew-point sounding indicates that the air below the inversion at 600 mb is moist, but dries within the synoptically induced subsidence layer above. The structure in the lowest 30mb, with brief encounters with warm air indicated, is suggestive of significant low level heating. This is interesting in itself in that unstable low level air is not generally associated with a snow covered surface. Miller (1956) has suggested that in such an environment coniferous trees can have a major impact on the surface layer heat budget by absorbing insolation which would otherwise be reflected away by the snow surface.

Figures 5.3 and 5.4 show maps of concentration of IN active at -20°C for 0 - 250 m and 250 - 500 m above terrain respectively, for 15 December 1973. The analysis is based on averages of the aircraft data in 250 m squares over the experimental day. About 700 such squares contained observations. The large area of high concentration should be noted. The acoustical counter saturates for concentrations in excess of 10,000 per liter.

At least three features of these concentration patterns are of interest. Firstly, it is clear that there is important channeling of the concentration pattern by the terrain. High concentrations extend southeast of the generator site through Camp Hale and then follow the

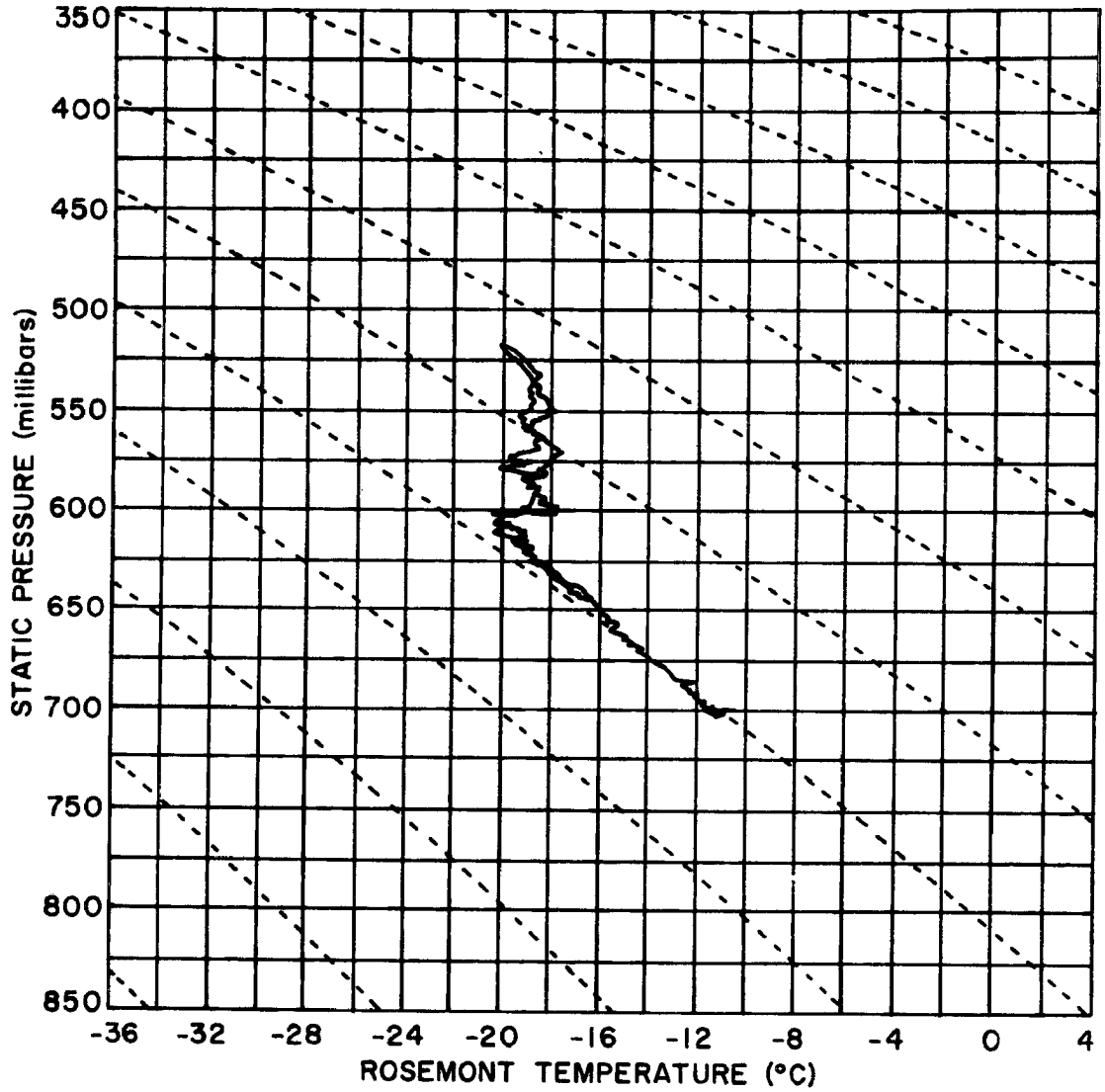

Figure 5.2. Aircraft vertical temperature profile for noon 15 December 1973, north of Camp Hale.

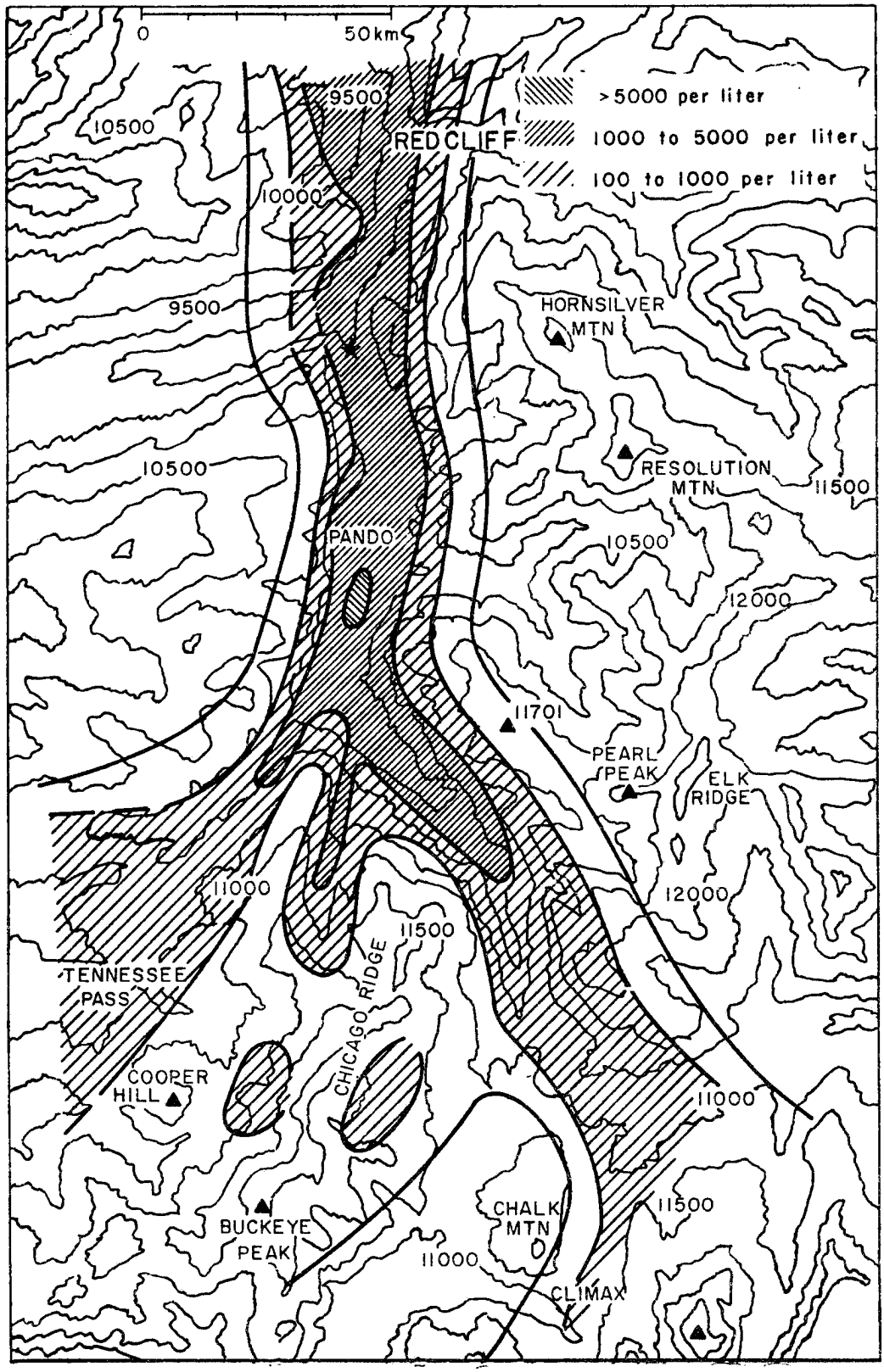

Figure 5.3. Concentration of Ice Nucleant effective at -20° C, 15 December 1973, Surface to 250 meters above surface. Outter contour indicates concentrations above background. ★ indicates generator site.

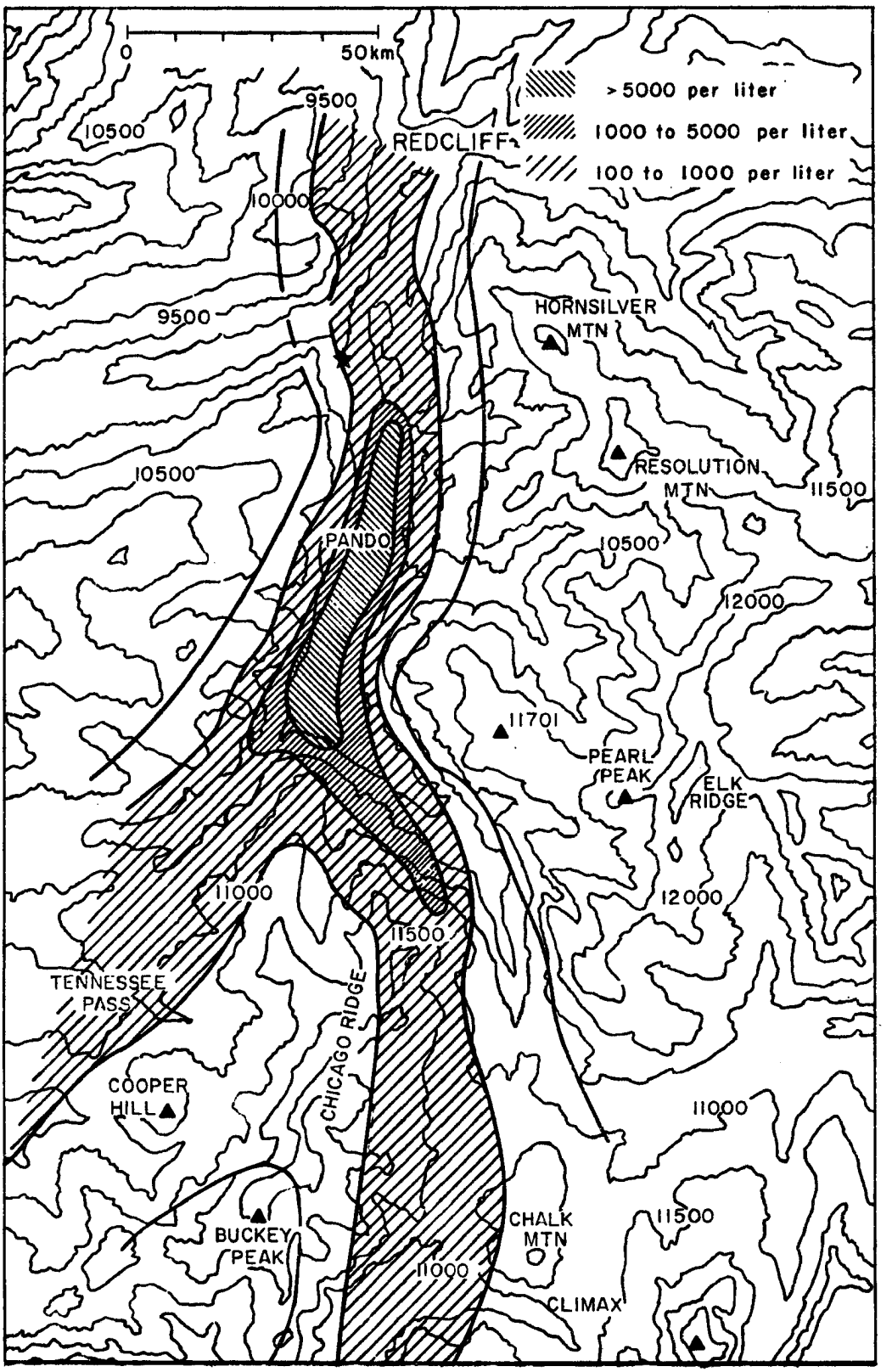

Figure 5.4. Concentration of Ice Nucleant effective at -20°C, 15 December 1973, 250 to 500 meters above the surface. Outer contour indicates concentrations above background. ★ indicates generator site.

valleys to Fremont and Tennessee Passes. Even a small valley such as Jones Gulch (between Taylor Ridge and Chicago Ridge) shows higher concentrations. It is interesting to compare this concentration pattern with that found for the barostromatic condition in the wind tunnel simulation of Orgill (1971). Barostromatic conditions are stable conditions, see Scorer (1953). Figure 5.5 shows a comparison of the non-dimensional potential temperature profiles for our case and the barostromatic case. Although the barostromatic case is less stable overall, the stability characteristics are quite similar in the lowest 600 meters. Figure 5.6 is Orgill's simulation for the surface concentration pattern for surface based seeding at Redcliff, within 5 Km of the S Bend seeding site. It is clear that the terrain effects are rather different, the wind tunnel producing a slight change in direction and distortion in the symmetry of the classic Gaussian plume compared to marked channeling in the field case. The reason for such a discrepancy is not clear. Snyder (1972) has emphasized the problems of simultaneously meeting all similarity criteria in the wind tunnel, particularly Reynolds number similarity. Orgill (1971) indicated practical problems in obtaining truly barostromatic wind tunnel conditions. Even if the problem of meeting all similarity criteria together turns out not to be prohibitive, there is still an unsolved technological problem in imposing realistic surface heat fluxes in the wind tunnel.

A second feature to note is that within Camp Hale higher concentrations are found over a wider area at the upper level than at the lower level. It has already been noted that the lowest levels of the atmosphere were unstable and topped by an inversion at about 600 mb, above the upper (250-500m) level within Camp Hale. These conditions are quite

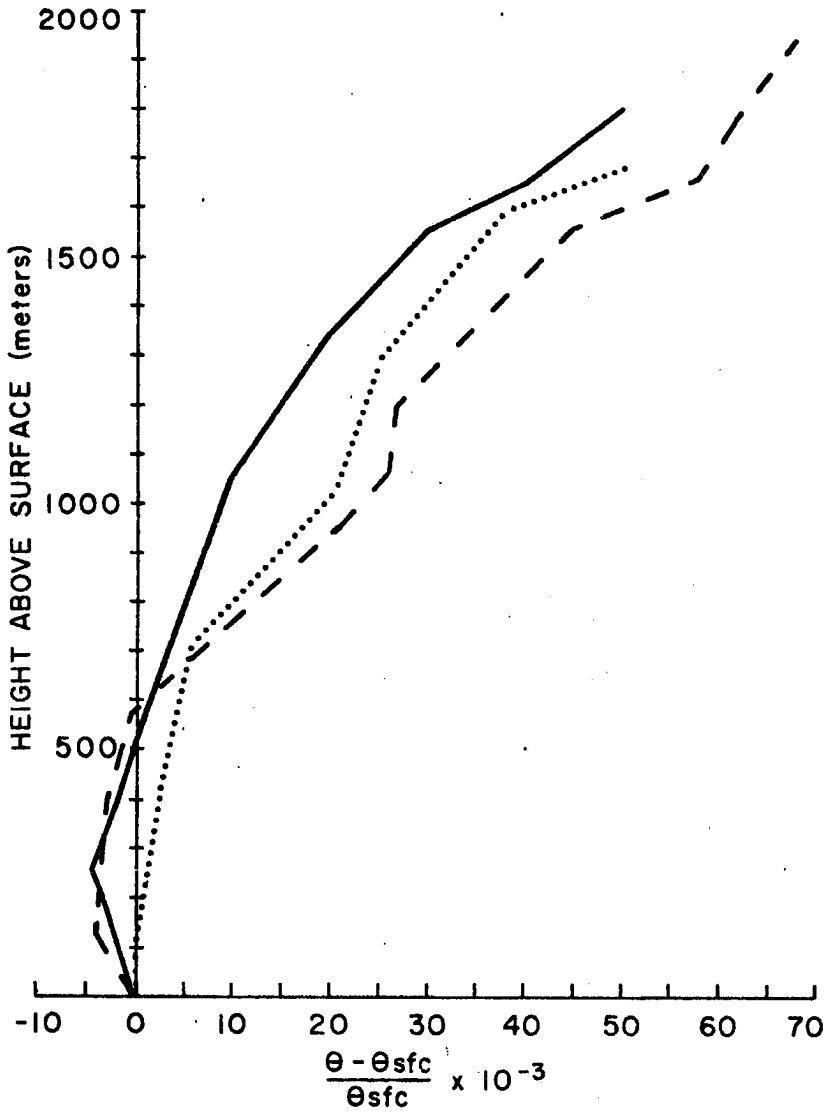

Figure 5.5. Comparison of non-dimensionalized potential temperature vertical profiles from S Bend site 15 December 1973 with barostromatic simulation profile; ·····10 am, - - - 2 pm, ——— Barostromatic.

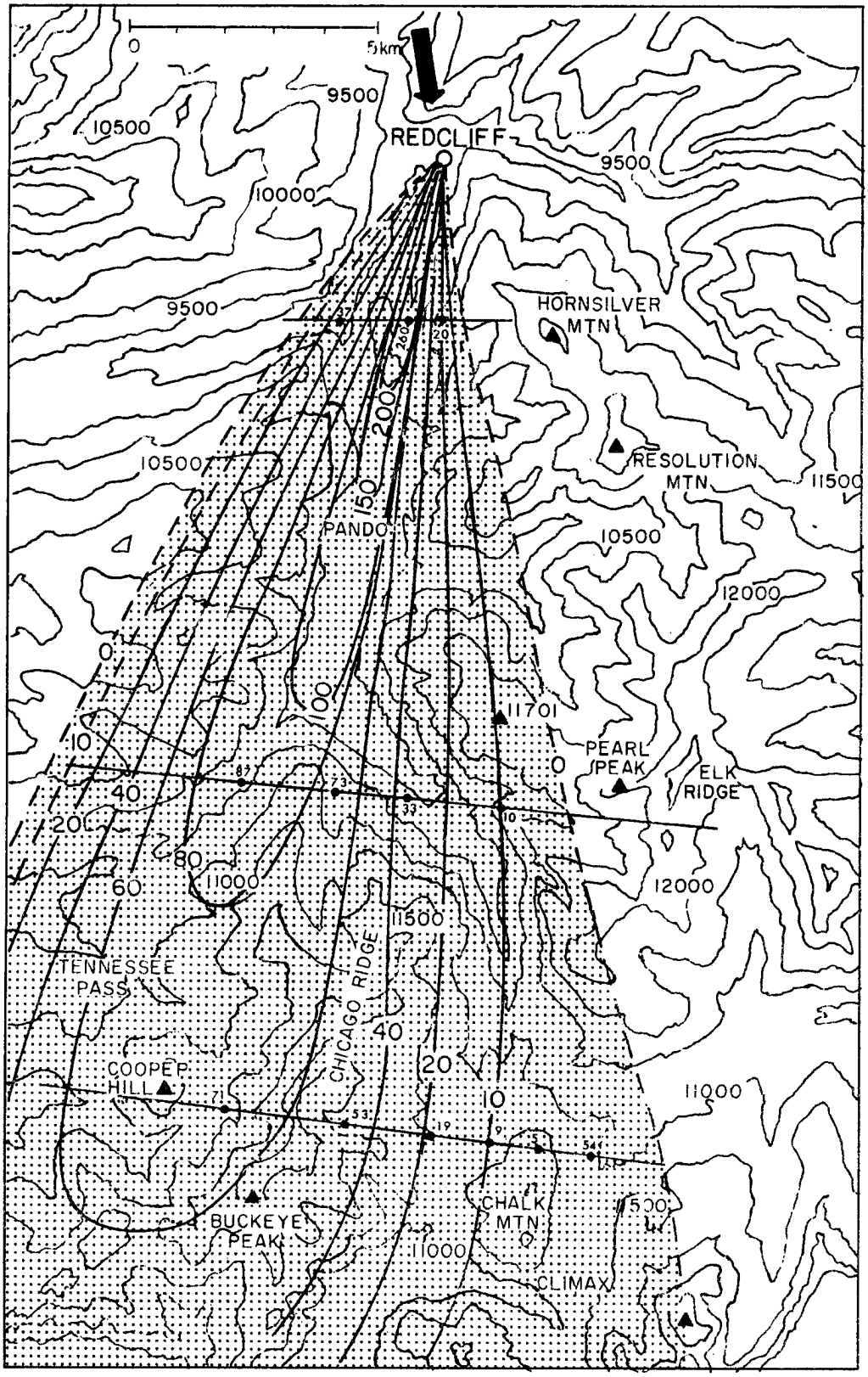

Figure 5.6. Surface concentration $\overline{C}\,\overline{U}/Qx10^{-9}m^{-2}$ downwind from Redcliff source. Barostromatic airflow. Thin lines are measurement locations. (After Orgill, 1971.)

similar to those modelled in a water tank by Deardorff and Willis (1974). They also found higher concentrations occurring beneath the inversion than at source height or at the surface for intermediate downstream distances. This observation does not conform to the more typical Gaussian plume dispersion models.

A third significant feature of the observed concentration patterns is that important concentrations of IN can be found "upwind" of the generator. While it is true that the time delay in the acoustical IN counter could give this effect over a small distance, the data has been scrupulously quality controlled to ensure this was not a factor. The reason for this apparent anomaly is clear upon considering the surface wind direction variation. Table 5.3 shows the wind variations for a number of stations on the day in question. The generator was turned on at about 8 am. Thus for about two to three hours the surface drainage wind was carrying the seeding agent northward, "upwind" relative to the large-scale flow. In the three hours between 8 am and 11 am on this day the anemometer at S Bend corner registered a mean wind speed of 1.5 mps from the southeast. This is enough, if constant throughout the valley, to advect AgI 16 Km "upwind".

The above conclusion is supported by ice nucleus observations taken at the surface at Chalk Mountain and HAO. At Chalk Mountain a CSU Rapid Expansion Counter found 13 IN per liter active at -20°C at 10:30 am, only slightly above background. By 11:30 am the count had increased to 250 IN per liter and stayed at these levels until observations ceased at 1:00 pm. At HAO data between noon and 2:00 pm showed counts in the range 100 to 200 per liter.

	TIME (MST)																		
	0100	0300	0500	0700	0700	0900	1000	1030	1100	1130	1200	1230	1300	1330	1400	1500	1700	1900	2100
CHALK MOUNTAIN	306 9.0	312 14.0	330 10.0	303 10.0	300 15.5	297 13.5	285 11.0	273 15.0	285 15.0	282 9.5	270 8.0	270 3.0	252 5.5	288 7.5	342 5.0	348 8.0	12 9.0	18 8.0	54 4.5
TAYLOR RIDGE	12 1.5	6 4.5	12 3.0	30 3.0	36 1.5	360 1.5	358 1.0	24 1.5	50 3.0	6 4.5	6 3.5	38 3.5	360 3.5	6 3.0	15 4.0	12 3.5	34 4.5	38 7.0	81 7.0
JOHN'S PLACE	180 1.0	189 0.5	186 0.5	192 0.5	186 0.5	198 1.0	66 0.5	48 0.5	51 0.5	48 2.0	54 7.0	57 7.0	42 6.5	39 6.5	42 6.0	45 8.0	282 8.0	183 2.0	186 1.0
HAO	45 1.0	52 2.5	60 3.5	54 5.0	51 6.0	57 4.5	60 5.5	46 8.5	51 6.0	42 6.5	44 5.5	36 3.0	120 2.5	132 1.0	177 1.5	171 2.5	204 1.0	225 1.5	237 2.0
CAMP HALE	123 0.5	C	C	C	C	C	108 0.5	174 3.5	78 0.5	312 4.5	305 7.5	300 8.0	310 11.0	306 10.0	306 17.5	297 10.0	140 2.0	129 1.5	132 1.0
CATERACT CREEK	C	C	132 0.5	150 0.5	C	C	276 3.0	224 5.0	235 8.0	249 6.0	267 7.0	234 6.0	249 7.0	246 6.5	231 5.5	268 1.5	114 2.0	C	C

Table 5.3. Wind variation at a number of stations for 15 December 1973. C indicates calm.

5.3.2 January 13, 1975

The synoptic charts, figure 5.7, from the 12Z soundings show a surface trough of low pressure in northeast Colorado associated with a broad low pressure system over South Dakota and Nebraska. At 500 mb a low amplitude short wave trough was embedded in a general strong (35 mps) northwesterly (310°) airflow above the surface system. Although not analysed on the NOAA surface chart it appears that the weather situation in the Climax region during the day was characterized by a cold frontal passage. Thus, on arriving at the area in the morning the aircraft was unable to enter the region because of poor flying conditions. Snowfall ceased around noon. This case represents the closest to a true orographic precipitation situation that was observed in this project. The 500 mb winds were stronger than is typical however.

The composite upper air sounding obtained from the flight, figure 5.8, shows two significant inversions. The upper level inversion is inferred from the 500 mb temperature given by the synoptic charts and conditions at the highest level flown, approximately 620 mb. Cloud above this level prohibited taking complete aircraft soundings. The exact level of this upper inversion is thus uncertain. The lower inversion is better defined in the individual soundings making up the composite than in the composite. It appears between 670 mb and 700 mb depending on the location. Below this inversion the air is quite stable, almost isothermal. Above the lower inversion the lapse rate is between moist and dry adiabatic. The air is close to saturation with dew point depressions 1 to 2°C at all levels.

The wind regime for this situation is quite interesting. At the lowest levels at which the aircraft measured (below 700 mb, the height

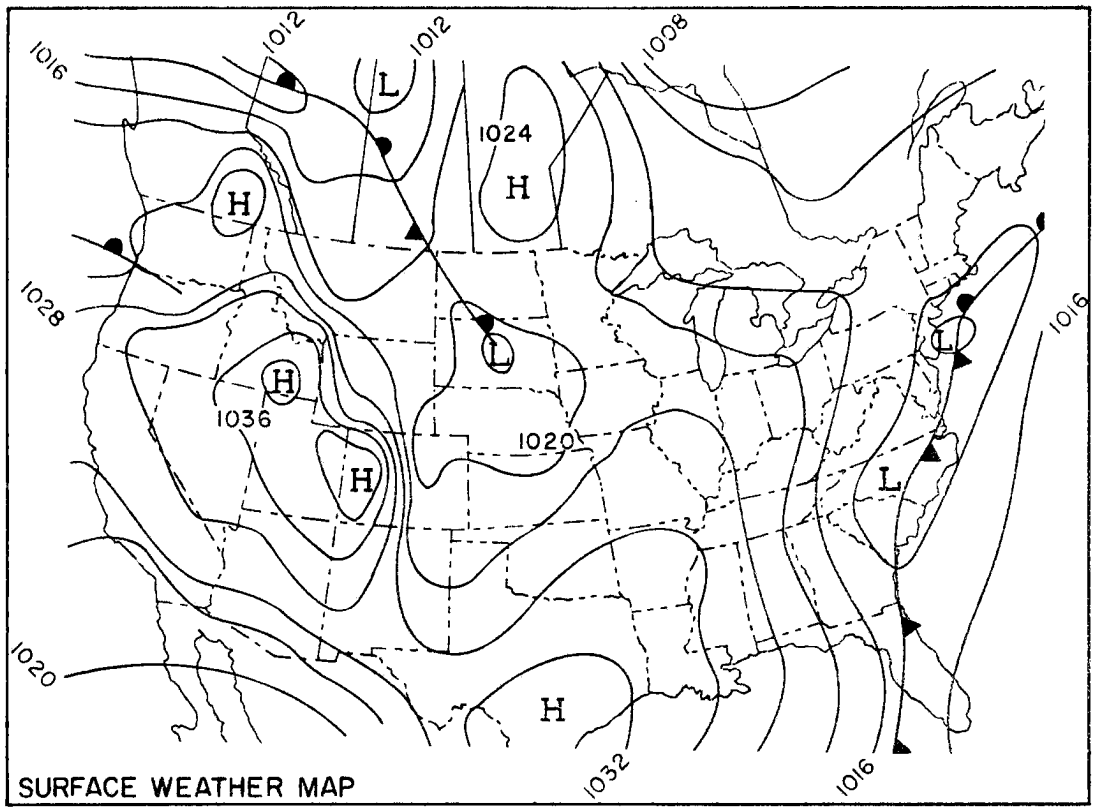

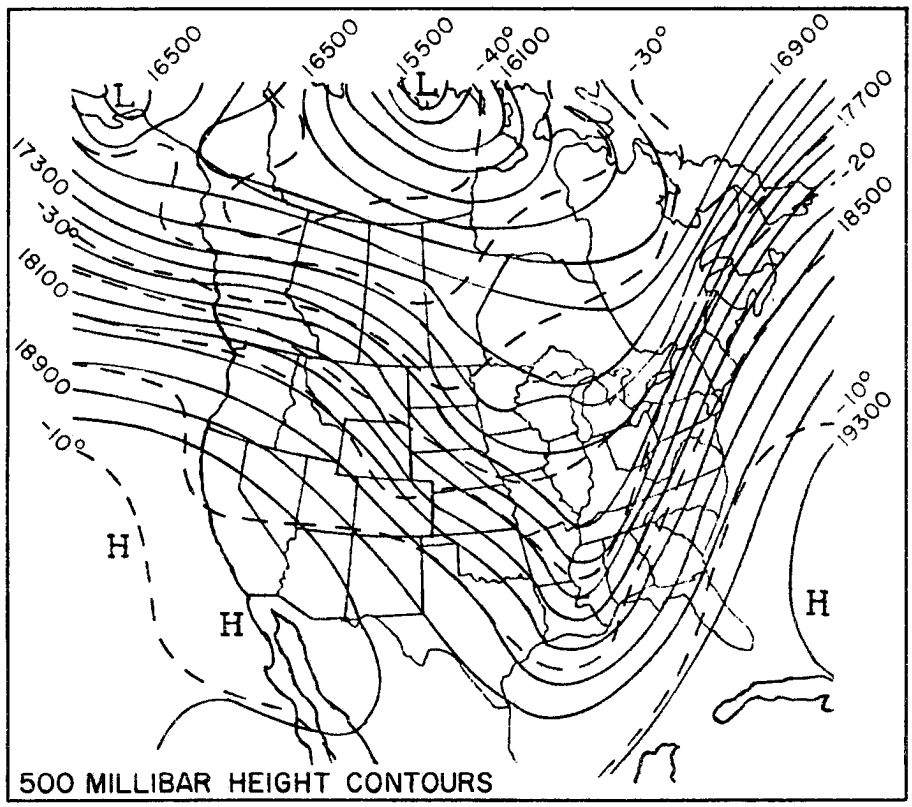

Figure 5.7. Surface and 500 millibar charts for 13 January 1975.

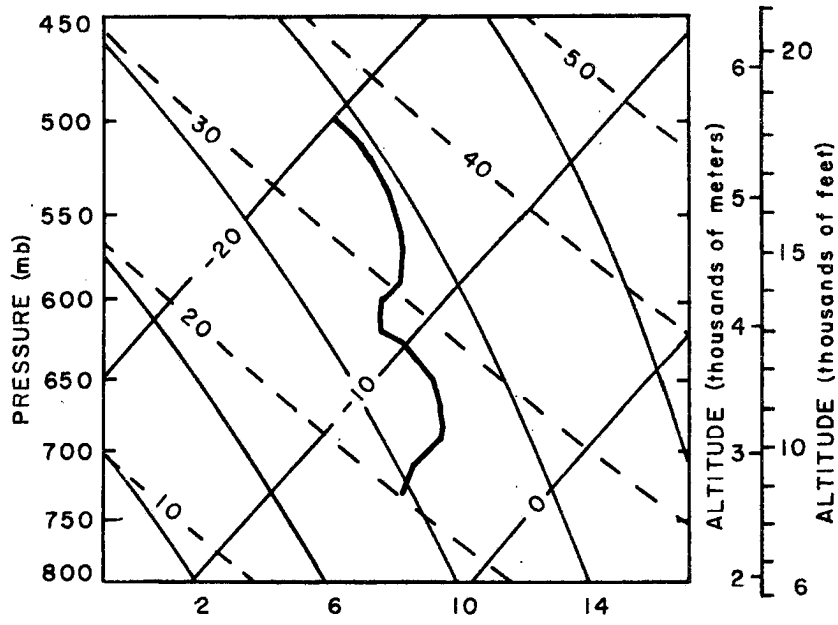

Figure 5.8. Composite Aircraft Sounding 1300-1530 MST 13 January 1975 in vicinity of Climax, Colorado.

of the lowest inversion) the winds were almost all up-valley, but with considerable deviation to follow local terrain contours. Within Homestake Creek the wind deviated to blow up-valley from about 60°. Near the seeding site at S Bend Corner a few measurements indicated a weak down-valley flow. Within this lowest layer winds were generally 0 to 3 mps. Above 700 mb the winds were from about 310° with the spread in direction decreasing with height. Wind speeds remained less than 5 mps below the lower inversion increasing above this level to 20 mps at 620 mb, not approaching 500 mb synoptic geostrophic values at the highest levels measured.

Seeding started at about 1000 MST on this day and continued to about 1500 MST. Figure 5.9 shows the surface level (average for observation below 250 m AGL) ice nucleus concentration pattern. Again it is clear that the distribution is strongly influenced by the terrain contours with highest concentrations found in Camp Hale and Homestake Creek. The maximum in Homestake Creek is interesting in that in order for tracer to enter this valley it would be necessary for air to be moving against the predominant wind between the seeding site and junction of the Creek with the main valley. The aircraft confirms this with observation of local low level drainage flow in this region.

Convergence between drainage flow and prevailing flow leads, by continuity, to enhancement of the flow normal to the along valley direction. This accounts for considerably enhanced flow up Homestake Creek and the concentration maximum. The convergence also favors upward vertical motion in this region. Figure 5.10 shows a cross section along the 310° azimuth and through the generator site. The concentration pattern suggests enhanced concentrations aloft associated with the zone

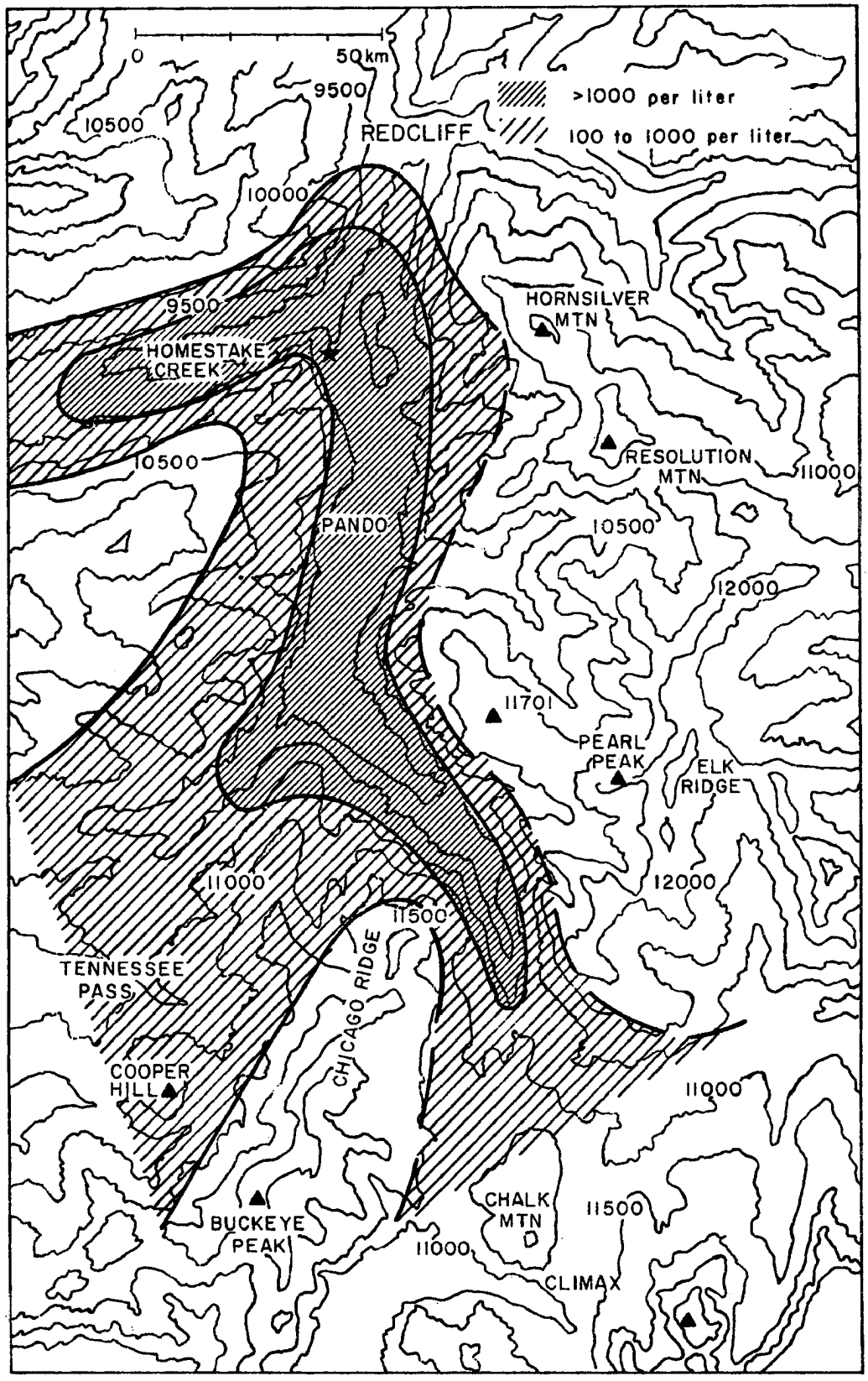

Figure 5.9. Surface (average of observations below 250 m AGL) ice nucleus concentration pattern for 13 January 1975.

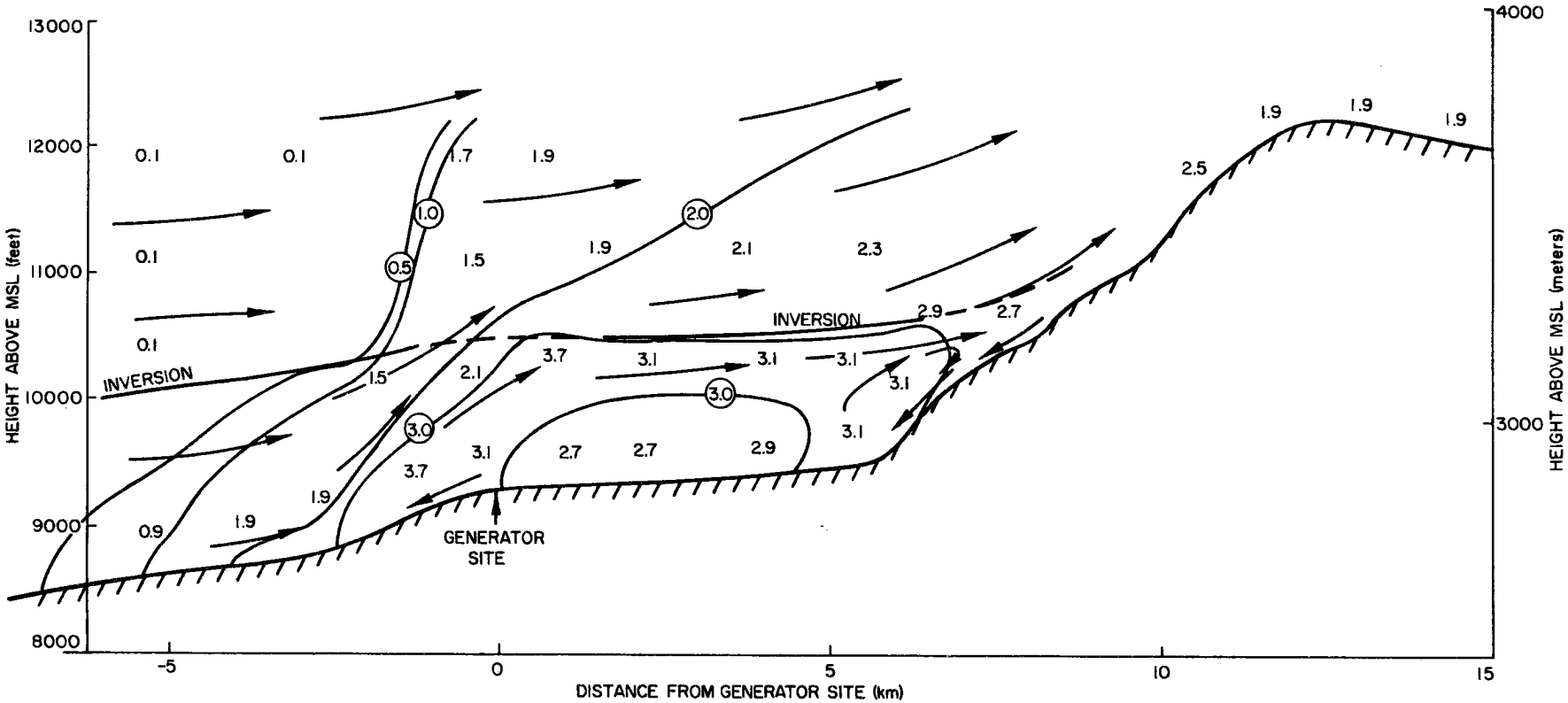

Figure 5.10. Cross section along the mean flow direction through the generator site showing concentrations of Ice Nuclei (active at -20° C) and Schematic Airflow for 13 January 1975 case study. Concentrations are given in common logarithms.

of convergence. The IN appears to be transported through the inversion at this location. The concentration pattern also suggests a second convergence region at the south end of Camp Hale, however there are no wind observations to confirm its presence.

5.3.3 January 14, 1975

An experimental day was declared on this day to investigate carry-over effects, ice nuclei lingering in the environment long after seeding had ceased the previous day (see the previous case study). Direct evidence of such persistence has been given by Rottner et al. (1974). Figure 5.11 shows that the synoptic configuration had changed little since the previous day. At 500 mb a strong (35 mps), generally north-westerly flow continued but with a more westerly component than the previous day (290°). The 500 mb temperature had returned to -18°C after the passage of the weak disturbance the previous day. At the surface the pressure had built over southwest Colorado and lee troughing prevailed east of the mountains. The day was characterized by encroaching subsidence, a high level orographic cloud which had apparently persisted overnight gradually dissipating during the day. With solar heating of the surface enhanced as the cloud dissipated and subsidence warming, the total depth of the atmosphere of interest here warmed considerably over the course of the day. Unfortunately, because of the flight sequence adopted this day it is impossible to accurately determine the warming at each level. The observations were organized so as to investigate the lower levels first and then move to progressively higher levels. A sounding at the start of observations shows a 20 mb deep isothermal layer at the surface capped by a layer of near moist adiabatic lapse rate to 670 mb. Above this is a subsidence inversion topped at 640 mb.

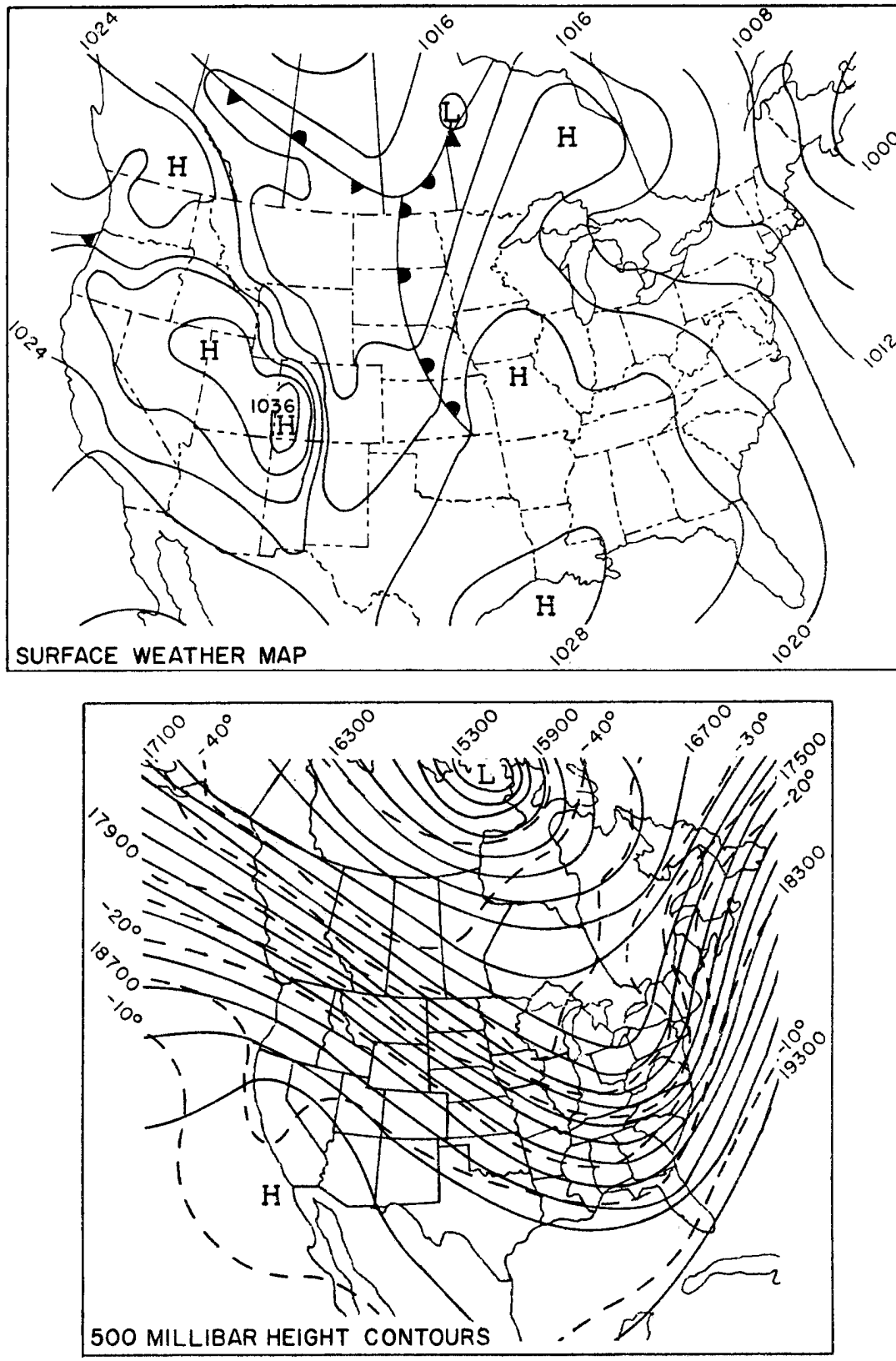

Figure 5.11. Synoptic situation at 12Z 14 January 1975.

The structure above this level is not defined by observation but the synoptic 500 mb pattern suggests another inversion below that level.

Analysis of the observations in the lowest levels, within 250 m of the surface, shows weak wind predominated about evenly divided between the drainage and prevailing directions. All observations at these levels are prior to 1230 MST. It may be that the drainage winds occurred in the observations in the lowest part of this 250 m layer and the prevailing winds in the upper part but the data has insufficient resolution to determine this. There is considerable carry-over of IN from the previous day, when seeding had stopped at about 3:00 pm. The concentration pattern is quite erratic, but high concentrations were again confined to the valley. Concentrations in excess of 100 per liter effective at -20°C extended from the junction of the Eagle Valley with Vail Valley through Camp Hale to Tennessee Pass and HAO. A few isolated locations of concentrations just over 1000 per liter were found.

Observations at higher levels later in the day showed winds from 290° through north to 45° with speed increasing to average 8 mps at 3600 m, the highest level measured. Concentrations at this highest level were mainly 10 to 100 per liter in the area above background with a few readings above 100 per liter at the south end of Camp Hale and into Tennessee Pass region where the terrain rises to approach this height.

The conclusion from this case study is that, even for a situation which, indexed to the 500 mb level, is a strong wind situation there is considerable carry-over of seeding agent trapped in the mountain valley to the next day.

5.4 Conclusions

The preceeding physical and climatological studies of the transport and dispersion of seeding agent from a ground-based generator to cloud base in the region northwest of Climax show that the total process is extremely complex. Numerous orographic cloud seeding experiments, however, testify that such transport does commonly occur.

Inversion layers, which are common during the nighttime and early morning hours in mountain valleys, retain seeding agent at low altitudes for considerable periods of time and isolate air within the valley from the drag effects of the prevailing flow. In these circumstances the airflow at the lowest levels is controlled by diurnal diabatic effects which are strongest during clear sky conditions. Under such circumstances turbulent dispersion is at a minimum and it is difficult to conceive that seeding agent in significant concentrations could directly penetrate such layers. Such a conclusion is consistent with high residual concentration levels as found 24 hours after seeding terminated during the 13-14 January 1975 experimental period.

When cloud is present over a mountain valley the net radiative energy loss at the surface is restricted and so the mechanism for maintaining strong inversions is lacking. Typically the low level stratification is neutral to isothermal. The low level flow is again dominated by diabatic effects, but in closer balance with the prevailing synoptic flow so that in some circumstances the synoptic flow can predominate. The case study for January 13, 1975 shows such a circumstance where down-valley flowing air, predominating on the steeper slopes, forms convergence zones with the synoptic flow, predominating where the slope is shallower. The case study suggests that such a convergence zone can

force vertical motions which locally aid transport of seeding agent out of the lowest levels. Another favorable location for convergence is likely to be in the vicinity of the edge of the shadow of the orographic cloud during the morning hours.

It is important that the picture resulting from the inherently limited definition of the processes provided in this investigation not be misunderstood. The actual detail of transport through the inversion, even in the vicinity of the low level convergence zone, is likely to be highly complex, non-linear and non-steady state. Although the importance of these small-scale processes, such as the breaking of Kelvin-Helmholtz waves, can now be appreciated, the interaction of such waves generated at a variety of locations in complex topography situations produces an effect which can likely only be treated statistically. Detailed treatments of these phenomena is beyond the scope of this investigation.

Additional mechanisms which may be effective in promoting the vertical transport of seeding agent during stable situations are mechanical turbulence where the stable layer intersects the valley wall and preferential solar heating on a slope facing the sun, both effectively breaking the stable layer locally.

The lack of any pronounced diurnal variation of seeding effect in the Climax precipitation record indicates that seeding agent can reach and interact with the orograhic cloud most of the time. The overall conclusion is that in orographic cloud cases the low level stability, as modified by the cloud presence, is such that significant vertical transport and dispersion occur. The significant parameters influencing

seeding effect, which also influence the transport and dispersion to the cloud, are generator location relative to the target and windspeed.

CHAPTER SIX

SIMULATION OF MOUNTAIN ENVIRONMENT AIRFLOW

A quantitative description of the mean airflow is one important input required in predicting pollutant dispersion. Because airflow is highly dependent on location in mountainous terrain its description is complex. In this chapter one approach to the solution of this problem, numerical modeling, is investigated. After reviewing previous attempts to numerically model mountain environment airflow, the desirable features of such a model are discussed. The current state of the art in this area is insufficiently developed to permit use of a model incorporating many of these features. A relatively simple, but still complex model, the University of Virginia two-dimensional mesoscale model is employed to investigate the qualitative aspects of airflow, and so dispersion, in a simple mountain ridge situation. We look for the different general classes of solution obtained as the input parameters are varied. In particular the effects of diabatic forcing at the surface are investigated.

6.1 Previous Modelling Studies

Attempts to understand airflow over mountainous terrain based on the Newtonian equations of motion have accelerated as computer capabilities have increased. Until about 1960, when computers started to become commonly available, efforts in this area were directed at finding analytical solutions to simplified equations for two-dimensional airflow. There was considerable interest in understanding the mountain lee wave phenomena which was a problem for early aviation. This work is reviewed by Queney (1960). Analytical studies of slope and valley flow

were also pursued, and are reviewed by Gleeson (1953). Such work suffers in that in order for analytic solutions to be found, possibly significant terms, particularly non-linear terms, in the complete equations must be omitted. Solutions can be unrealistic, or even worse, realistic for the wrong reasons.

As computers became commonplace, facility was developed in simulating simple situations which had first been investigated analytically. Previously neglected terms were included. Emphasis remained on two-dimensional flow [Hovermale (1965), Deaven (1974), Klemp and Lilly (1975)]. Cold orographic clouds were simulated in two-dimensions by Plooster and Fukuta (1972, 1975), Fraser et al. (1973) and Young (1974) including more or less sophisticated cloud physics. The Lavoie (1968) model has been applied to orographic flow by groups at the University of Wyoming and South Dakota School of Mines. Mahrer and Pielke (1975) have included sophisticated parameterization of boundary layer processes.

Computer limitations have delayed the development of three-dimensional simulations. The early efforts of Thyer (1967) to model valley winds with a vorticity model and Hino (1968) to model dispersion in complex terrain are noteworthy. In the USSR, Shershkov (1972) has developed a comprehensive dry model. Gal Chen (1973) has continued development of coordinate transformations to optimize accuracy of three-dimensional models. Development of three-dimensional models, including cloud microphysics, is actively being pursued by Nickerson at NOAA in Boulder, Colorado, by Anthes at Pennsylvania State University, by Deaven at NCAR, and for summer-time situations by Cotton at CSU.

6.2 Modelling Constraints and Requirements

From a practical viewpoint the objective of modelling is to determine the result of the interaction of various processes under defined conditions. An efficiently defined model will minimize the number of interacting processes needed to describe the result, by consideration of the time and space scales of the events, and the magnitude of the processes.

Consider the problem of modelling a typical event of orographic snowfall. The significant chain of processes is as follows. Air rises as the large-scale flow forces it over a mountain barrier. The airflow near the surface is influenced by the low level stability which may change as the surface energy balance changes with changes in surface temperature, moisture, roughness and albedo. An orographic cloud is formed over the barrier if the air is sufficiently moist. The air also contains natural ice nuclei whose activity is a function of temperature. Ice crystals formed around nuclei may grow, collide and multiply. Below cloud base falling precipitation particles may evaporate in sub-saturated regions and only reach the ground if they survive passage through such layers. Clouds and precipitation, by acting on the radiative exchange, modify the energy balance at the surface, which influences the airflow. Latent heat released during cloud and precipitation formation act to modify the airflow.

If seeding from the surface is occurring, nuclei properties depend on the generation process including windspeed at the generator. Artificial nuclei are dispersed and transported to the cloud level by the airflow. Depending on the radiative environment nuclei may photo-deactivate. They may react with the cloud to form ice crystals and thus

release additional latent heat. Additional or thicker cloud alters the radiative balance at the surface.

It is helpful to think of the problem as four interacting sub-problems.

1. The problem of determining the atmospheric airflow, temperature, and moisture structure.
2. The problem of the cloud microphysics.
3. The problem of the radiative interactions.
4. The problem of the transport of the artificial nucleant.

Previous studies [e.g., Young (1974), Fraser et al. (1973)] have simplified the problem by circumventing the details of the seeding process and specifying the artificial nucleant concentration upwind of the cloud. If the radiative effect on the airflow is largely limited to near the surface the need to treat radiation in detail is obviated. Plooster and Fukuta (1975) consider the dispersion from a ground based generator but employ only a simple Gaussian plume model formulated for non-mountainous terrain.

In this study the prime interest is in the dispersion and transport of the nucleant at low levels and into the cloud. The atmospheric airflow is of prime concern. The radiative-diabatic effect is highly significant, but lacking the facility to treat the surface energy budget in detail the diabatic surface effects are parameterized in terms of specified surface temperature. The details of cloud microphysics are ignored in the airflow modelling as they are not the basic concern of this investigation.

The horizontal resolution required will determine the grid spacing in the model (if a grid point formulation is used). The desirability of

large grid spacing for computational efficiency must be balanced by resolution requirements for accuracy. Examination of figure 4.2 makes it clear that there is considerable topographic structure on scales down to 1 Km in our area of interest. Accurate resolution of structure of this scale will require considerably smaller horizontal grid point spacing, say 100m. Shershkov (1972) used 400m horizontal resolution in calculating the flow in the vicinity of Sado Island which has much simpler topography than our region.

For our problem vertical resolution will need to be sufficient to resolve details of the low level structure. In particular, inversions and shallow layers of drainage flow, which are very significant to dispersion from a ground based generator need to be resolved. Aloft the resolution can be relaxed. It is the author's perspective that the computer capable of dealing with this three-dimensional airflow problem with reasonable cost and time expenditure, is not yet available to the atmospheric science community. In order to examine the problem further we reluctantly resort to two-dimensional modelling. The two-dimensional mesoscale model of the University of Virginia is employed.

6.3 The University of Virginia Two-Dimensional Mesoscale Model

As shown by Pielke (1974b), a two-dimensional mesoscale model can be used to investigate many of the properties of atmospheric circulations even though spacial variations of the dependent variables in the third direction are ignored. A complete discussion of this model, taken in large part from Mahrer and Pielke (1975), is given in Appendix A.

The basic equations for hydrostatic flow in cartesian coordinates are structured in a terrain following coordinate system (x, y, z*, t) by the transformation $z^* = \bar{s}(z - z_G)/(s - z_G)$, where $\bar{s}$ is the initial

height of the top of the model, s is the material surface top of the model (initially $\bar{s} = s$) and z_G is the ground elevation. Latent heat effects are ignored. The conservation equation for specific humidity is written assuming moisture is a passive scaler.

A detailed treatment of the boundary layer is incorporated using a profile function representation of the boundary layer fluxes. More details on this parameterization may be found in Appendix A. In this respect the parameterization in this model is considerably more sophisticated than in previous models of orographic airflow, and it is this aspect of the model that makes it especially appropriate for our purposes.

6.3.1 Restrictions on the Applicability of the Model

Prior to demonstrating some of the model results, its limitations are now described. It is important to appreciate these so that the model is only applied in appropriate circumstances and the temptation to over-interpret the voluminous output generated can be resisted.

In the atmosphere perturbations from balanced flow (i.e., gradient flow) leads to wind oscillations which are damped out by at least three mechanisms; longitudinal and lateral transient pressure fluctuations and eddy viscosity. These first two correspond to the mechanism of geostrophic adjustment. Specification of a constant geostrophic wind in the model is equivalent to imposing a constant lateral pressure gradient. Thus one of the mechanisms of geostrophic adjustment is lacking and we might expect that transients will continue longer in the model solution than in the atmosphere.

A second restrictive assumption in this model is that it is a dry model. If a parcel of air ascends in the atmosphere it eventually

becomes saturated and additional ascent causes liquid or solid water to form releasing latent heat. In the model no such phase change process is accounted for, the specific humidity of an air parcel changes only as a result of eddy diffusion. It might at first seem that this is a severe restriction for an orographic cloud environment model. There is evidence, however, that dry models can be quite helpful in modelling cloud environment situations. Thus Pielke (1974a) was able to predict the favorable areas for formation and the movement of mesoscale cumulonimbus cloud areas in south Florida with a dry model. Of course, details in the immediate cloud vicinity were not modelled. It would be reasonable to expect that as orographic clouds are, by comparison, shallower than cumulonimbus clouds and environmental absolute humidities are lower in the high elevation winter orographic situations at Climax, the effect of latent heat release will be less.

Fraser et al. (1973) have closely examined the effect of moisture on airflow in an orographic environment, with particular reference to environmental conditions over the Washington Cascades. They conclude that:

1. The latent heat effect "is significant in some cases but depends on details of the flow".
2. "The effect generally becomes less significant near the ground where the flow is constrained by the boundary".
3. "Under stable conditions the latent heat effects appear to be secondary to the barrier effects of the mountain".

As we are primarily interested in effects near the surface this study then supports the use of a dry model for our purposes. In fact, as Fraser et al. assume inviscid flow we might expect that in the planetary

boundary layer the surface effect will outweigh the latent heat effect even more substantially.

A final argument for employment of a dry model is that, for the circumstance where the atmosphere is saturated, a dry model with a uniform potential temperature should give a reasonable representation of this flow, to the extent that the moist adiabatic lapse rate is proportional to the dry adiabatic lapse rate. This is a similarity argument, similar to that used in wind tunnel studies where isothermal conditions are used to simulate neutral flow.

There are several additional deficiencies of the University of Virginia Model:

1. The parameterization of the surface layer employs an assumption of horizontally homogeneous turbulence which is of particularly limited validity in mountainous terrain. This is part of a more general deficiency in present understanding of atmospheric boundary layer processes.
2. Use of the hydrostatic approximation; although this may not be a serious problem as the horizontal scales of interest in this study are greater than a few kilometers.
3. Use of a simple upstream finite difference operator which introduces an artificial diffusion.
4. Lack of an explicit surface energy budget, although skillful specification of surface temperatures will minimize the errors here.
5. The approximations inherent in the treatment of the upper boundary.

In summary, the model applied here has numerous deficiencies, particularly those resulting from its two-dimensional nature and lack of treatment of latent heat effects. For terrain which can reasonably be represented in two-dimensions the model can be expected to give useful insights into the airflow regime within the planetary boundary layer. Particularly useful simulation of situations with no saturation or complete saturation conditions can be expected.

6.4 Case Studies with the University of Virginia Model

The model is applied to a few atmospheric situations to investigate the flow solutions obtained. In a later chapter a Monte Carlo dispersion simulation is run using these flow solutions, to illustrate important features of dispersion in mountainous terrain.

As we are primarily interested in low level features of the model flow solution only the lower part of the solution is displayed. Horizontally the displays run from 40 Km upwind to 5 Km downwind of the mountain crest. The mountain profile is shown in the figures. Vertically the region displayed is 1875 m deep and the mountain rises 1 Km above base height. The pressure at the base height is nominally 700 mb. These parameters are specifically chosen to illustrate features of the northwest flow situation near Climax; however the terrain features are highly smoothed. Adequate data defining surface heat fluxes in this type of environment do not appear to exist, thus the surface temperatures chosen are estimates for these situations designed to show the range of solutions obtainable.

6.4.1 The Daytime Case

During a typical daytime situation, without cloud present, the surface energy budget is such that there is a weak heat flux to the air.

When cloud is present the incoming short-wavelength radiation is depleted and only a relatively weak heat flux at the surface may be found.

Consider the case where the air is in thermal equilibrium with the surface beneath it, the remainder of the atmosphere being neutrally stratified, an analogy with moist-adiabatic flow. Figures 6.1 and 6.2 show respectively streamlines and isotachs of vertical velocity for a geostrophic wind of 10 mps, after 28 hours of integration time. Although weak transitory oscillations are still evident in the solution the flow is, for practical purposes, steady state. The computer solution is well behaved. Upward vertical velocities are confined upwind of the mountain and subsidence downwind. The vertical velocity attains a maximum a few hundred meters above ridge crest level, within the boundary layer. Outside the region of strong vertical motions the role of the mountain is to enhance the kinetic energy of the downslope flow at the expense of the static energy of the total column and the kinetic energy of the flow normal to the terrain slope.

Figure 6.3 shows streamlines for the situation where the air entering the integration domain is neutrally stratified and the geostrophic wind is 10 mps but the surface is maintained cooler than the air above it. The potential temperature of the surface is specified to be 2°K cooler than that of the air initially in contact with it, except that on the crest of the mountain from 10 Km upwind of the crest to 2 Km downwind the surface potential temperature is specified to be 3°K cooler than elsewhere. This combination of parameters is designed to simulate the situation that might be encountered in the early hours after sunrise where the incoming solar radiation almost balances longwave radiative

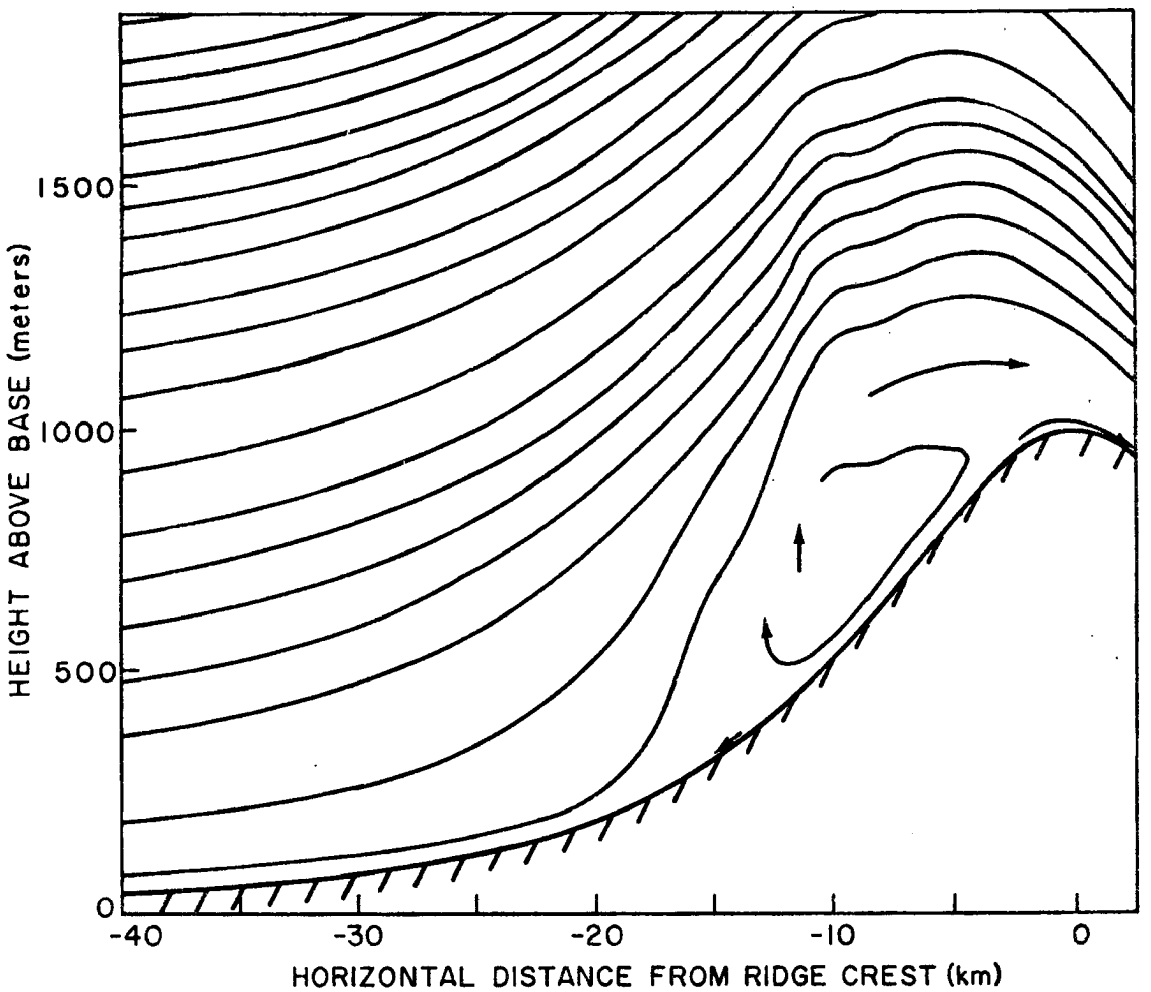

Figure 6.3. Streamlines of orographic flow for an early morning situation with an orographic cloud present, geostrophic wind 10 mps.

loss at the surface, except under an orographic cloud hanging over the mountain crest where the temperature is thus less. A closed circulation in the vertical is evident on the upwind face of the mountain formed by drainage flow under the cloud, ascent of the air at the upwind edge of the cloud where the drainage flow converges with the prevailing flow, and a recycling of this air to form a closed circulation. The streamline nearest the surface upwind of the mountain is forced over this circulation, passing almost 1000 feet above the ridge crest. It is clear that for this case the low level convergence of drainage flow and prevailing flow is a viable mechanism, in addition to the diffusion mechanism, for vertical transport of the seeding agent from near the surface to well above the ridge crest. Further investigations show that the closed circulation can occur under a wide variety of circumstances where the drainage flow opposes the prevailing wind. For a given stability condition at the surface, light prevailing winds allow the drainage flow to drive far upwind relative to the prevailing flow. For stronger prevailing winds the closed circulation becomes restricted to the steeper slopes and a strong enough wind will eliminate the slope wind entirely.

6.4.2 The Nighttime Case

At the mountain surface during nighttime conditions a strong flux of sensible heat to the surface can be expected for clear sky conditions, while a weak to moderate flux of heat to the surface can be expected in cloudy conditions.

Figure 6.4 shows streamlines for a stable (lapse rate 6.6°C Km^{-1}) nighttime situation simulating clear sky conditions, except for an orographic cloud over the mountain from 10 Km upwind to 2 Km downwind of

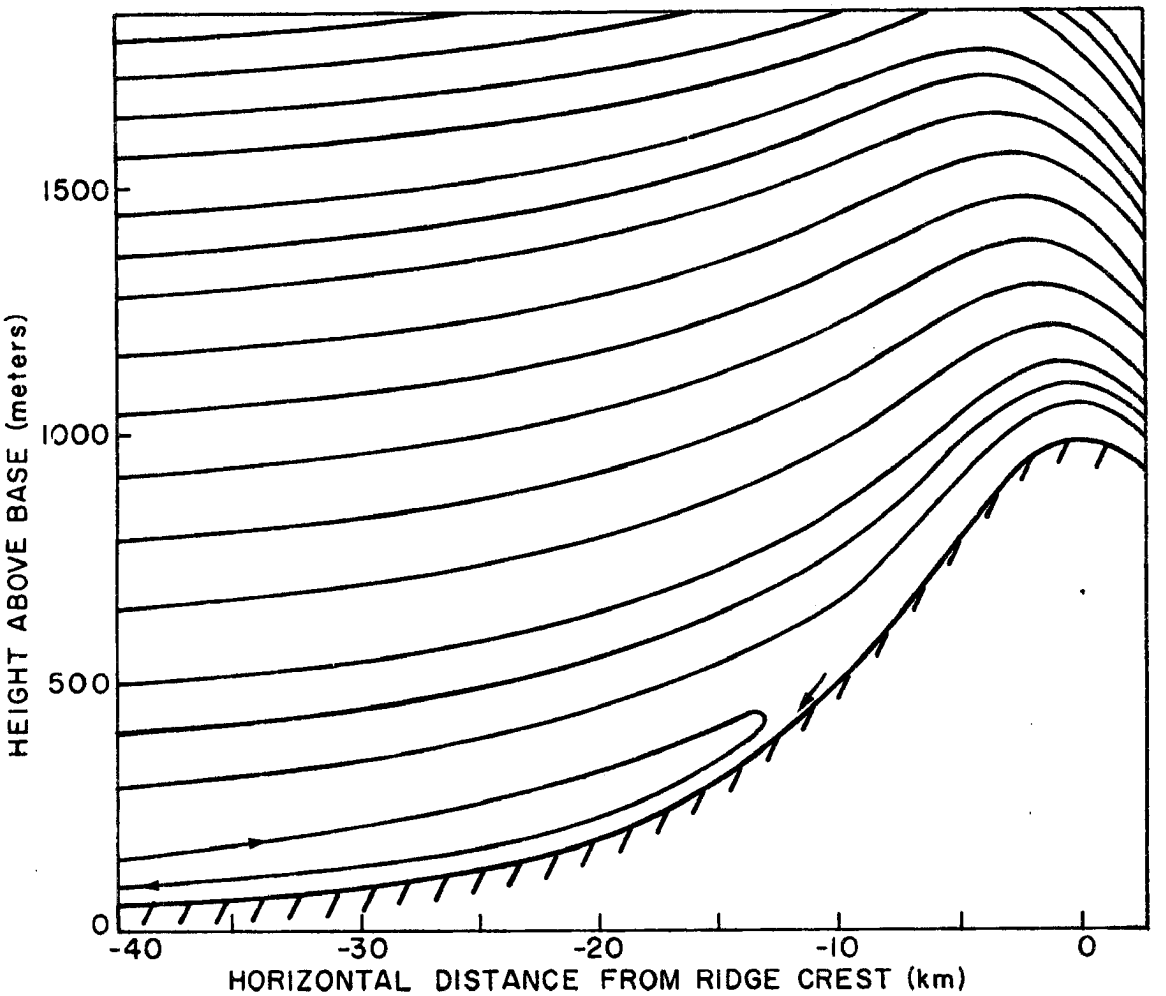

Figure 6.4. Streamlines of stable (6.6° C/km) stratification airflow for a nighttime orographic cloud situation, geostrophic wind 10 mps.

the crest. The initial surface potential temperature deficit is 20°K, consistent with the extreme inversions seen in clear sky nocturnal conditions. On the mountain surface under the cloud the temperature deficit is specified as only 5°K. On the upwind side of the mountain a shallow drainage flow is predicted which extends horizontally to the upwind boundary. This drainage flow averages 2 mps. There is strong evidence that such drainage flows frequently drive far upwind relative to the prevailing flow. Ice nucleus counts elevated above background have been observed upwind of Climax at Glenwood Springs on several occasions when the Climax seeding was in progress and a drainage wind was in evidence. Glenwood Springs is about 80 Km west and downstream of the Minturn seeding site employed for the Climax experiments. Such a drainage flow, because of its observed persistence, has the capability of being a mechanism for widespread transport of pollutants, and in particular ice nuclei, to produce effective seeding locations far from the physical site of the surface based seeding generator.

For nighttime cases where an extensive cloud deck is present the temperature deficit at the surface is less than for clear skies. A similar evolution of the low level wind regime with prevailing windspeed to that found for cloudy daytime case is found. That is, for low wind speeds a predominant drainage flow; for intermediate an eddy circulation on the steeper slopes of the upwind mountain face; and for strong wind speed an absence of any drainage flow.

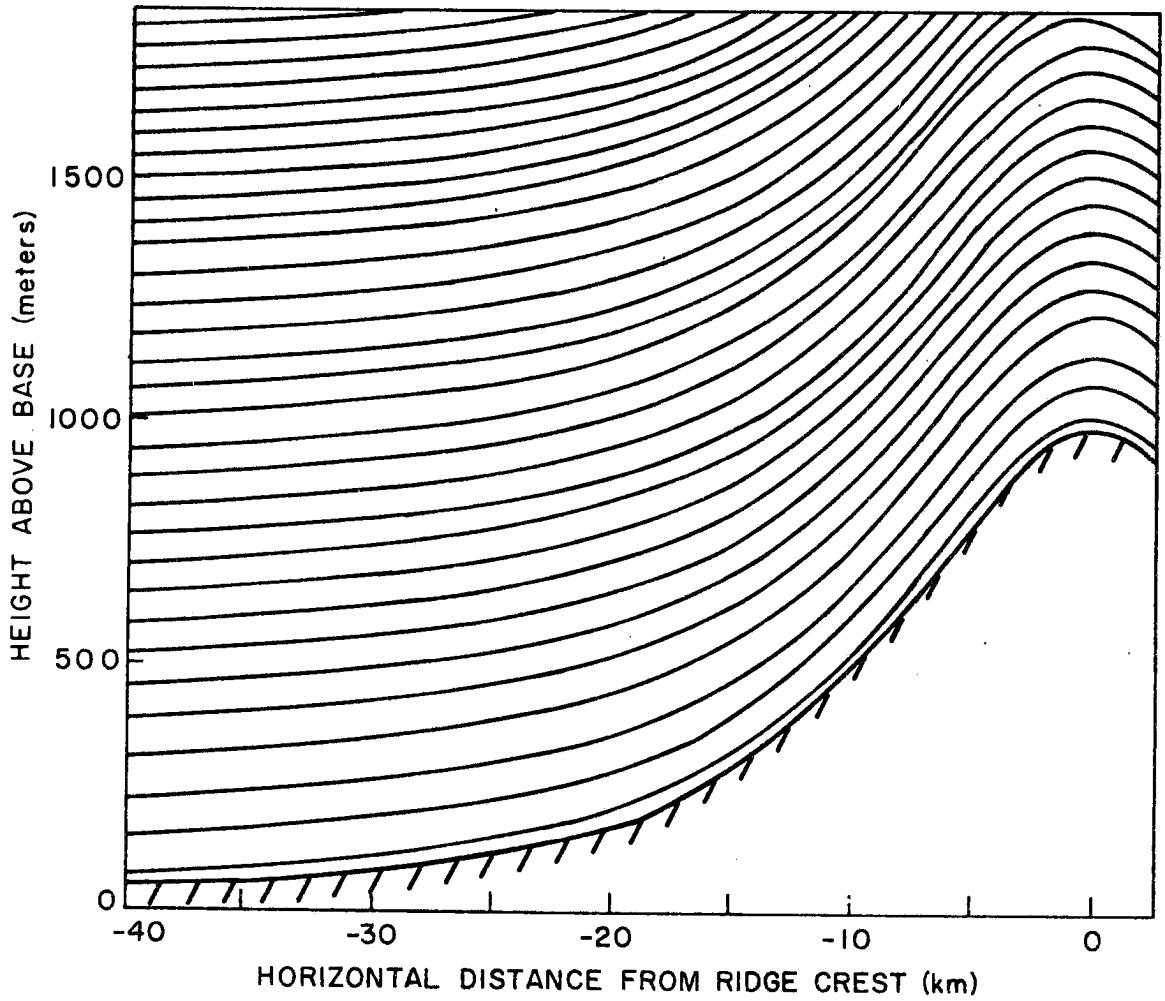

Figure 6.1. Streamlines of neutral stratification airflow over a mountain ridge for a case with geostrophic wind 10 mps.

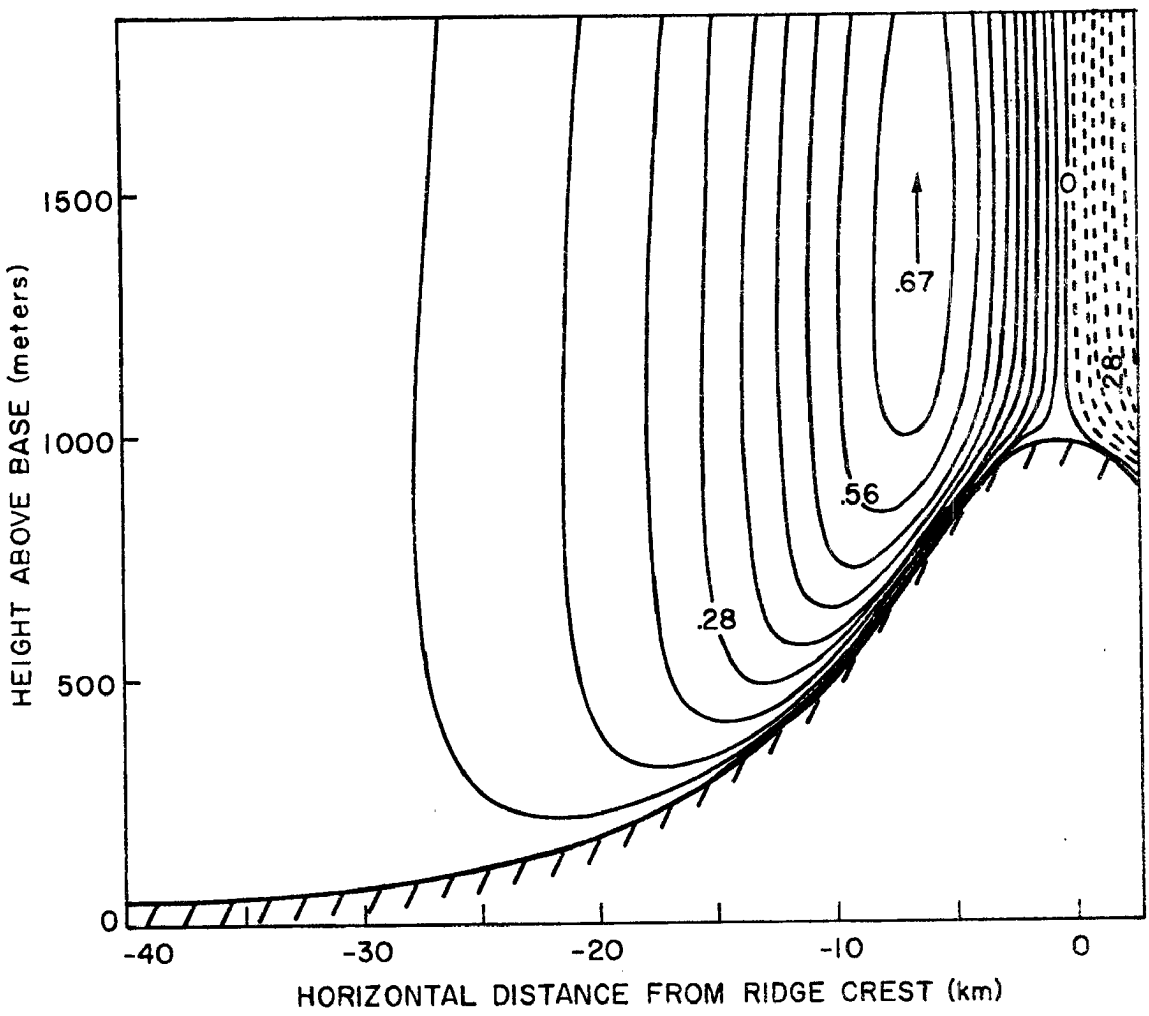

Figure 6.2. Isotachs of vertical velocity for the case of Figure 6.1.

CHAPTER SEVEN

MONTE CARLO METHODS FOR ATMOSPHERIC DISPERSION STUDIES

The Monte Carlo method is employed in an attempt to calculate dispersion by parameterization of the turbulence which leads to dispersion. If the turbulence is treated sufficiently realistically the dispersion will be accurately predicted. By contrast, eddy diffusivity theory is an attempt to parameterize the dispersion directly by analogy to molecular diffusion. The Monte Carlo method employs those flow parameters that can be resolved explicitly and a statistical representation of the flow properties at unresolved scales. This permits statistical treatment of a class of intermediate scale transport processes neither susceptible to efficient direct computation nor to a gradient transport parameterization.

The method is formulated in a Lagrangian frame so that it is easy to extend the treatment to account for other processes influencing dispersion such as inertia and gravitational settling. Processes such as radioactive decay, photo-deactivation, collection on and resuspension at boundaries, nucleation and growth of cloud droplets and ice particles can also be rather simply taken into account.

7.1 The Monte Carlo Method

Dispersion is the result of the action of a fluctuating wind on particles released in the atmosphere. Specification of the movement of such particles is achieved by specifying resolved and unresolved wind components. The resolved component is, by definition, given as a function of space and time explicitly. The unresolved components are

determined from physical-statistical models appropriate to the systems they represent.

With the wind thus specified a large number of particle trajectories are calculated. The volume of atmosphere of concern is divided into cells which are the smallest volumes for which concentration can be resolved. Total time all particles spend in each cell is proportional to concentration in that cell.

In practice, particle displacements are calculated for short time increments (Δt) and the number of increments (n_i) all particles spend in each cell of volume $DV_i = Dx \cdot Dy \cdot Dz$ accumulated. If the source strength is Q and total number of trajectories N, then the concentration C_i in cell i is given by

$$C_i = \frac{n_i \, Q\Delta t}{N \, DV_i}$$

The method gives minimum and maximum definable concentrations for $n_i = 1$ and $n_i \Delta t \approx N \, Dx_i/U$ respectively, where U is the mean wind speed, assumed constant in the x (along mean wind) direction. In any particular problem it is necessary to make a careful choice of the definable parameters to ensure that the concentration range of interest is covered.

For simple one-dimensional and homogeneous turbulence we saw in Chapter Two that the statistics required to specify the dispersion are the distribution of turbulent velocities and spectrum of turbulence. For general and fully three-dimensional turbulence, Lindberg and Thompson (1974) have shown how turbulence structure with specified spectral properties may be formulated in an Eulerian framework. From a practical viewpoint, even under the best of practical atmospheric

circumstances, only part of the data required for this formulation is available. Fortunately, it appears, as evidenced by the success of K theory, that for cases of practical interest only rather limited information regarding the turbulence is needed to adequately predict dispersion.

7.1.1 Specification of Component Winds

This division of the wind into resolved and unresolved components is one of convenience rather than fundamental. For global scales and long-term dispersion, synoptic scale systems have been treated as unresolved. Naturally, the smaller the scale cut-off of the resolved component the better will be the prediction. The statistical treatment of unresolved components will only approximate the truth. Deardorff (1972) has performed calculations resolving scales down to 10's of meters. The unresolved scales were then well in the inertial sub-range where the eddy diffusivity approximation is claimed to perform adequately. It can be hoped that by careful parameterization of various unresolved components, and for a considerably larger scale cut-off than employed by Deardorff, adequate dispersion predictions can be achieved. The parameterization is guided by physical studies of the properties of unresolved systems and facilitated by the Lagrangian nature of the Monte Carlo formulation.

The formulation of models of unresolved wind components is detailed in the next two sections. First the formulation for situations where K theory has given reasonable results, near neutral conditons, is given. This is essentially just the numerical application of Taylor's statistical treatment of homogeneous turbulence. Secondly, the situation of the

unstable boundary layer is investigated. A treatment of the unresolved convective plume effects is given in Appendix B.

7.2 Numerical Method for Statistical Simulation of Near Neutral Stability Condition Dispersion

Specification of the spectrum and distribution function of turbulent velocities does not give a complete representation of turbulent structure. Information such as the relative phases of the various spectral components is also needed in the general case. For the near neutral condition the information about the phases does not seem to be important. The problem is thus to simulate a velocity series with specified spectrum and distribution function for this case.

While it is quite possible to generate a series with a given general distribution and spectrum the process can require much computer time. For certain choices of spectrum and distribution function, turbulent velocities can be generated quickly.

In Chapter Two it was noted that turbulent velocities were distributed in a very nearly Gaussian manner. Given random deviates from a uniform distribution, fast computer algorithms such as the Box-Muller scheme are available for generation of random deviates from a Gaussian distribution. By neglecting non-normal distributions the sampling procedure can be speeded up with little loss in the representation of actual conditions.

Pasquill (1962) has shown that the exact shape of the spectrum is not important in defining the spread of pollutants, but rather the Lagrangian time scale is more significant. Accuracy in the magnitude of the Lagrangian time scale is, in turn, less important than accurate

specification of the turbulent intensity. For computational purposes a spectrum corresponding to a Lagrangian time correlation

$$R_L(t) = \exp(-t/T_L)$$

is convenient. The Lagrangian time scale can be calculated from the integral length scales found for the von Kármán spectra, for example, in the LO-LOCAT study.

The approximations above lead to an elementary equation for calculating turbulent velocities. Given a turbulent velocity at time t from a normal distribution $(0,\overline{u_i'^2})$, the turbulent velocity at time $t + \Delta t$, where $\Delta t << T_L$, is given by

$$u_i(t + \Delta t) = \alpha u_i(t) + \beta r$$

where r is a normally distributed random variable $(0,\overline{u_i'^2})$, α is given by $\exp(-\Delta t/T_L)$, and β is given by $(1 - \alpha^2)^{\frac{1}{2}}$. It is interesting to note that if $\overline{u_i'^2}$ varies in space and/or time the above formulation quite simply accounts for advection of turbulence.

The stability of concentration estimates will increase as the number of independent contributions to that estimate increases. For the particular Lagrangian time correlation used here the number of independent contributions is given by

$$n_{eff} = \frac{n_i(1 - \rho_1^2)}{(1 + \rho_1^2)}$$

where ρ_1 is the correlation for lag Δt. It is easy to see that if $\Delta t = T_L/100$, then very closely for each Lagrangian time scale length of trajectory there is one independent contribution.

To illustrate the validity of the Monte Carlo numerical scheme for almost the simplest case, consider dispersion from an infinite line source orientated normal to a uniform wind field along the y axis, and in a homogeneous turbulence field. This situation has an analytical solution for concentration

$$C(x,z) = \frac{Q}{U\sqrt{\pi}} \left[\frac{1}{2\sigma_z^2}\right]^{\frac{1}{2}} \exp\left(-\frac{z^2}{2\sigma_z^2}\right)$$

where for our choice of spectrum

$$\sigma_z^2 = 2\,\overline{w'^2}\,T_L\left[\frac{x}{U} - T_L + T_L \exp\left(-\frac{x}{UT_L}\right)\right]$$

if Q is the source strength and U the mean wind. Figure 7.1 compares the analytic and Monte Carlo numerical solutions for 500 trajectories, $U = 5$ m sec^{-1}, $Q = 10$ g sec^{-1}m^{-1}, $\overline{w'^2} = 0.1$ m^2 sec^{-2}, and $T_L = 100$ sec. Concentrations up to 3.5 km downwind of the source and 300 m vertically from the source axis were considered. Cells for concentration resolution were 100 m along the wind and 20 m vertically. A linear correlation coefficient of 0.997 between Monte Carlo and analytical concentrations was found. The deviation from 1.00 can be explained in that we employed only a small number of trajectories. Clearly, for most purposes the Monte Carlo method is adequate in this situation.

7.3 Numerical Method for Statistical Simulation of Dispersion in Energy Containing Eddy Fields

In simulating dispersion in more complex situations a simple description of the unresolved motions in terms of a spectrum function and velocity distribution may become insufficient because information on relative phases of different spectral components is ignored. This phase information may be retained most directly by explicit generation of

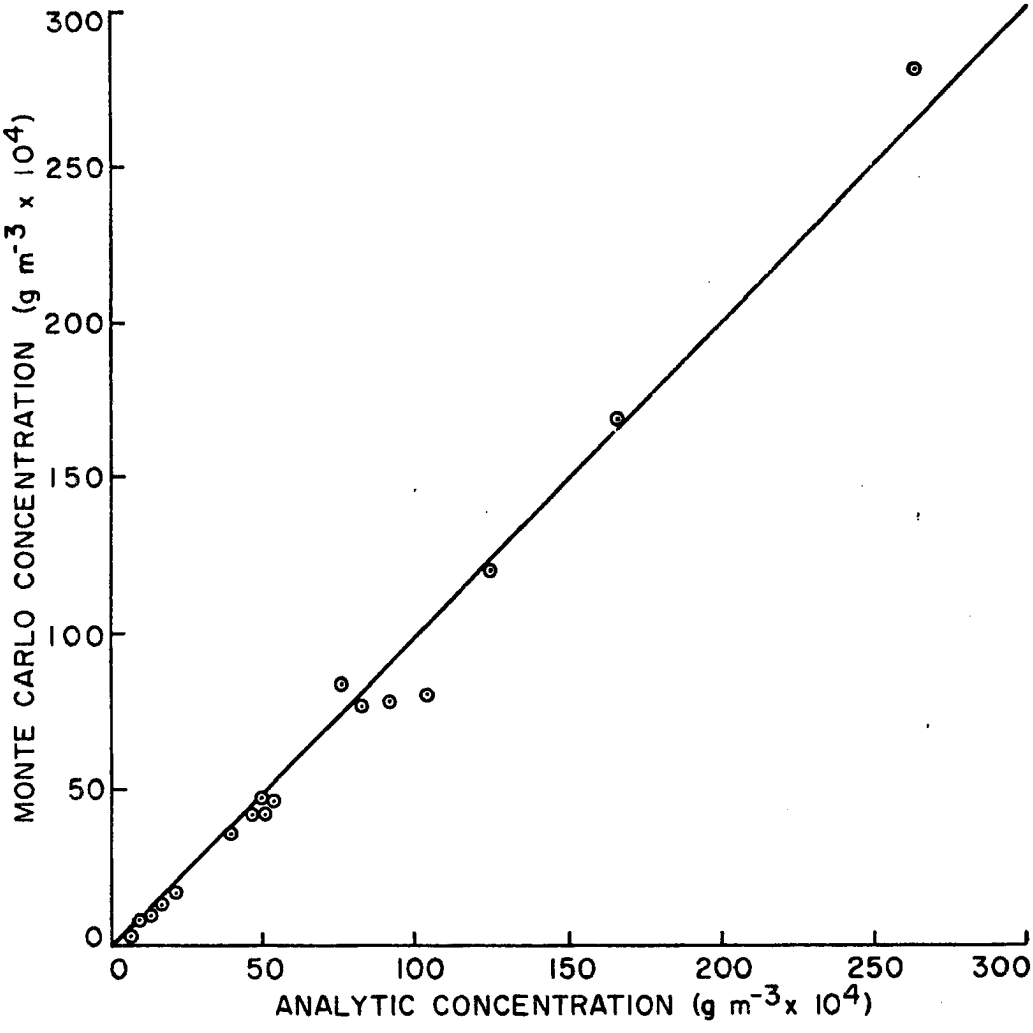

Figure 7.1. Comparison of Monte Carlo volume mean concentration with analytic concentration for Lograngian time scale 100 seconds.

winds given by a model of the significant, but unresolved, systems. An example of such a system, the convective plumes of the unstable boundary layer, is considered in Appendix B.

The appendix calculations show that some of the qualitative aspects of dispersion found in a physical simulation of the unstable planetary boundary layer, which cannot be explained by a rational application of the eddy diffusivity approach, can be explained employing the Monte Carlo approach. A more complete understanding of the physical nature of the convective plume field will be required before quantitative agreement can be expected.

7.4 Variance Reduction Techniques

It soon becomes apparent in attempting to apply this method to numerical simulation of an actual case that a tremendous amount of computer time is required. This becomes increasingly the case as the number of particles followed and downstream distance from the source increase, and wind speed and Lagrangian time scale decrease. A number of techniques have been devised to considerably speed up the simulation. Through skillful computer programming the techniques can be employed together to obtain optimum results.

7.4.1 Random Number Sharing

A considerable part of the time involved in computing trajectories is used in calculating the random numbers employed. By careful use of the same random number for different purposes a considerable saving can be effected. Consider the simple numerical simulation of turbulence as in the first example above, but in three dimensions. For each time step three random numbers are required to advance each of the three turbulent velocity components. However, by taking the particles in threes it is

possible to use only three random numbers to advance all three particles one time step. Thus, the first random number advances the u turbulent velocity component of the first particle, the v component of the second and the w component of the third. The second random number advances the v turbulent velocity component of the first particle, the w component of the second and the u component of the third. Likewise in rotation for the third random number.

7.4.2 Time Step Expansion for Quasi-Uniform Regions

We have noted before the Kampé de Feriet version of Taylor's equation

$$\sigma^2_{x_i}(t) = 2\,\overline{u_i'^2}\int_o^t (t-\tau)\,R_L(\tau)d\tau$$

Consider dispersion for a time t where $R(\tau)$ remains unity (the same turbulent velocity component is retained). It is easy to see that $\sigma^2_{x_i}$ can be equal to that for the $R(\tau)$ varying case only if an effective velocity variance $\overline{u_{i_{eff}}'^2}$ is defined to compensate. Thus

$$\overline{u_i'^2}\int_o^t (t-\tau)\,R(\tau)d\tau = \overline{u_{i_{eff}}'^2}\int_o^t (t-\tau)d\tau$$

If $R(\tau)$ is specified the integration can be performed. For the exponential decay case

$$\overline{u_{i_{eff}}'^2} = 2\frac{T_i^2}{t^2}\,\overline{u_i'^2}\left[\exp\left(-\frac{t}{T_L}\right)+\frac{t}{T_L}-1\right]$$

By choosing the turbulent velocity component from a Gaussian distribution with this reduced effective variance the time step can often be greatly increased as long as the resolved flow structure, statistics of

the other unresolved components, and statistics of this turbulence remain sensibly constant within the distance covered by the particle during this time. The technique is particularly helpful in cases where the Lagrangian time scale is short.

7.4.3 Cloning and Russian Roulette

The simple Monte Carlo method is inefficient because in order to define low concentrations many particles have to be followed through high concentration regions. To overcome this two methods have been devised. In cloning, particles which move into regions which have been identified in a previous run as low concentration regions are split into m particles, each carrying 1/m th of its weight in contributing to concentration. Each of these m particles is then followed as a separate entity. Particles moving into yet lower concentration regions may again be cloned as required.

The reverse process may also be applied to particles in regions of high concentration. Particles close together may be combined to give one or a few particles having a total weight the same as that of the contributing particles. These particles which remain are randomly selected and retain their previous velocities and positions. The other particles are eliminated. This process has been called Russian Roulette.

7.5 Disadvantages of the Method

There are a few disadvantages to the Monte Carlo method. Because of the statistical formulation, such that each particle moves in a flow field with the unresolved turbulence components independent in phase of those acting on a neighbor particle, the method as formulated here cannot predict instantaneous concentrations but only time means. Another problem, that is common to other parameterizations, is that adequate

data to quantify the parameterization is not currently available. Unlike the K parameterization, however, the parameters required in the Monte Carlo formulation are physically meaningful [Scorer (1972)]. Finally, the method is new and not formulated in a traditional differential equation format with which most workers in the discipline feel at ease.

CHAPTER EIGHT

A MOUNTAIN ENVIRONMENT DISPERSION SIMULATION

In this chapter the airflow model is incorporated with a parameterization of unresolved motions to produce predictions of pollutant concentrations as a function of space. The model of unresolved motions employed is outlined. Computational details are discussed. A number of case studies are used to elucidate the influence of various parameters on cloud seeding efficiency.

8.1 The Turbulence Model

In parameterizing the motions on unresolved scales which contribute to dispersion it is necessary to reluctantly admit that our knowledge of such scales of motion is inadequate to parameterize these in any manner other than as simple turbulence specified only by a turbulence velocity variance and time scale.

Even with the parameterization task simplified to this extent, it is still formidable. This is especially true because our region of interest is mountainous where the forcings are considerably more complex than over smooth terrain. In the smooth terrain case the surface frictional and thermal stresses are overwhelmingly restricted to the lower boundary. In mountainous terrain this is not the case, there are effective higher level sources such as from the sides of valleys and from cross-valley advection of turbulent air from ridge top to high levels above the valley floor. This problem has been recognized by Wooldridge (see figure 2.8) who displayed eddy diffusivity variation as a function of height scaled by valley depth.

The turbulence model adopted here is based solely on observational data from the LO-LOCAT project discussed in Chapter Two. This does scant justice to the complexity of the situation, but does insure that the values employed are reasonable for the terrain considered as only values found in wind-conforming flights near Climax were considered.

Tabulations of LO-LOCAT flight data made during the winter months over the mountains west of Colorado Springs and just east of our area of interest in this research, were examined. A total of 78 legs of 4 1/2 minutes each were found where the aircraft heading was within 20° of directly upwind or downwind. This resulted in a rather small data set to perform stratifications upon, particularly for the L_{u_i} parameter which was calculated for only 33 of these cases.

Jones et al. (1970) concluded that the von Kármán spectra were the best fit to their experimental data. They noted that the scale length is influenced by surface roughness and altitude. Gunter et al. (1969) found an influence of stability on scale length at the higher altitudes. Except for very stable conditions the scale length was nearly constant with height. The evidence from the wind conforming subset is not convincing for any systematic variations. As can be seen in table 8.1, the most noticeable feature is the noise. The best descriptors are L_u = 260m, L_v = 190m, L_w = 135 m.

A preliminary test of the model showed that the directional variation made only very minor changes in the result from assuming a constant scale length applicable to all directions. The difference found was within the noise level of the Monte Carlo method. A constant value of L = 200 meters was used in all the following case studies. This is transformed to a time scale using the Taylor frozen turbulence

STABILITY	HEIGHT RANGE	L_u	L_v	L_w
VERY STABLE	250	158 (14) 2	217 (98) 3	99 (22) 2
	750	286 (169) 4	241 (124) 3	154 (83) 2
STABLE	250	258 (88) 8	179 (43) 8	156 (47) 8
	750	224 (57) 5	216 (85) 5	131 (10) 4
NEUTRAL	250	267 (75) 5	182 (45) 5	107 (19) 4
	750	259 (59) 2	162 (15) 2	141 (10) 2
UNSTABLE	250	298 (15) 2	184 (15) 2	112 (9) 2
	750	253 (77) 3	140 (26) 3	151 (56) 3

Table 8.1. Von Karman integral scale lengths (meters) (standard deviation of scale lengths), and number of samples in each category. Wind conforming sub-set of LO-LOCAT phase III data collected over high mountain terrain west of Colorado Springs, Colorado during winter months. All flights below 1000 ft AGL classified as nearer 750 ft or 250 ft AGL.

Very Stable $\equiv$ Lapse Rate $>$ -2°F/1000 ft
Stable $\equiv$ -2°F/1000 ft $<$ Lapse Rate $\leq$ -5°F/1000 ft
Neutral $\equiv$ -5°F/1000 ft $<$ Lapse Rate $\leq$ -6°F/1000 ft
Unstable $\equiv$ -6°F/1000 ft $<$ Lapse Rate

STABILITY	σ_u	σ_v	σ_w
VERY STABLE	1.02 (0.31) 19	1.12 (0.28) 19	0.93 (0.29) 19
STABLE	1.39 (0.52) 26	1.57 (0.70) 26	1.35 (0.44) 26
NEUTRAL	1.66 (0.48) 22	1.71 (0.64) 22	1.49 (0.39) 22
UNSTABLE	1.68 (0.76) 11	1.65 (0.63) 11	1.51 (0.43) 11

Table 8.2. Turbulent velocity rms values (meters/second), (standard deviation of the rms value), and number of samples as a function of stability. Data from the wind conforming subset of LO-LOCAT phase III data collected over high mountain terrain west of Colorado Springs, Colorado, during winter months. Flights below 1000 ft AGL. See Table 8.1 for definition of stability categories.

assumption with a mean wind for the case and employing a constant value of the parameter β equal to four in the expression

$$T_L = \frac{L\,\beta}{\bar{U}}$$

Turbulent velocity RMS values were found to be greater for rougher terrain, at low altitude, and for more unstable conditions in the LO-LOCAT data set. The effect of altitude was not significant for the rough terrain cases. Pritchard (1966) gives somewhat similar conclusions. Table 8.2 shows the effect of stability for the wind conforming LO-LOCAT subset. The important influence of decreasing stability increasing the turbulent velocity RMS values is clear. LO-LOCAT also found that increasing wind speed was accompanied by increasing levels of turbulence, but this was a less significant effect than that of stability and could not be adequately defined for the wind conforming subset. The turbulent velocity variances were parameterized as functions of stability only. The regression equations

$$\ln \sigma_u = -0.058 + 0.053\gamma$$

$$\ln \sigma_v = 0.133 + 0.033\gamma$$

$$\ln \sigma_w = -0.112 + 0.050\gamma$$

were found, where γ is the lapse rate of temperature in °C Km^{-1} and the turbulent velocity variances are in m^2 sec^{-2}.

8.2 Application

In application to a specific situation the airflow model is first run to the required stage using the upwind sounding and surface forcing appropriate to the situation. The results of this computation are saved. Only gridpoint values of the various parameters are available. In running the Monte Carlo simulation, values everywhere in the region

are required. The method for interpolation of the gridpoint values which gave the smoothest fields, while still agreeing with the gridpoint data, was found to be interpolation using bi-splines under tension. Still greater accuracy was achieved when the logarithm of height was used in the interpolation. This method has the additional advantage of being quite rapid compared to other methods tried.

It was previously noted that the Monte Carlo method has minimum and maximum resolvable concentrations. The task of calculating concentration of artificial ice nuclei is considerably more demanding than that of calculating the gram concentration of the seeding agent. This is because the same gram concentration has a greater effect as an ice nucleant the lower the temperature, figure 4.3. Define the range 10 to 100 IN per liter as the effective range of concentrations for seeding. When the effect of temperature is considered this implies that for a range of temperatures of interest from -8°C to -14°C a gram concentration range of 2.9×10^{-9} to 7.3×10^{-12} g m^{-3} must be resolved. A seeding rate of 10 g hr^{-1} is employed so the criteria given in section 7.1 can be met by adapting cells of dimension Dx = 1000 m, Dy = 100 m, Dz = 100 m with 1800 particle trajectories calculated and the timestep varying from 20 seconds for the 15 mps geostrophic wind case to 60 seconds for the 5 mps case.

8.3 Case Studies

In the following sections case studies of seeding concentrations for a variety of different situations are presented. Because of uncertainties in the representativness of the model conditions compared to actual atmospheric conditions and particularly the statistical fluctuations inherent in the Monte Carlo method the values given below,

particularly areas subject to seeding, should be regarded as estimates only. The trends however can be considered reliable and it is these which will be the prime concern.

8.3.1 The Daytime Situation

For simulating the daytime situation a strictly neutral stratification flow is considered. The surface heat fluxes are usually quite small during this time of the day and for conditions where clouds are present a similarity between the model dry, neutral stratification airflow and moist-adiabatic flow conditions can be expected. Table 8.3 shows the area at cloud base subject to inflowing air with various concentrations of ice nuclei active. The situation treated here is one where the seeding generator is 40 Km upwind of the ridge crest and the effective source height is 10 meters above the surface. The effective source is considerably higher than the physical source owing to the buoyancy of the generator effluent. Geostrophic wind speed cases of 15, 10 and 5 mps are shown. The countervailing actions of cloud base becoming more remote from the source tending to decrease concentrations, and lower temperatures for higher cloud bases, are evident.

For the 5 mps geostrophic windspeed case table 8.3 shows little change in area seeded with height, except that a notable decrease in area is seen at the 300 m above crest level. Area subject to overseeding shows the same trend with notable decreases in area starting at lower altitudes. Detailed examination of the concentrations for this case shows that concentrations sufficient for seeding are confined to within about 15 Km downwind of the generator. The seeding agent disperses to below effective seeding levels by the time it has travelled this short distance.

Cloud Base Altitude Relative to Crest Altitude(m)	Cloud Base Temperature (°C)	Neutral 15 mps		Neutral 10 mps		Neutral 5 mps	
		OSI	SEI	OSI	SEI	OSI	SEI
-100	- 8	-	0.9	-	0.9	-	0.9
	-10	0.3	58.7	0.1	89.4	0.5	41.8
	-12	6.7	77.3	13.9	109.9	11.4	67.4
	-14	24.2	70.5	52.7	88.4	23.7	77.1
0	- 8	-	-	-	-	-	-
	-10	-	37.9	-	80.2	-	41.2
	-12	1.7	72.2	3.7	118.0	9.8	69.1
	-14	10.1	77.3	32.0	107.6	21.7	76.8
100	- 8	-	-	-	-	-	-
	-10	-	15.0	-	54.7	-	39.1
	-12	-	51.0	0.2	107.5	7.0	67.3
	-14	1.1	68.2	10.2	118.8	19.5	72.5
200	- 8	-	-	-	-	-	-
	-10	-	4.7	-	33.6	-	35.3
	-12	-	26.3	0.1	90.3	5.5	61.3
	-14	0.2	46.2	4.2	107.7	15.0	74.9
300	- 8	-	-	-	-	-	-
	-10	-	1.2	-	19.0	-	31.9
	-12	-	14.5	-	69.3	2.1	59.5
	-14	-	28.5	1.9	92.2	12.3	67.0

Table 8.3. Seeding Efficiency Index (SEI) (Area, Km^2, at cloud base with inflow concentrations 10 to 100 IN per liter) and Overseeding Index (OSI) (Area, Km^2, at cloud base with inflowing concentration greater than 100 IN per liter) for neutral stratification and various prevailing windspeed.

The intermediate, 10 mps geostrophic, windspeed case shows the largest areas subject to seeding, but with overseeding only significant at the lower altitudes. The effect of turbulent diffusion is balanced by the rise in the surface terrain height as the crest is approached to keep nearly the same concentrations at cloud base for considerable regions between the generator and ridge crest.

The 15 mps windspeed case allows only a short transit time between the generator and ridge crest. The plume remains "tight" so that a smaller area is subject to seeding than at the same altitude in the 10 mps case. Highest concentrations at any altitude above the crest are found near and over the crest.

Table 8.4 shows area subject to seeding and overseeding for an overall neutral stratification, 10 mps geostrophic wind case, but considering the effect of reducing the radiation input to the surface under an orographic cloud hanging over the upwind slope of the mountain. The first case in the table is the strictly neutral case, reproduced from table 8.1 for comparison purposes. The second case is for the surface potential temperature under the cloud 2°K less than the initial potential temperature of the air in contact with the surface. Generally somewhat smaller areas subject to seeding, and overseeding, are evident at all levels. When the temperature deficit under the cloud is reduced one more degree the areas subject to seeding, and overseeding, are increased over those found in the neutral case. Examination of the flow solution for this case indicates a drainage flow situation, similar to that in figure 6.3, so that low level convergence is forcing a vertical transport of seeding agent in addition to that due to turbulent dispersion and orographic lift.

Cloud Base Altitude Relative to Crest Altitude(m)	Cloud Base Temperature (C°)	Neutral 10 mps		Neutral Stable T-2 10 mps		Neutral Stable T-3 10 mps	
		OSI	SEI	OSI	SEI	OSI	SEI
-100	- 8	-	0.9	-	0.9	-	0.4
	-10	0.1	89.4	0.3	77.6	0.1	91.0
	-12	13.9	109.9	9.8	106.9	20.6	119.7
	-14	52.7	88.4	41.2	91.7	49.5	112.5
0	- 8	-	-	-	-	-	-
	-10	-	80.2	-	66.5	-	77.1
	-12	3.7	118.0	2.4	108.2	10.9	119.6
	-14	32.0	107.6	23.6	107.1	39.3	115.0
100	- 8	-	-	-	-	-	-
	-10	-	54.7	-	43.0	-	66.2
	-12	0.2	107.5	0.5	93.4	4.3	114.1
	-14	10.2	118.8	8.6	105.6	26.6	116.8
300	- 8	-	-	-	-	-	-
	-10	-	19.0	-	19.1	-	41.4
	-12	-	69.3	-	62.3	-	97.0
	-14	1.9	92.2	1.3	81.9	6.8	117.8
500	- 8	DATA		-	-	-	-
	-10			-	5.3	-	15.6
	-12	MISSING		-	34.1	-	65.1
	-14				55.4	0.7	93.9

Table 8.4. Same as table 8.3 except for initial temperature on the upwind face of the ridge 0, 2 and 3°C cooler than the air above it, 10 mps prevailing windspeed. This simulates daytime conditions with an orographic cloud present.

In summary of these results for daytime conditions, the countervailing actions of lower concentrations at higher altitudes and lower temperatures at higher altitudes are evident. The variation of seeding concentration at a given altitude is dependent on the compensation between the rate at which the turbulent dispersion proceeds and the rate at which the higher concentrations nearer the surface are forced to that altitude as the terrain underneath rises to the ridge crest. Higher windspeeds (10 to 15 mps) are indicated as optimal for seeding lower based clouds and lower windspeeds (5 to 10 mps) for higher based cloud in this neutral stratification. If the energy balance on the side of the mountain is modified, such as by shielding by an orographic cloud to introduce local low level stability, the area subject to seeding is at first reduced owing to the poorer vertical spreading. Somewhat greater cooling induces a downslope drainage flow which promotes vertical transport of seeding agent at the upwind edge of the cloud where the drainage flow converges with the prevailing flow.

8.3.2 The Nighttime Situation

Under clear night skies the mountain snow-covered surface radiates away energy rapidly and strong surface-based inversions are formed. The dynamic simulation of such a situation yields persistent drainage flow as shown in Chapter Six. Based on the thermal stratification predicted by the flow model and the parameterization of turbulent velocity variances adopted, it is unlikely that any important quantity of pollutant could move vertically by turbulent diffusion to above a strong surface based inversion. Thus no cloud seeding effect can be expected in such a situation, and this evidence is sufficiently clear that it would be fruitless to run a Monte Carlo simulation for this case.

A seeding effect similar to daytime is found, however, for nighttime hours at Climax so it must be that a vertical transport does occur. Of course, during conditions under which seeding will occur there is, hopefully, an orographic cloud to seed and the cloud will substantially modify the stability at the surface. Strong surface based inversions are not found under cloudy skies.

Table 8.5 shows the Monte Carlo model estimate of areas subject to seeding, and overseeding, for overall neutral stratification except stable near the surface by 3°K relative to the initial temperature. Calculations for 10 and 15 mps geostrophic wind cases are shown, and the equivalent areas for strictly neutral conditions from table 8.3 included for comparison.

The most interesting feature of these results is that, despite the decreases in turbulence levels which accompany the stable low level stratification cases, appreciable quantities of seeding agent can still rise to above typical cloud base heights. Cloud base areas subject to seeding, although generally less than for the corresponding neutral stratification case, are still substantial. A reasonable explanation for this is that the stable cases have considerably lower wind speed than the neutral cases in the lowest 100 meters due to the enhanced drag, and so the travel time to the crest is greater in these stable cases. This additional time for dispersion is apparently sufficient to counterbalance to a considerable extent the reduction in turbulent velocity variances and allow seeding agent to move to higher altitudes in effective concentrations. The additional mechanism of low level convergence between drainage flow over the steeper part of the mountain

Cloud Base Altitude Relative to Crest Altitude (m)	Cloud Base Temperature (C°)	Neutral 10 mps		Low Level Stable, T-3 10 mps		Neutral 15 mps		Low Level Stable, T-3 15 mps	
		OSI	SEI	OSI	SEI	OSI	SEI	OSI	SEI
-100	- 8	-	0.9	-	0.4	-	0.9	-	0.5
	-10	0.1	89.4	0.1	23.0	0.3	58.7	0.1	47.9
	-12	13.9	109.9	4.1	54.6	6.9	77.3	9.9	64.2
	-14	52.7	88.4	8.6	73.4	24.2	70.5	22.8	63.6
0	- 8	-	-	-	0.2	-	-	-	0.2
	-10	-	80.2	0.1	20.8	-	37.9	-	39.8
	-12	3.7	118.0	4.3	49.1	1.7	72.2	5.6	65.7
	-14	32.0	107.6	8.9	67.4	10.1	77.3	16.7	65.7
100	- 8	-	-	-	0.1	-	-	-	-
	-10	-	54.7	-	16.2	-	15.0	-	30.7
	-12	0.2	107.5	3.6	40.3	-	51.0	3.8	55.0
	-14	10.2	118.8	7.2	55.2	1.1	68.2	12.0	60.8
300	- 8	-	-	-	-	-	-	-	-
	-10	-	19.0	-	14.1	-	1.2	-	19.3
	-12	-	69.3	1.7	36.8	-	14.5	0.3	44.8
	-14	1.9	92.2	6.0	51.0	-	28.3	5.3	54.7
500	- 8	DATA		-	-	DATA		-	-
	-10			-	12.7			-	7.6
	-12	MISSING		0.4	31.0	MISSING		-	24.8
	-14			3.8	44.1			1.0	40.3

Table 8.5. Same as table 8.3 except for initial temperature 0 and 3°C cooler than the air above it, 10 and 15 mps prevailing windspeed case. This simulates a cloudy nighttime condition.

side and prevailing flow over the shallower slope up-wind leading to a forced vertical transport is found for the 10 mps low level stable case.

Overall, these experiments for low-level stable stratification show similar trends to those for neutral stratification. For strong nocturnal inversions, such as can be found under clear skies, the inversion can frequently trap all seeding agent near the surface. However, for cloudy nighttime situations where the inversions at the surface are weak significant vertical dispersion is indicated. The prime controlling factor appears to be windspeed as for the neutral case. There is an indication that the optimum windspeed for stable stratifications is higher than for the neutral stratification.

The model studies in this chapter have important implications for air pollution studies. Conditions most favorable for accumulation of pollutant are clear sky, light wind, nocturnal conditions. Less accumulation of pollutant can be expected for stronger wind situations and for cloudy sky nocturnal or clear sky daytime situations. The optimum location for a pollution source within a mountain environment as far as dispersion is concerned would appear to be ridge crest where the occurrence of trapping inversions will be a minimum. Another good location would be an open park area where drainage flows and associated low level stability can be most easily overcome by stronger prevailing winds.

CHAPTER NINE

SUMMARY AND CONCLUSIONS

The overall objective of this research has been to improve the understanding of the physical processes contributing to, and so ability to predict, dispersion in mountainous terrain. In particular the understanding of the transport and dispersion of seeding agent from a ground based seeding generator to a cold orographic cloud has been a motivation. In the following section the research is summarized, and the general conclusions and the specific conclusions from each facit of the research noted. These specific conclusions are then integrated in the form of a conceptual model of orographic cloud seeding which emphasizes the role of windspeed. Finally suggestions for additional research are made.

9.1 Summary and Specific Conclusions

This research shows that there is normally a strong diabatic control of the low level mountain valley airflow in the Eagle River valley northwest of Climax, Colorado. For cloudy conditions, of interest in orographic cloud cases, this control is less marked. Dispersion of cloud seeding agent from the surface to cloud base is enhanced by the radiative suppression of strong inversions and low level airflow convergence aiding the vertical transport. Based on statistical studies of the Climax orographic cloud seeding experiment and a model simulation, including use of a promising new Monte Carlo dispersion prediction technique, the important parameters governing dispersion of seeding agent to the orographic cloud are generator location and wind speed.

Climatological studies of the surface wind regime in the Eagle River Valley to the northwest of Climax were undertaken. The wind regime in this valley follows the archetype diurnal pattern for the most part, with downslope flow during the night and upslope flow during a few hours of the daytime. The downslope flow tends to be superseded during strong prevailing northwesterly flow situations when cloud is present by an upslope flow.

Field studies of the transport and dispersion regime were conducted in the valley northwest of Climax for northwesterly flow situations during the winters of 1973-74 and 1974-75. Cases tended to be more stable than is typical for storm conditions, showing considerable downslope drainage flow which dispersed the tracer many kilometers upwind relative to the prevailing flow. These drainage situations also trapped the tracer at low levels within the valley so that it persisted for many hours at these levels after the release had been terminated. A case study with northwesterly flow performed just after a storm had ended indicated that seeding agent released from the surface could rise rapidly above the stable lower levels to typical cloud base heights. There was some indication that this process can be aided by the occurrence at low levels of convergence between drainage flow over the steeper slopes and prevailing synoptic flow over the shallower slopes.

Ten years of a randomized seeding experiment on orographic clouds, the Climax experiment, provide a substantial data set with which to infer some of the dispersion characteristics, although, these are considerably confounded with the other processes occurring. It should be remembered that these are strictly post hoc analyses. The very fact that numerous seeding effects are observed with a high degree of

confidence in the precipitation record is evidence that seeding agent is being dispersed to the cloud, and in sufficient quantity with timeliness to have an effect on the precipitation. The Climax precipitation data show that the target precipitation efficiency is naturally high for 700 mb windspeed cases less than 8 mps. For warm temperature cases seeding reduces this efficiency for northwest flow, but increases it for southwest flow. Moderate windspeed cases show the most significant seeding effect on precipitation, particularly the 12 to 14 mps 700 mb speed category. Higher windspeeds appear to yield precipitation decreases on seeding. Finally, there is no apparent diurnal effect of seeding on precipitation.

A flexible Monte Carlo dispersion model has been developed and applied within the environment of the University of Virginia two-dimensional dry mesoscale model for airflow over a mountain ridge. Ice nuclei in concentrations adequate for seeding are indicated at cloud base for environmental conditions considered representative of the Climax area in northwest flow. Simulations show that, with seeding from a surface based generator, the area at cloud base fed by inflowing air with artificial ice nuclei concentrations in the effective seeding range changes with wind speed and low level stability. For neutral stratification a 10 mps geostrophic wind gives greater cloud base area seeded than either 5 mps or 15 mps. For stable conditions near the surface, such as would be encountered in an orographic cloud situation, maximum area seeded appears to occur at somewhat higher geostrophic wind speed. The mechanism of low level convergence between down-slope and prevailing flow forcing vertical transport appears in the model simulations for conditions not unlike those observed in the field.

9.2 A Conceptual Model of the Orographic Cloud Seeding Process

In figure 3.1 a schematic representation of the orographic cloud seeding process was given. Chappell (1970) has demonstrated the critical nature of the ice crystal growth stage occurring between t_1 and t_2, namely that the cloud must be relatively warm so that the natural precipitation mechanism is inefficient and can be made more efficient by the addition of artificial ice nuclei. In this section the critical nature of the transit time from the generator to the ridge crest is expounded. The transit time is primarily governed by the wind speed and the distance from the generator to the crest. The contribution of this, admittedly crude, conceptual model lies in its ability to integrate the observations with the model simulations in a consistent manner.

Based on the Monte Carlo dispersion simulation for neutral stratification an artificial ice nucleant released from the ground can reach cloud base at ridge crest height in concentrations significant for seeding in a minimum of about 1000 seconds transit time downwind from the generator. Based on the equations of Hobbs et al. (1973) an unrimed planar crystal of 0.05 cm radius can grow in an environment typical of that at Climax in about 500 seconds transit through the cloud. Crystals this size are typical, weighted for contribution to precipitation, of those found at Climax under seeded conditions. Of the total transit time then, only 1500 seconds approximately is required for the first two phases. The final phase is that of settling of the crystal, without additional growth, to the surface against the orographic uplift. If the barrier is 1000 meters high and rises to this height over a 30 Km distance, the mean vertical velocity imposed by the terrain is 17, 33, and 50 cm sec^{-1} for the 5, 10, 15 mps prevailing wind speed cases

respectively. Estimates of the terminal velocity of a 0.05 cm crystal vary from 30 to 70 cm sec^{-1}. Using these two extremes of velocity the distance that a 0.05 cm radius crystal could fall during the remainder of the transit time is 845 to 3445 meters for the 5 mps case, less than 925 meters for the 10 mps case, and less than 233 meters for the 15 mps case.

Consider the high wind speed case. The Climax statistical experiment showed that these clouds are naturally not very efficient, and that seeding is likely to decrease this efficiency at the target. These observations can be understood in that seeding is indicated not to be effective for cloud base higher than 250m above ridge crest in these conditions, the ice crystals having only slight net fall velocity relative to the surface. Further, much of the area at cloud base subject to the seeding agent is overseeded for this case and so precipitation decreases can be expected.

Moderate wind speed cases showed the maximum seeding effect at Climax, although again natural precipitation efficiency was not high at the target. The lowest one Km above ridge top is subject to effective seeding, and a large part of the moisture flux over the barrier is found in this lowest kilometer. However, a large area at cloud base is subject to such effective seeding concentrations for these conditions.

Low wind speed conditions offer the most complex situation. Precipitation efficiencies at the target are naturally high and seeding reduces these efficiencies for warm, northwest flow cases at Climax. The high natural precipitation efficiencies are likely due to the action of ice crystals formed at high levels in the cloud having a considerable time to fall through the lower layers and collect their moisture,

falling to the surface upwind of the crest. The dispersion simulation for this case showed seeding agent lofted high into the cloud only a few kilometers downwind of the generator. This must considerably enhance the competition for moisture and smaller ice crystals than natural can be expected to form. Because these have smaller terminal velocity they stand more chance of being blown over the barrier. An additional factor also may be effective. There is considerable area in this low wind speed case between the ridge crest and the area subject to effective seeding concentrations which is subject to seeding concentrations too low for effective seeding. Without seeding occurring these levels provide the moisture which is collected by ice crystals from higher levels. With seeding this moisture can remain uncollected as only a few ice crystals aloft grow large enough to fall to these levels upwind of the crest.

It is clear that the dispersion regime associated with orographic airflow is the crucial factor causing the marked variation of cloud seeding effect with wind speed at Climax in northwesterly flow, and likely the cause of similar wind speed effects found in the Wolf Creek, Bureau of Reclamation Pilot Project, and Bridger Range seeding experiments.

9.3 Suggestions for Further Research

The results of this study, in particular the effect of wind speed on the dispersion, are dependent on the flow regime and turbulence parameterization adopted. These should be improved. Particularly, a number of three-dimensional airflow models are becoming available and, in time, it should become feasible to run these on a fine enough grid to model the flow in the Climax region. The parameterization of turbulence

velocity should be placed on a more solid base with more extensive field observations of turbulence in mountainous terrain. New basic research is needed on the structure and development of mountain valley inversions.

The statistical results found in this study need to be tested on an independent data set. Finally, future orographic cloud statistical experiments should emphasize the routine collection of as much auxillary meteorological data as possible, such as ice nucleus counts, low level wind flow, radiosonde data at frequent intervals, cloud information, acoustic sounder data, ice crystal type and size, etc, etc.

REFERENCES

Benjamin, T.B., 1968: Gravity Currents and Related Phenomena. J. Fluid Mech., 31(2):209-248.

Bergen, J.D., 1967: Some Aspects of Cold Air Drainage on a Forested Mountain Slope. Colorado State Univ., Dept. of Atmospheric Science, Ph.D. Dissertation, 188 pp.

Bergeron, T., 1949: The Problem of Artificial Control of Rainfall on the Globe. 1. General Effects of Ice-Nuclei in Clouds. Tellus, 1(1):1-12.

Burns, A. and C.K. Rider, 1965: Project Topcat: Power Spectral Measurements of Clear Air Turbulence Associated with Jet Streams. Royal Aircraft Establishment. Tech. Rept. No. 65210.

Businger, J.A., J.C. Wyngaard, Y. Izumi and E.F. Bradley, 1971: Flux-Profile Relationships in the Atmospheric Surface Layer. J. Atmos. Sci., 28:181-189.

Cross, C.M., 1950: Slope and Valley Winds in the Columbia River Valley. Bul. Amer. Met. Soc., 31(3):79-84.

Deardorff, J.W., 1972: Numerical Investigation of Neutral and Unstable Planetary Boundary Layers. J. Atmos. Sci., 29:91-115.

_____, 1974: Three-Dimensional Numerical Study of the Height and Mean Structure of a Heated Planetary Boundary Layer. Bound. Layer Meteor., 7:81-106.

_____, and G.E. Willis, 1975: A Parameterization of Diffusion into the Mixed Layer. J. Appl. Met., 14:1451-1458.

Deaven, D.G., 1974: A Solution for Boundary Problems in Isentropic Coordinate Models. Pennsylvania State Univ., Ph.D. Dissertation, 136 pp.

Defant, A., 1933: Der Abfluss Schwerer Luftmassen auf geneigtem Boden, nebst einigen Bemerkungen zu der Theorie stationärer Luftströme; Sitzungberichte der Preuss. Akad. Wiss. Phys.-Math. Klasse, XVIII(3):624-635.

_____, 1949: Zur Theorie der Hangwinde, nebst Bemerkungen zur Theorie der Berg-und Talwinde. Arch. Meteorol. Geophys. Bioklim., Ser. A, 1:421-450.

Flohn, H., 1969: Local Wind Systems in World Survey of Climatology. Volume 2. Elsevier Publishing Co., New York, 266 pp.

Fraser, A.B., R.C. Easter and P.V. Hobbs, 1973: A Theoretical Study of the Flow of Air and Fallout of Solid Precipitation over Mountainous Terrain: Part I. J. Atmos. Sci., 30:801-812.

Gal Chen, T., 1973: Numerical Simulation of Convection with Topography. Columbia Univ., Faculty of Pure Science, Ph.D. Dissertation, 170 pp.

Gleeson, T.A., 1953: Effects of Various Factors on Valley Winds. J. Met., 10:262-269.

Grant, L.O., 1963: Indications of Residual Effects from Silver Iodide Released into the Atmosphere. Proc. Western Snow Conference, 109-115.

_____, C.F. Chappell, and P.W. Mielke, Jr., 1971: The Climax Experiment for Seeding Cold Orographic Clouds. Proc. Intl. Conf. on Weather Modification, Canberra, Australia, 78-84.

_____, (Compiler), 1971: The Second International Workshop on Condensation and Ice Nuclei: Report on Workshop Goals, Program, Instruments, Observations and Preliminary Analysis. Colorado State Univ., Dept. of Atmospheric Science, 149 pp.

_____, C. Chappell, L. Crow, J. Fritsch and P. Mielke, 1974: Weather Modification - A Pilot Project. San Juan Mountains, Colorado River Basin Final Rept., Bureau of Reclamation Contract 14-06-D-6467.

_____, and A.M. Kahan, 1974: Weather Modification for Augmenting Orographic Precipitation. In Weather and Climate Modification, W.H. Hess (Ed.), 282-317.

_____, and R.E. Elliott, 1974: The Cloud Seeding Temperature Window. J. Appl. Met., 13(5):355-363.

Gunter, D.E., G.W. Jones, J.W. Jones and K.R. Monson, 1969: Low Altitude Atmospheric Turbulence. LO-LOCAT Phases I and II, ASD-TR-69-12. Wright-Patterson Air Force Base, Ohio, 395 pp.

Hay, J.S. and F. Pasquill, 1959: Diffusion from a Continuous Source in Relation to the Spectrum and Scale of Turbulence. In Atmospheric Diffusion and Air Pollution, F.N. Frenkiel and P.A. Sheppard (Eds.), Advances in Geophysics, 6:345, Academic Press.

Hino, M., 1968: Computer Experiment on Smoke Diffusion Over a Complicated Topography. Atmos. Environment, 2(6):541-558.

Hobbs, P.V., R.C. Easter and A.B. Fraser, 1973: A Theoretical Study of the Flow of Air and Fallout of Solid Precipitation Over Mountainous Terrain: Part II. Microphysics. J. Atmos. Sci., 30:813-823.

Hosler, C., 1961: Low-Level Inversion Frequency in the Contiguous United States. Mon. Weather Rev., 89:319-339.

Hovermale, J.B., 1965: A Non-Linear Treatment of the Problem of Airflow over Mountains. Pennsylvania State Univ., Ph.D. Dissertation, 88 pp.

Hovind, E.L., T.C. Spangler and A.J. Anderson, 1974: The Influence of Rough Mountainous Terrain upon Plume Dispersion from an Elevated Source. Proc. Symposium on Atmospheric Diffusion and Air Pollution, Santa Barbara, California, 214-217.

Jelinek, A., 1937: Über den thermischen Aufbau der periodischen Hangwinde. Beit. z. Phy. d. fr. Atm., 24:85-97.

Jones, J.W., R.H. Mielke, G.W. Jones, D.E. Gunter and K.R. Monson, 1970: Low Altitude Atmospheric Turbulence. LO-LOCAT Phase III, Vols. 1 and 2 (parts 1 and 2), AFFDL-TR-70-10, Wright-Patterson Air Force Base, Ohio.

Kampé de Fériet, M.J., 1939: Les Fonctions Aléatoires Stationnaires et la Théorie Statistique de la Turbulence Homogène. Ann. Soc. Sci. Brux., 59:145.

Kao, S.K., J.N. Paegle and W.E. Normington, 1974: Mountain Effect on the Motion in the Atmosphere's Boundary Layer. Bound. Layer Meteor., 7:501-512.

Klemp, J.B. and D.K. Lilly, 1975: The Dynamics of Wave-Induced Downslope Winds. J. Atmos. Sci., 32(2):320-339.

Langer, G., J. Rosinski and C.P. Edwards, 1967: A Continuous Ice Nucleus Counter and its Application to Tracking in the Troposphere. J. Appl. Met., 6(1):114-125.

Lavoie, R.L., 1968: A Mesoscale Numerical Model of Lake-Effect Storms. Pennsylvania State Univ., Ph.D. Dissertation, 102 pp.

Lenschow, D.H., 1970: Airplane Measurements of Planetary Boundary Layer Structure. J. Appl. Met., 9(6):874-884.

Lettau, H., 1967: A New Turbulent Transfer Theory based on Eulerian Concepts of Eddy Displacement Structure. Symposium on Turbulence and Diffusion, Sandia Labs, Albuquerque, New Mexico.

Lindberg, W.R. and R. Thompson, 1974: Simulation of three-dimensional Turbulence with given Second-Order Statistical Structure. Quart. J. Roy. Met. Soc., 100:608-623.

Ludlam, F.H., 1955: Artificial Snowfall from Mountain Clouds. Tellus, 7:277-290.

Lumley, J.L. and H.A. Panofsky, 1964: The Structure of Atmospheric Turbulence. Interscience Publishers, New York, 239 pp.

Mahrer, Y. and R.A. Pielke, 1975: A Numerical Study of the Air Flow Over Mountains Using the Two-Dimensional Version of the University of Virginia Mesoscale Model. J. Atmos. Sci., 32(11):2144-2155.

Miller, D.H., 1956: The Influence of Open Pine Forest on Daytime Temperature in the Sierra Nevada. Geogr. Rev., 46:209-218.

Myers, Vance A., 1962: Airflow on the Windward Side of a Large Ridge. J. Geophys. Res., 67(11):4267-4291.

National Center for Atmospheric Research (NCAR), 1973: Atmospheric Technology No. 1. 76 pp.

O'Brien, J.J., 1970: A Note on the Vertical Structure of the Eddy Exchange Coefficient in the Planetary Boundary Layer, J. Atmos. Sci., 27:1213-1215.

Orgill, M.M., 1971: Laboratory Simulation and Field Estimates of Atmospheric Transport-Dispersion over Mountainous Terrain. Colorado State Univ., Dept. of Atmospheric Science, Ph.D. Dissertation, 302 pp.

Panofsky, H.A. and T. Mizuno, 1974: Horizontal Coherence and Pasquill's Beta. AMS Symposium on Atmospheric Diffusion and Air Pollution, p. 31-34.

Pasquill, F., 1962: Atmospheric Diffusion. Van Nostrand, London, 297 pp.

Pielke, R.A., 1974a: A Three-Dimensional Numerical Model of the Sea Breezes over South Florida. Mon. Weather Rev., 2:115-139.

_____, 1974b: A Comparison of Three-Dimensional and Two-Dimensional Predictions of Sea Breezes. J. Atmos. Sci., 31(6):1577-1585.

_____, 1975: Representation of the Heated Planetary Boundary Layer in Mesoscale Models with Coarse Vertical Resolution. J. Atmos. Sci., 32:2288-2308.

Plooster, M.N. and N. Fukuta, 1972: A Numerical Model of Ice Phase Precipitation from Orographic Clouds. Proc. 3rd Conf. on Weather Modification, Rapid City, South Dakota.

_____, and N. Fukuta, 1975: A Numerical Model of Precipitation from Seeded and Unseeded Cold Orographic Clouds. J. Appl. Met, 14(5): 859-867.

Pritchard, F.E., C.C. Easterbrook and G.E. McVehil, 1965: Spectral and Exceedance Probability Models of Atmospheric Turbulence for Use in Aircraft Design and Operation. Cornell Aeronautical Lab., Inc., VC-1954-F-I, AFFDL-TR-65-122, 80 pp.

Queney, P., et al., 1960: The Airflow Over Mountains. WMO Tech. Note No. 34, 135 pp.

Reid, J.D., 1974: Predicting Nucleant Concentrations from Ground Based Generators. Proc. Fourth Conference on Weather Modification, November 18-21, Fort Lauderdale, Florida, p. 447-453.

Richtmyer, R.D., 1957: Difference Methods for Initial Value Problems. Interscience Publishers, New York, 238 pp.

Rottner, D., S.R. Brown and O.H. Foehner, 1974: The Effect of Persistance of AgI on Randomized Weather Modification Experiments. Proc. Fourth AMS Weather Modification Conf., Fort Lauderdale, Florida, p. 301-306.

Schaefer, J.T., 1973: On the Solution of the Generalized Ekman Equation. Mon. Weather Rev., 101(6):535-537.

Schulman, E.E., 1970: The Antarctic Circumpolar Current. Proc. 1970 Summer Computer Simulation Conference, Denver, Colorado, p. 955-961.

Scorer, R.S., 1953: Theory of Airflow over Mountains II - The Flow over a Ridge. Quart. J. Roy. Met. Soc., 79:70-83.

_____, 1972: The Meaningfulness of Mathematical Theories of Atmospheric Dispersion. Symposium on "External" Flows, Bristol Univ., July 4-6.

Shershkov, V.V., 1972: One Method of Computing the Meteorological Variables for Mesoscale Processes. Izv., Atmos. and Oceanic Physics, 8(7):695-703.

Smith, D.B., 1968: Tracer Study in an Urban Valley, J. Air Pollu. Con. Assoc., 8:600-604.

Smith, E.J., 1967: Cloud Seeding Experiments in Australia. Proc. 5th Berkeley Symposium on Mathematical Statistics and Probability, Volume 5, p. 161.

Snyder, W.H., 1972: Similarity Criteria for the Application of Fluid Models to the Study of Air Pollution Meteorology. Bound. Layer Meteor., 3:113-134.

Start, G.E., C.R. Dickson and N.R. Ricks, 1974: Effluent Dilutions over Mountainous Terrain and Within Mountain Canyons. Proc. Symposium on Atmospheric Diffusion and Air Pollution, Santa Barbara, California, 226-232.

Sutton, O.G., 1949: Atmospheric Turbulence. Methuen and Co., Ltd., London, 107 pp.

Taylor, G.I., 1921: Diffusion by Continuous Movements. Proc. London Mathematical Society, Ser. 2, XX:196-212.

Telford, J.W., 1970: Convective Plumes in a Convective Field. J. Atmos. Sci., 27:347-358.

Thyer, N.H., 1967: A Theoretical Explanation of Mountain and Valley Winds by a Numerical Method. Arch. Meteorol. Geophys. Biokl., Ser. A, 15(3-4):318-348.

Vinnichenko, N.K., N.Z. Pinus, S.M. Shmeter and G.N. Shur, 1973: Turbulence in the Free Atmosphere. Translation by Consultants Bureau, New York, 263 pp.

Willis, G.E. and J.W. Deardorff, 1974: A Laboratory Model of the Unstable Planetary Boundary Layer. J. Atmos. Sci., 31(5):1297-1307.

Wooldridge, G.L., 1974: Atmospheric Dispersion Characteristics of a Large Mountain Valley. Preprint, Utah State University, Logan, Utah, 16 pp.

_____, and J. Lewis, 1975: Dispersion in Mountain Valleys Using Measured Constants in a Modified Plume Model. 12th AMS Conf. on Agriculture and Forest Meteorology, Tucson, Arizona.

Young, K.C., 1974: A Numerical Simulation of Wintertime, Orographic Precipitation, Parts I and II. J. Atmos. Sci., 31(7):1735-1767.

APPENDIX A

THE UNIVERSITY OF VIRGINIA TWO-DIMENSIONAL MESOSCALE MODEL

As shown by Pielke (1974b), a two-dimensional mesoscale model can be used to investigate many of the properties of atmospheric circulations even though spacial variations of the dependent variables in the third direction are ignored. This discussion of the model given below is taken, in large part, from Mahrer and Pielke (1975).

The basic equations for hydrostatic flow in cartesian co-ordinates are structured in a terrain following co-ordinate system (x, y, z*, t) by the transformation $z^* = \bar{s}\ (z - z_G) \ /\ (s - z_G)$. Here $\bar{s}$ is the initial height of the top of the model, s is the material surface top of the model (initially $\bar{s} = s$) and z_G is the ground elevation. Using this transformation the equations of motion with no variation in the y direction permitted become

$$\frac{du}{dt} = fv - \theta \frac{\partial \pi}{\partial x} + g \frac{z^* - \bar{s}}{\bar{s}} \frac{\partial z_G}{\partial x} - g \frac{z^*}{s} \frac{\partial s}{\partial x} + \left(\frac{\bar{s}}{s - z_G}\right)^2 \frac{\partial}{\partial z^*} \left(K_z^m \frac{\partial u}{\partial z^*}\right) \qquad \text{A.1}$$

$$\frac{dv}{dt} = - fu + fu_g + \left(\frac{\bar{s}}{s - z_G}\right)^2 \frac{\partial}{\partial z^*} \left(K_z^m \frac{\partial v}{\partial z^*}\right), \qquad \text{A.2}$$

the first law of thermodynamics for an ideal gas under adiabatic conditions becomes

$$\frac{d\theta}{dt} = \left(\frac{\bar{s}}{s - z_G}\right)^2 \frac{\partial}{\partial z^*} \left(K_z^\theta \frac{\partial \theta}{\partial z^*}\right), \qquad \text{A.3}$$

the conservation equation for specific humidity without evaporation, melting or sublimation becomes

$$\frac{dq}{dt} = \left(\frac{\bar{s}}{s-z_G}\right)^2 \frac{\partial}{\partial z^*}\left(K_z^q \frac{\partial q}{\partial z^*}\right), \qquad \text{A.4}$$

and the continuity equation for hydrostatic flow becomes

$$\frac{\partial u}{\partial x} + \frac{\partial w^*}{\partial z^*} - \left(\frac{u}{s-z_G}\right)\frac{\partial z_G}{\partial x} + \frac{1}{(s-z_G)}\left(\frac{\partial s}{\partial t} + u\frac{\partial s}{\partial x}\right) = 0. \qquad \text{A.5}$$

Symbols are defined in the Table of Symbols and the following identities apply

$$\frac{\partial \pi}{\partial z^*} = -\left(\frac{s-z_G}{\bar{s}}\right)\frac{g}{\theta} \qquad \text{A.6}$$

$$\pi = C_p\left(\frac{p}{p_{oo}}\right)^{R/C_p} \qquad \text{A.7}$$

$$w^* = \frac{\bar{s}\, w}{s-z_G} - \frac{z^*}{s-z_G}\left(\frac{\partial s}{\partial t} + u\frac{\partial s}{\partial x}\right) + \left(\frac{z^*-\bar{s}}{s-z_G}\right)u\frac{\partial z_G}{\partial x} \qquad \text{A.8}$$

$$\frac{d}{dt} = \frac{\partial}{\partial t} + u\frac{\partial}{\partial x} + w^*\frac{\partial}{\partial z^*} \qquad \text{A.9}$$

A prognostic equation for the free surface height is obtained by integrating eq. A.5 from $z^* = 0$ to $z^* = \bar{s}$ with boundary condition $w^* = 0$ on both surfaces. The resultant equation is

$$\frac{\partial s}{\partial t} = -\frac{1}{\bar{s}}\int_0^{\bar{s}} \frac{\partial}{\partial x}\left[u(s-z_G)\right] dz^* \qquad \text{A.10}$$

This treatment of the upper surface as a free material surface is an attractive feature of this model as it circumvents the inconsistency of the other commonly employed approach, a fixed upper surface height but with varying pressure.

A.1 Boundary Layer Formulation

The unique feature of this model is the comprehensive treatment of the boundary layer. Vertical exchange coefficients in the surface layer

are given by

$$K_z^m(z^*) = k_o u_* z^*/\phi_i(|\xi|)$$

and

$$K_z^\theta(z^*) = \beta K_z^m(z^*)$$

where the subscript i = 1 denotes unstable stratification in the surface layer and subscript i = 2 denotes stable surface layer stratification. The nondimensional stability length ξ and the parameter β are defined as

$$|\xi| = z^*/|L_*|$$

and

$$\beta = \begin{cases} 1/\phi_i(|\xi|) & i = 1 \\ 1 & i = 2 \end{cases}$$

where

$$L_* = -\bar{\theta}\, u_*^2/\sigma k_o g \theta_*$$

Expressions for the ϕ_i nondimensional wind, potential temperature and specific humidity profile functions are those given by Businger (1971).

$$\phi_m = \begin{cases} (1-15\xi)^{-1}, & \xi \leq 0 \\ 1+4.7\xi, & \xi > 0 \end{cases}$$

$$\phi_q = \phi_H = \begin{cases} 0.74(1-9\xi)^{-\frac{1}{2}}, & \xi \leq 0 \\ 0.74+4.7\xi, & \xi > 0 \end{cases}$$

$$\frac{\partial \phi_m}{\partial \xi} = \begin{cases} 3.75\phi_m^5, & \xi \leq 0 \\ 4.7, & \xi > 0 \end{cases}$$

$$\frac{\partial \phi_H}{\partial \xi} = \begin{cases} 8.22\phi^3, & \xi \leq 0 \\ 4.7, & \xi > 0 \end{cases}$$

where

$$\phi_m = \frac{kz}{u_*} \frac{\partial u}{\partial z} \quad \text{and} \quad \phi_H = \frac{kz}{\theta_*} \frac{\partial \theta_v}{\partial z} .$$

The exchange coefficients above the surface layer are determined using the polynomial formulation of O'Brien (1970), while the technique to determine the top of the planetary boundary layer is based on the work of Deardorff (1974). In this formulation the boundary layer grows as a function of surface heat and momentum fluxes, mesoscale vertical motion and overlying stability. Additional information on the boundary layer parameterization may be found in Pielke and Mahrer (1975).

A.2 Initial and Boundary Conditions

To avoid numerical integration problems arising from the initial accelerations, Deaven's (1974) procedure of diastrophism is used. The mountain is allowed to grow during the first two hours from an initial flat surface to its maximum height. The initial conditions are given for temperature and humidity by a measured or otherwise specified upwind sounding. Over the flat surface initially, the shear stress, Coriolis and pressure gradient forces are assumed in balance as expressed by

$$\frac{\partial}{\partial z}\left(K_z^m \frac{\partial u}{\partial z}\right) + f(v-v_g) = 0 \qquad \text{A.11}$$

and

$$\frac{\partial}{\partial z}\left(K_z^m \frac{\partial v}{\partial z}\right) + f(u_g-u) = 0 \qquad \text{A.12}$$

The initial wind profile in the planetary boundary layer is calculated from A.11 and A.12 by the method of Schaefer (1973). Above the planetary boundary layer the velocities are assumed geostrophic.

On the lower boundary at $z^* = 0$ the conditions

$u = v = w^* = 0$ and $\theta = \theta(t)$

are specified. On the upper boundary at $z^* = \bar{s} = 10$ Km the conditions

$$\frac{\partial u}{\partial z^*} = \frac{\partial v}{\partial z^*} = w^* - 0, \quad \pi = \pi(\bar{s}) - g\frac{(s\bar{s})}{\theta(s)}, \quad \frac{\partial \theta}{\partial z} = 0.4°C/100m$$

are implemented. At the upwind and downwind boundary the conditions are

$$w^* = \frac{\partial}{\partial x}(u,v,\theta,\pi,s) = 0.$$

A roughness parameter of $z_o = 0.2$ m is used in all experiments.

A.3 Numerical Aspects

The numerical integration of eqs. A.1 to A.6 and A.10, with the initial and boundary conditions as given above, are carried out by first order forward differences in time and upwind differences in space. The vertical eddy viscosity and eddy conductivity terms are replaced by a DuFort and Frankel difference scheme (Richtmyer, 1957). A full description of the numerical procedure and staggered grids used are given in Pielke (1974a).

In order to minimize lateral boundary effects, stretching is applied symmetrically about the center of the domain, after Schulman (1970). In this study the minimum grid spacing is chosen to be 2 Km with 33 horizontal grid points and a domain total length of 600 Km. While this 2 Km grid spacing is much larger than the approximately 100 m mentioned earlier, it is adequate to describe the along wind slope variation, which will be investigated here, when the vertical transformation is considered.

In the vertical, the atmospheric structure is specified at 12 levels at heights of 0, 50 m, 100 m, 1200 m, 1800 m, 2400 m, 3600 m, 4800 m, 6000 m, 7200 m, 8400 m, and 10,000 m. At these levels u, v, p, and w are computed. At intermediate heights r is computed. The time step in the integration is 15 seconds for a geostrophic wind of 10 mps.

APPENDIX B

NUMERICAL METHOD FOR STATISTICAL SIMULATION OF CONVECTIVE PLUME FIELD DISPERSION

In simulating dispersion it is apparent that it will frequently be desirable to explicitly handle certain "systems" or energy containing eddies as distinct entities. The flow properties accompanying such systems introduce unique dispersion characteristics. The convective plumes of the planetary boundary layer are such systems and are treated in this section.

Basically the role of the plumes in dispersion is in transporting the pollutant particles upward in the planetary boundary layer. Outside the plumes, air subsides to compensate for this. Continuity demands convergence toward the plumes at low levels and divergence at high levels.

Let a plume of radius R be surrounded by a compensating subsidence region concentric with the plume. For cylindrical symmetry the equation of continuity in cylindrical polar co-ordinates is

$$\frac{u}{r} + \frac{\partial u}{\partial r} = \frac{\partial w}{\partial z}$$

where u is the radial velocity component and w the vertical velocity component. Solving this differential equation by the method of separation of variables with $u = u(z).u(r)$ and $w = w(z).w(r)$, the equation becomes

$$\frac{u(r)}{r} + \frac{du(r)}{dr} = Mw(r)$$

and

$$\frac{dw(z)}{dz} = -Mu(z)$$

where M is a separation constant. Profiles of u(z), u(r), w(z) and w(r) need to be specified. Adopt simple analytic expressions which meet the physically determined boundary conditions.

For the radial components the boundary conditions are:

1. w(r) is a maximum at r = 0.
2. w(r) becomes constant at the outer edge of the subsidence region.
3. w(r) is positive (upward) within the plume and negative (downward) outside the plume. It is zero at the plume edge.
4. u(r) is zero at the plume center.
5. u(r) is zero at the outer edge of the subsidence region.
6. The net vertical flux at any level is zero.

The differential equation and boundary conditions are satisfied by the relations

$$w(r) = J_o(\alpha r) \qquad 0 < \alpha r < 3.83171$$

$$u(r) = -MJ_1(\alpha r)$$

where the J's are Bessel functions. The α is defined so that the first zero of $J_o(\alpha r)$ falls at the edge of the plume.

Vertical profiles are constrained by the boundary conditions:

1. u(z) = 0 at the earth's surface
2. w(z) = 0 at the earth's surface
3. w(z) = 0 at the top of the boundary layer
4. w(z) is positive.

Deardorff and Willis (1975) have simulated dispersion from an elevated point source in an unstable PBL using a water tank. They show

results for centerline concentration as a function of height and downstream distance, fig. B.1. Significant features of the water tank result are:

1. The height of maximum concentration lowers initially as most of the pollutant is released into the subsiding air outside the plumes.
2. After the initial lowering, the concentration maximum rises rapidly to about three-quarters of the boundary layer height. Most of the pollutant has been entrained into the convective plumes and has been transported aloft. The region of strongest entrainment to the plumes appears to be in the lowest tenth of the PBL. Detrainment appears to start at about half the PBL height.
3. The maximum lowers to the half height of the PBL as the pollutant is detrained from the plume, subsides and becomes uniformly mixed within the PBL.

This result provides information, additional to that of the boundary constraints, to aid in choosing the vertical profile. Specifically, the u(z) appears greatest toward the plume at lower levels and appears to go to zero while w(z) becomes a maximum, at about half the PBL height.

Figure B.2 shows a w(z) profile satisfying all the above constraints. The rapid variation in the lower part of the PBL makes this a difficult profile to fit with an analytical function. In addition, observation and theory do not appear well enough reconciled to allow a profile in z to be established. In this study, where the emphasis is to illustrate the approach rather than to reproduce details, the dispersion produced by a simple profile meeting only some of the criteria has been calculated.

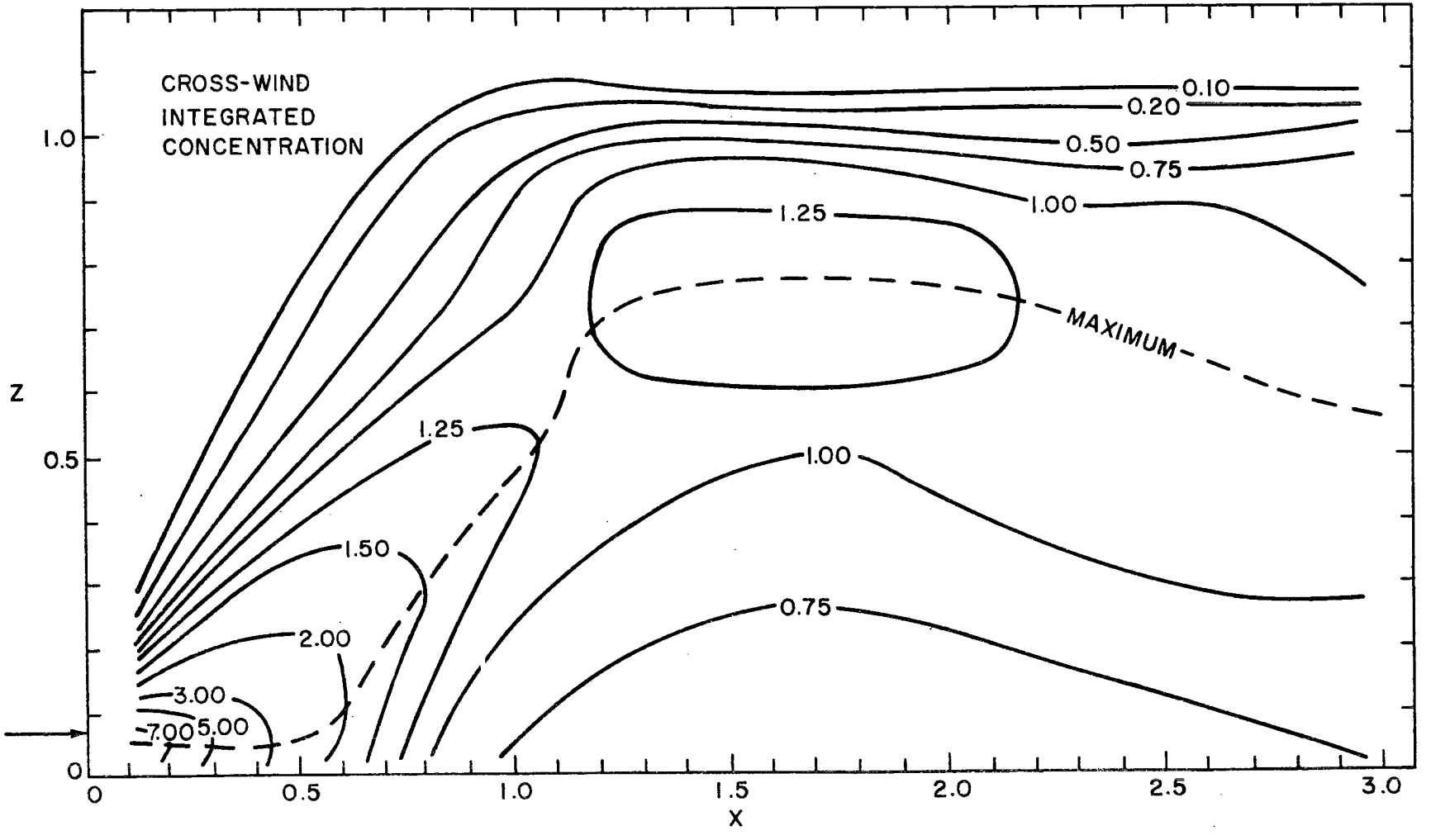

Figure B.1. Smoothed values of dimensionless cross-wind integrated concentration as a function of height and downstream distance. Arrow denotes source location. (After Willis and Deardorff, 1975.)

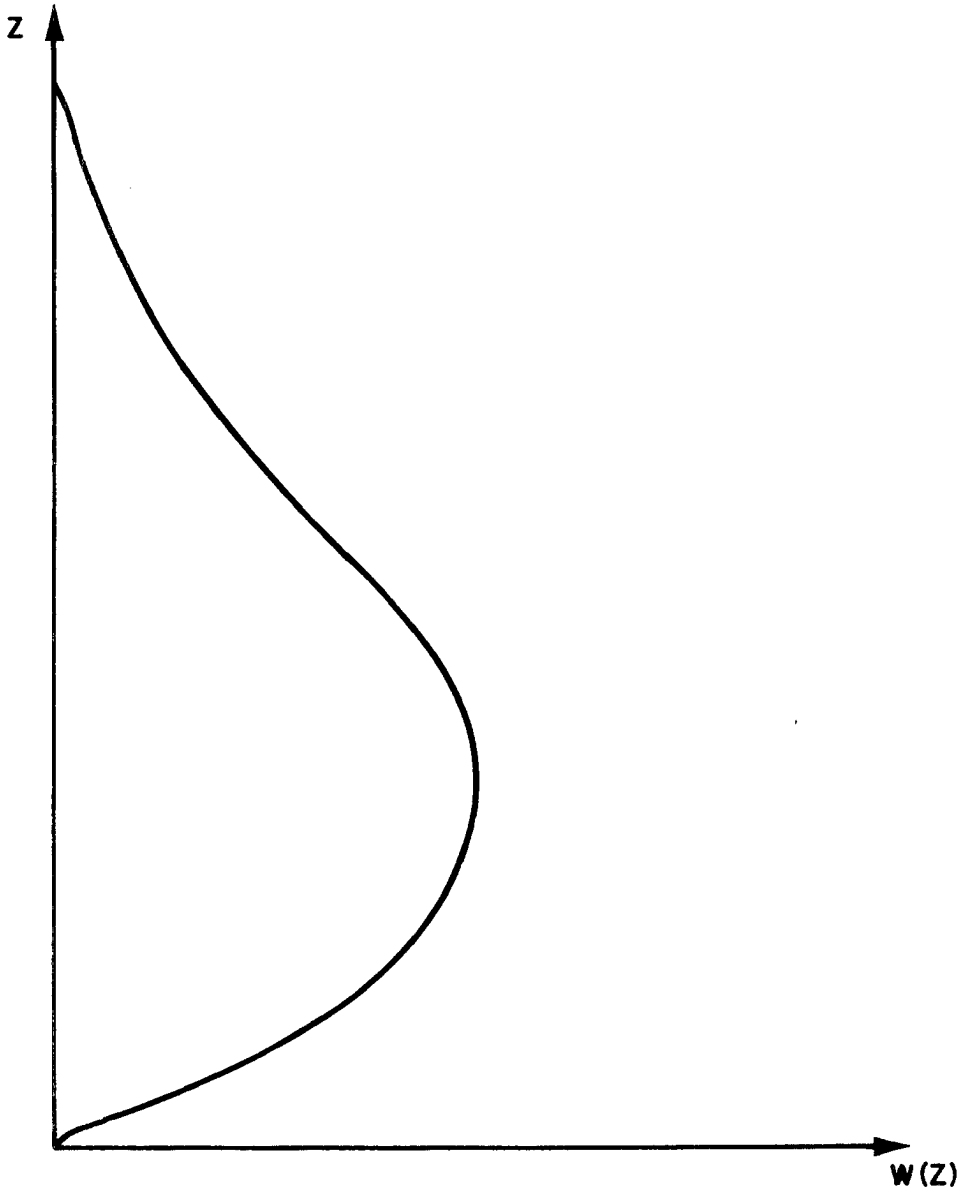

Figure B.2. Plume vertical velocity profile satisfying boundary constraints.

The assumption of a constant R which has been employed here has been found to be quite reasonable by Telford (1970). With the specifications above particle trajectories through the plume system can be calculated.

In application to dispersion in the unstable planetary boundary layer the motion of particles is calculated from components given by the resolved winds, the plume model and the small scale turbulence model (as used in the previous example). Horizontal winds are formed from components given by the resolved and small scale turbulence components. Vertical winds use a component from the plume model in addition. Parameters from the larger scales may be required in the smaller scale parameterizations. Thus, for example, the height of the convective boundary layer used in the plume model can be obtained from the resolved scale.

The result of the Monte Carlo simulation of dispersion from an infinite line source normal to the mean wind in an unstable boundary layer with 5,000 trajectories calculated is shown in figure B.3. In this simulation the mean (resolved) wind is assumed uniform in direction and speed with position, the small scale turbulence is assumed independent of position, which is in accord with the results of Telford (loc cit). Lacking definitive information on the vertical profile needed for the plume circulation specification the expression

$$w(z) = 20\, z(1-z)(1-z/2) \qquad 0 \leq z \leq 1$$ (z=1 at the top of the convective layer)

is employed, which fits boundary conditions 2, 3 and 4 and has a maximum of w(z) at about 0.4 of the convective layer height.

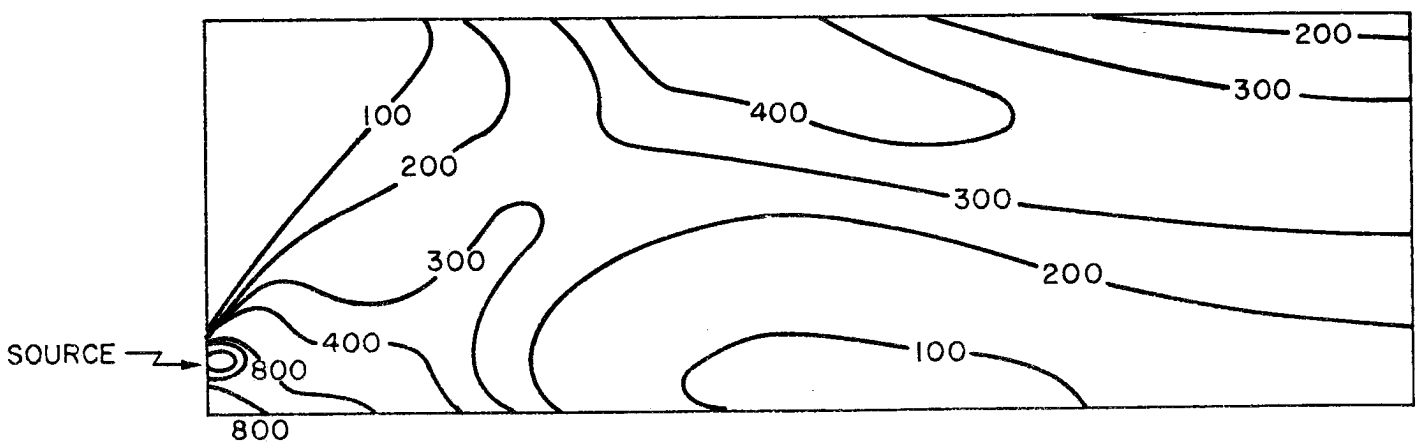

Figure B.3. Axial Concentrations in the Planetary Boundary Layer for dispersion from an infinite line source simulated by the Monte Carlo Method. Isopleth values are proportional to concentration.

It is interesting to compare the result of this simulation with the result for cross wind integrated concentration from a point source found in the water tank experiments simulating dispersion in an unstable planetary boundary layer of Deardorff and Willis (loc cit). Both simulations show the maximum concentration initially lowering too close to the surface. This is because most of the particles are released into the subsident air outside the plumes. These particles gradually become entrained into the plumes which carry them aloft. Thus an elevated maximum forms in both simulations. Differences in the concentration patterns can be attributed to lack of definitive knowledge of the vertical profile of vertical velocity in the plumes.